NASA CR 65604

[redacted]

FACILITY FORM 602

N67-23326	
(ACCESSION NUMBER)	(THRU)
94	1
(PAGES)	(CODE)
CR 65604	29
(NASA CR OR TMX OR AD NUMBER)	(CATEGORY)

LMSC/2-44-66-1

Final Report

Contract No. NAS 9-1587

PROTON-ELECTRON SPECTROMETER EXPERIMENTS ON GEMINI-4 AND GEMINI-7

by

J. B. Reagan
J. C. Bakke
M. A. Heinemann
W. L. Imhof
R. V. Smith

30 September 1966

LOCKHEED PALO ALTO RESEARCH LABORATORY
Lockheed Missiles & Space Company
A Group Division of Lockheed Aircraft Corporation
Palo Alto, California

FOREWORD

This final report is submitted to the National Aeronautics and Space Administration, Manned Spacecraft Center, covering work performed under Contract NAS 9-1587, Proton Flux Experiment.

The work was performed during the period 27 May 1963 to 30 September 1966, at the Lockheed Palo Alto Research Laboratory, Palo Alto, California.

ABSTRACT

This report describes two experiments which were performed aboard the Gemini-4 and Gemini-7 spacecraft to measure the external radiation environment. Omnidirectional fluxes and spectra of electrons in the 0.5-8.0-MeV energy range and of protons in the 25-80-MeV energy range as well as the omnidirectional proton flux greater than approximately 80 MeV were measured by scintillation spectrometers employing 16-channel pulse-height analyzers. A detailed description of the spectrometers including design philosophy, laboratory and in-flight calibration, and flight performance is included. Preliminary results from the experiments in the form of proton and electron flux contours and spectral shapes in B,L space are given. A comparison between the present data and previous experimental and theoretical results is also included. Proposed additional detailed data analysis is suggested.

TABLE OF CONTENTS

ILLUSTRATIONS

Illustrations, cont'd

Illustrations, cont'd

Illustrations, cont'd

Section 1

INTRODUCTION

Two experiments designed by the Space Radiation Group of the Lockheed Palo Alto Research Laboratory and designated as the MSC-2 experiments have been conducted aboard Gemini spacecraft to measure in detail the external proton and electron environment. The flux and spectrum of electrons in the 0.5-8.0-MeV energy range and of protons in the 25-80-MeV energy range were measured aboard the Gemini-4 spacecraft from 3-7 June, 1965, with a sintillation spectrometer employing a 16-channel pulse-height analyzer. From 4-18 December, 1965, a similar experiment with somewhat different energy ranges was performed on the Gemini-7 spacecraft.

These experiments have provided detailed flux and spectrum measurements in the vicinity of the South Atlantic anomaly, where the population, lifetime, and behavior of particles trapped on low magnetic shells are greatly influenced by the earth's atmosphere. Therefore, it is possible to study loss and redistribution mechanisms as well as the overall time variations encountered in the inner radiation belt by means of detailed comparisons between experimental data and atmospheric scattering theory. Previous comparisons of this sort have been limited by the number of detailed experimental measurements [Imhof, et al., 1963; Mann, et al., 1963; Mozer, et al., 1963; Freden and Paulikas, 1964; Imhof and Smith, 1965a,b, c,d; West, et al., 1965]. Data acquired from higher altitude satellites are not so directly applicable to the understanding of phenomena in this low-altitude region. Therefore, the Gemini-4 and -7 radiation experiments will allow more scientific analysis and understanding than had been possible heretofore concerning the lower edge of the inner radiation belt.

In addition, and of particular interest to NASA-MSC, virtually all of the radiation encountered by the Gemini and early Apollo missions will be accumulated in this region. A detailed knowledge of the flux and spectrum of the radiation experienced in these orbits is essential to an accurate prediction of doses to be received by astronauts and equipment on these flights. This information is also of importance to satellite-borne scientific experiments which require a knowledge of the radiation environment. Since the available data are limited and because the behavior of the trapped radiation is time dependent, frequent updating of the lower inner radiation belt model is required. Experiments performed periodically on low-altitude spacecraft have provided our best source of such information.

Our knowledge of the origin of the natural radiation belts and of the mechanisms involved in their continual losses and regeneration is still rather limited after several years of investigation. At low altitudes it has been established, however, that the atmosphere encountered by both trapped protons and electrons in their trajectories dominates their behavior [Welch, et al., 1963; Lenchek and Singer, 1963; Walt and MacDonald, 1964a]. The interaction for electrons is primarily scattering, producing diffusion in both energy and pitch angle. A fraction of those which are scattered toward lower mirror points in the dense atmosphere are permanently lost. The replenishment of these electrons to maintain the natural belts occurs in a manner which is not clearly understood. Unlike electrons, trapped protons lose their energy primarily through ionization interactions with the atmosphere in their path. The replenishing source of these protons is also not clearly understood although the decay of cosmic-ray albedo neutrons [Lenchek and Singer, 1963] appears to be one of the significant mechanisms. Difficulty in predicting the behavior of these trapped particles arises from the lack of detailed knowledge of the source term in both cases.

The Starfish high-altitude nuclear detonation of 9 July, 1962, provided a unique opportunity to investigate the time behavior of trapped electrons since it created an intense artificial belt of electrons with fission-like energies at low L shells. In this situation, the source term was reasonably known, and several satellite experiments were performed shortly after the event. Based on these early time data, Walt [1964b] has shown that the predominant loss mechanism for these fission electrons at L $\lesssim$ 1.25 is atmospheric scattering. In particular, the narrow but important anomaly region of the inner radiation belt dominates the lifetime of these electrons. Several experiments have been performed [Mozer, et al., 1963; Imhof and Smith, 1965a,b,c,d; West, et al., 1965] to investigate the intensity, spectrum, and decay of this radiation belt.

The Gemini-4 and -7 experiments offer a valuable opportunity to measure in detail the intensity, spectrum, and decay of this radiation some three to four years after the event. By comparing early time data and the current results with the predictions based on atmospheric scattering, we should be able to learn a great deal about the atmosphere controlling the decay rate and whether other loss mechanisms are also important.

In addition to the two spatial parameters, B and L, it has been shown [Welch, et al., 1963; Paulikas and Freden, 1964; Imhof and Smith, 1965b; Vernov, et al., 1965] that longitude also becomes an important controlling parameter for electrons observed at low altitudes on almost any L shell. The fluxes of electrons for $L \leq 1.7$ trapped with mirror points at B,L positions for which the minimum altitude is less than 100 km exhibit a strong dependence on longitude. Fluxes just west of the magnetic anomaly region are typically about an order of magnitude greater than those measured just east of the anomaly at comparable values of B and L. In addition, at a given B,L value the spectrum west of the anomaly is softer than that east of the anomaly. This effect has been attributed to large-angle coulomb scattering of trapped electrons resulting in their shift to high B values. The phenomenon has been compared to a windshield wiper in that trapped electrons on magnetic shells $L \leq 1.7$ which in their eastward drift around the earth encounter the anomaly region from the west are "swept out" by small-angle atmospheric scattering and then "built up" again just east of the anomaly perhaps by large-angle scattering effects. Clearly, a very intriguing and important source and loss mechanism is involved in this region. The Gemini experiments may provide interesting longitudinal-dependent data obtained during solar minimum for comparison with earlier results.

Experimental data [Freden, et al., 1964] have shown that the equilibrium flux and spectrum of energetic protons in the inner radiation belt are quite stable. Since protons lose their energy primarily through ionization processes with the atmospheric constituents, a change in the flux should be observed as the atmospheric density changes during the solar cycle [Blanchard and Hess, 1964]. The present data should provide detailed proton flux and spectra during solar minimum for comparison with earlier results obtained closer to solar maximum. This comparison, particularly when combined with a similar analysis of electron data obtained from the same spectrometer, should result in an accurate definition of the atmosphere over this period.

A detailed knowledge of the flux and spectra of both electrons and protons at low L shells is also important from an operational aspect. The capability of predicting and calculating radiation doses to be received ay astronauts and equipment on typical Gemini, earth-orbiting Apollo and MOL flights must be based on current and accurate knowledge of the radiation environment. This can only be provided by conducting periodic experiments such as the present ones. The limited quantity of available data on protons and electrons on low L shells is illustrated by Vette's [1966] model of the trapped radiation environment. For magnetic shells of $L \leq 1.7$ only three sets of experimental electron data were available to Vette. Many more measurements were available for higher L shells. The situation is identical for protons. The present Gemini data should prove valuable in updating and substantiating the current environmental model in this region.

Section 2

DESCRIPTION OF THE EXPERIMENTS

2.1 Proton-Electron Spectrometer—Gemini-4

The experiment performed aboard the Gemini-4 spacecraft to measure the external proton and electron environment utilized a scintillation detector in conjunction with a multichannel pulse-height analyzer. A photograph and cross-sectional view of this spectrometer is shown in Figures 1 and 2, respectively. The basic detector for both protons and electrons was a large plastic scintillator (Pilot-B) 7.87 cm in diameter and 5.08 cm high. The size and shape of the scintillator were chosen to provide high sensitivity and uniform path length over the entire acceptance solid angle of 1.2π steradians for electrons of energy from 0.5-8.0 MeV and protons of energy from 25-80 MeV.

Separation of electrons and protons was accomplished by the different ranges of energy deposit in the detector and the known relative intensities of the two types of particles within these ranges. In particular, there are a negligible number of electrons to be expected with energies above 8 MeV [Imhof and Smith, 1965c] compared with the expected proton flux above 25 MeV [Freden, et al., 1964]. The spectrometer was located at the center of the equipment-adapter module of the spacecraft with an aft view cone of 68.2 degrees half-angle. A thermal curtain which covered the rear of the module in combination with a thin (1 mg/cm^2) aluminized-mylar covering over the entrance aperture of the spectrometer eliminated protons with incident energy in the 0.5-8.0 MeV range.

The light from the detector scintillator was coupled to a ruggedized type 4439 photomultiplier by a lead-glass light pipe 2.54 cm in diameter by 1.27 cm thick. This also provided approximately 5.1 gm/cm^2 of shielding for the detector scintillator in the backward direction. The lead glass combined with the shielding provided by the photomultiplier, electronics,

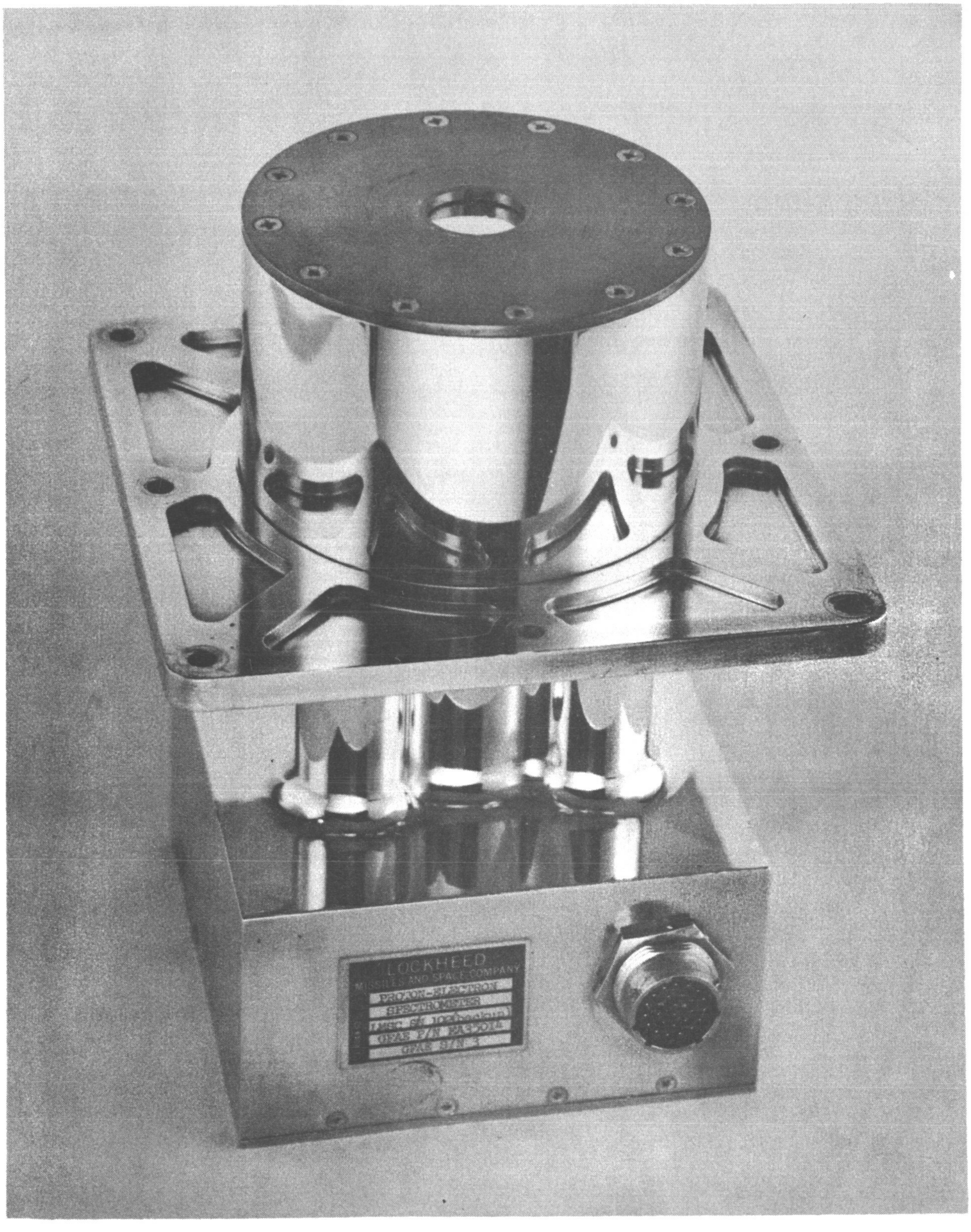

FIGURE 1. Photograph of Gemini-4 Proton-Electron Spectrometer.

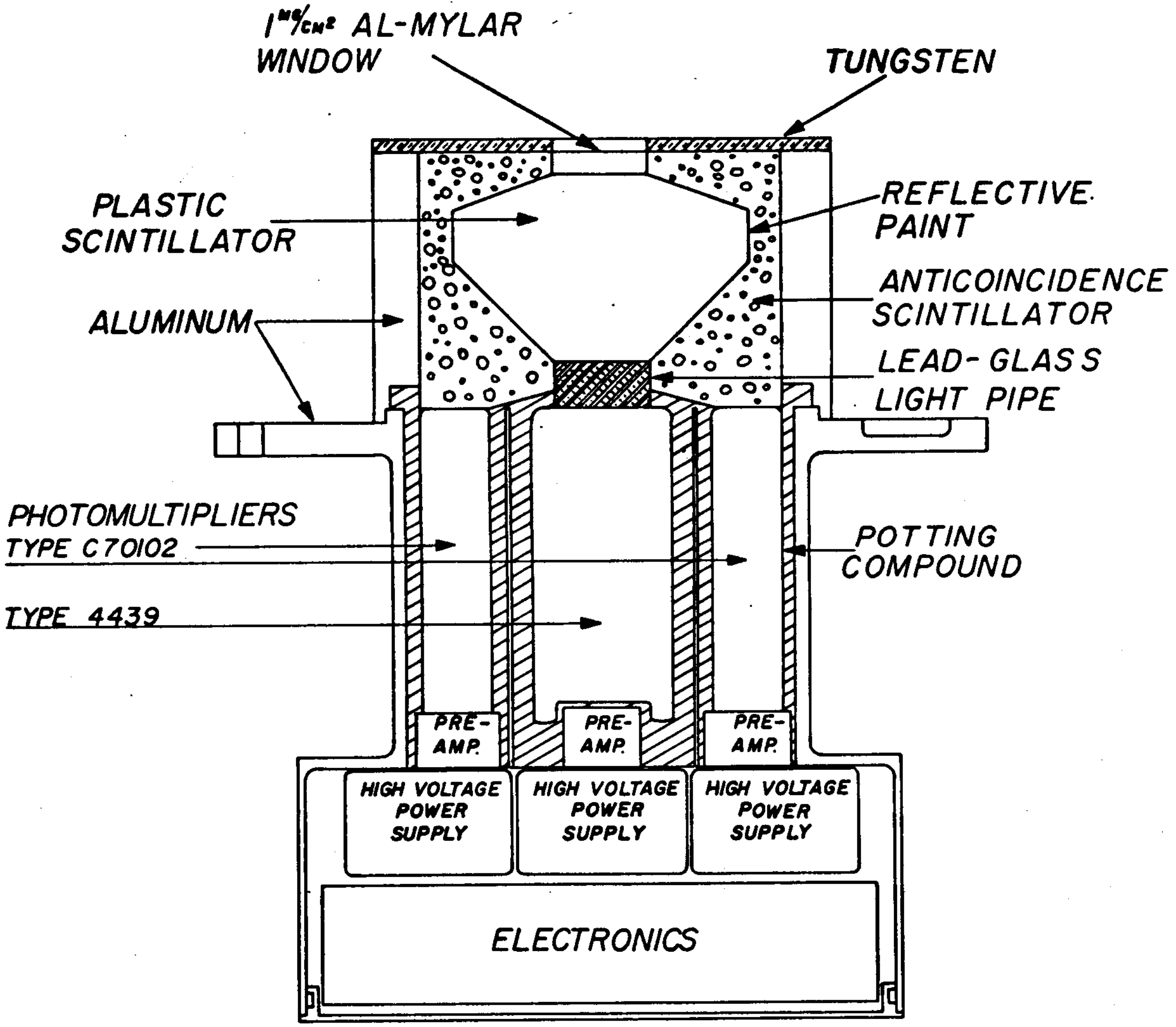

FIGURE 2. Cross-Section Diagram of Gemini-IV Proton-Electron Spectrometer

aluminum containers, and the spacecraft reduced to a negligible quantity the effect of energetic particles entering the detector scintillator from the solid angle defined by the light pipe.

The entire detector scintillator except for the acceptance aperture was surrounded by a combination of shielding material and an ancicoincidence scintillator. The purpose of the shielding was to prevent the penetration of most of the energetic particles into the detector scintillator from directions other than the acceptance solid angle. The top of the scintillator was protected by a 0.218-cm thickness of tungsten (Fansteel-77) to provide a shielding of 5.41 gm/cm^2 corresponding to the range of an 8.5-MeV electron and a 53-MeV proton. The surrounding walls and bottom of aluminum provided a minimum shielding of 3.43 gm/cm^2, corresponding to the range of a 5.3-MeV electron and a 56-MeV proton. Completely surrounding the main scintillator, except for a 2.54-cm diameter acceptance aperture and the light pipe, was a plastic (Pilot-B) anticoincidence scintillator. This scintillator had an energy threshold of approximately 300 keV and was sufficiently thick to detect all particles above that energy, including cosmic rays. Thus, all particles not entering through the acceptance solid angle were rejected from further analysis. The aluminum shielding outside the anticoincidence detector was necessary to limit the anticoincidence dead time to a reasonable value by stopping most of the undesired energetic particles. Three photomultipliers, type C70102, viewed the light from the anticoincidence scintillator to obtain maximum detection sensitivity.

A block diagram of the data-handling system of the spectrometer is shown in Figure 3. Pulses from the detector-photomultiplier were coupled to the analysis system by a preamplifier stage with two discrete gain steps, in order to cover the broad range of energy involved. This gain change was accomplished in flight by means of an internal solid-state timer which allocated alternate time periods of 18 seconds to each of the two energy ranges. An analog voltage from the timer to the telemetry provided a monitor on the range under analysis.

Pulses from the three photomultipliers viewing the anticoincidence scintillator were coupled to a common integral discriminator by three

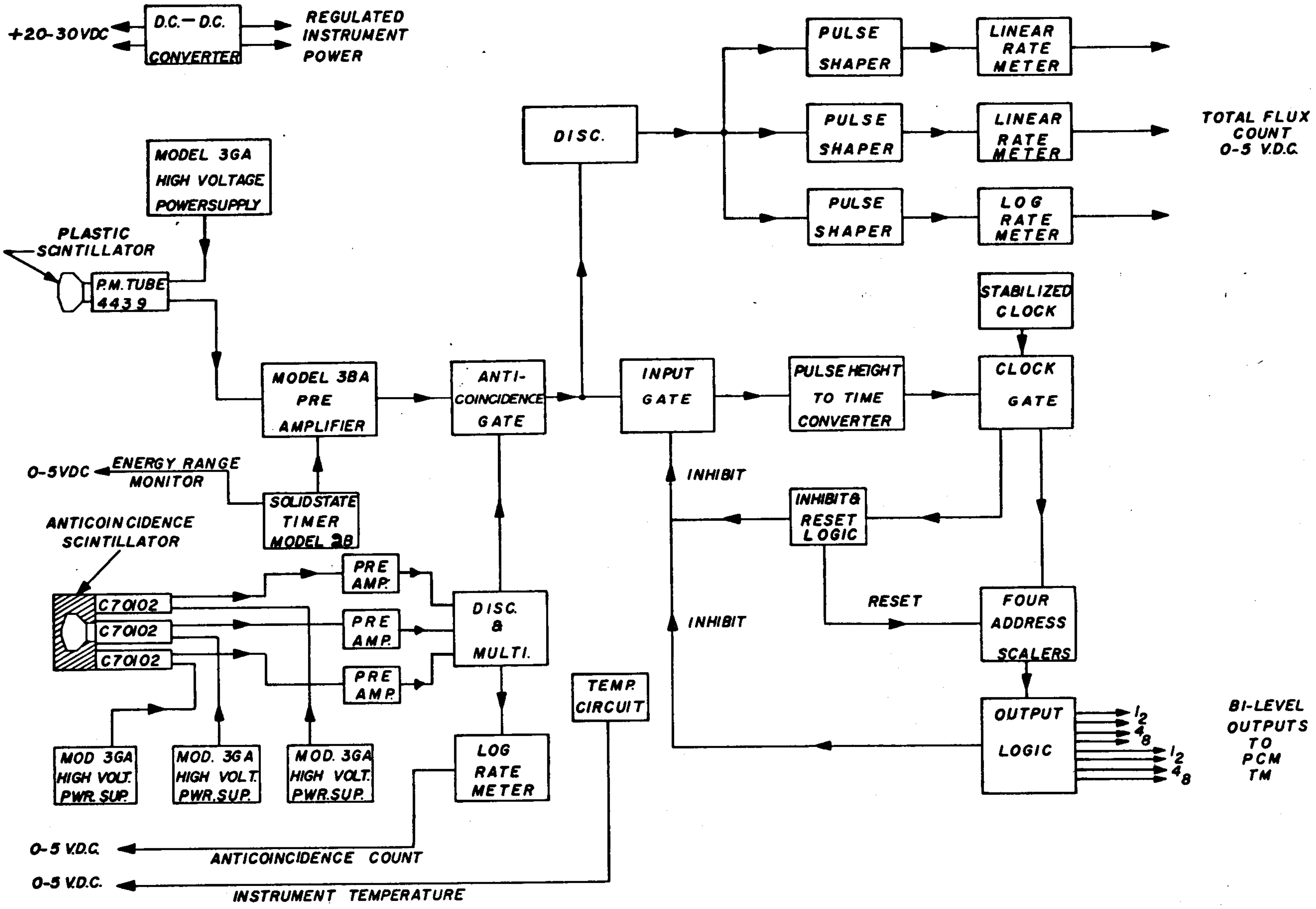

FIGURE 3. Block diagram of data analysis and handling system for Gemini-IV proton-electron spectrometer.

preamplifiers. When the discrimination level was exceeded, an enable signal was applied to an anticoincidence gate which then prevented any detector-scintillator signal from being analyzed during the following 3-microsecond period. The enable pulses were also fed to a logarithmic ratemeter to provide the anticoincidence or singles rate to the telemetry.

Pulses from the detector scintillator which passed through the anticoincidence gate were analyzed by a 16-channel pulse-height analyzer of the analog-to-digital conversion type [Rowland, et al., 1963; Reagan, et al., 1965]. The channel-address which corresponded to an input pulse-height from the detector was coded in binary format and was sampled in parallel as a four-bit bi-level word by the PCM telemetry system at a 20-sample-per-second rate. The input of the analyzer was inhibited from receiving any additional information until the pulse under analysis had been sampled by the telemetry. In this manner, a random spectrum sampling of the incoming radiation was obtained. Because of this relatively low-sampling-rate limitation, the absolute flux of incoming radiation was determined by a group of ratemeters. Pulses which passed the anticoincidence gate triggered a discriminator having a threshold which was matched to that of the pulse-height analyzer. Two linear ratemeters covered the counting range to about 800 counts per second. A logarithmic ratemeter which overlapped the linear ratemeter extended the counting rate capability to approximately 500,000 counts per second. The outputs of these ratemeters, which were analog voltages between 0 and 5 Vdc, were sampled by the telemetry and converted to an eight-bit binary word at a 1.25-sample-per-second rate.

A dc-to-dc converter was utilized to convert the unregulated input voltage to regulated instrument voltages and to provide required isolation from the spacecraft. A temperature circuit which was capable of measuring the internal instrument temperature between -30°C and +75°C was also incorporated to permit temperature corrections to be made to the data.

2.2 Proton-Electron Spectrometer—Gemini 7

At the request of NASA-MSC, the proton-electron spectrometer used in the Gemini-4 experiment was redesigned for the Gemini-7 flight to measure protons down to 5 MeV in addition to measuring electrons in the 0.5-4.0-MeV energy range. This is a difficult experiment to perform since one is required to measure a relatively low flux of natural protons in an energy and spatial region where an intense flux of fission-type electrons exist. The experiment becomes more difficult when a plastic scintillator is used to measure both types of particles since the light output efficiency in a scintillator is significantly lower for protons than that for electrons over the same energy region. In Figure 4, the electron pulse-height in MeV equivalent to the light output of protons in the 1-10-MeV is presented for two commercially available plastic scintillators [Evans and Bellamy, 1959]. For example, a 5-MeV proton produces a light output equivalent to a 2-MeV electron. This disadvantage of plastic scintillator is, however, offset by its many advantages, including its short decay time which allows detection to very high counting rates without pile-up of long-term fluorescence effects.

To identify unambiguously the type of particle producing the light output in the main detector, an additional plastic scintillator, 0.025 cm thick, was placed in front of and operated in coincidence with the main detector. Protons in this energy range in traversing this scintillator lose considerably more energy per unit path length than equivalent energy electrons because of their much higher specific ionization. On this basis a distinct separation of pulse heights for protons and electrons should then be possible. Figure 5 shows the calculated energy loss in the above scintillator for incident protons and electrons based on the known range-energy relationships of protons [Rich and Madey, 1954] and electrons [Nelms, 1956] in a hydrocarbon. The relative light output for these two particles based on the data shown in Figure 4 is also shown. A unique identification of protons would then be possible by accepting only those pulse heights which correspond to an energy loss of greater than

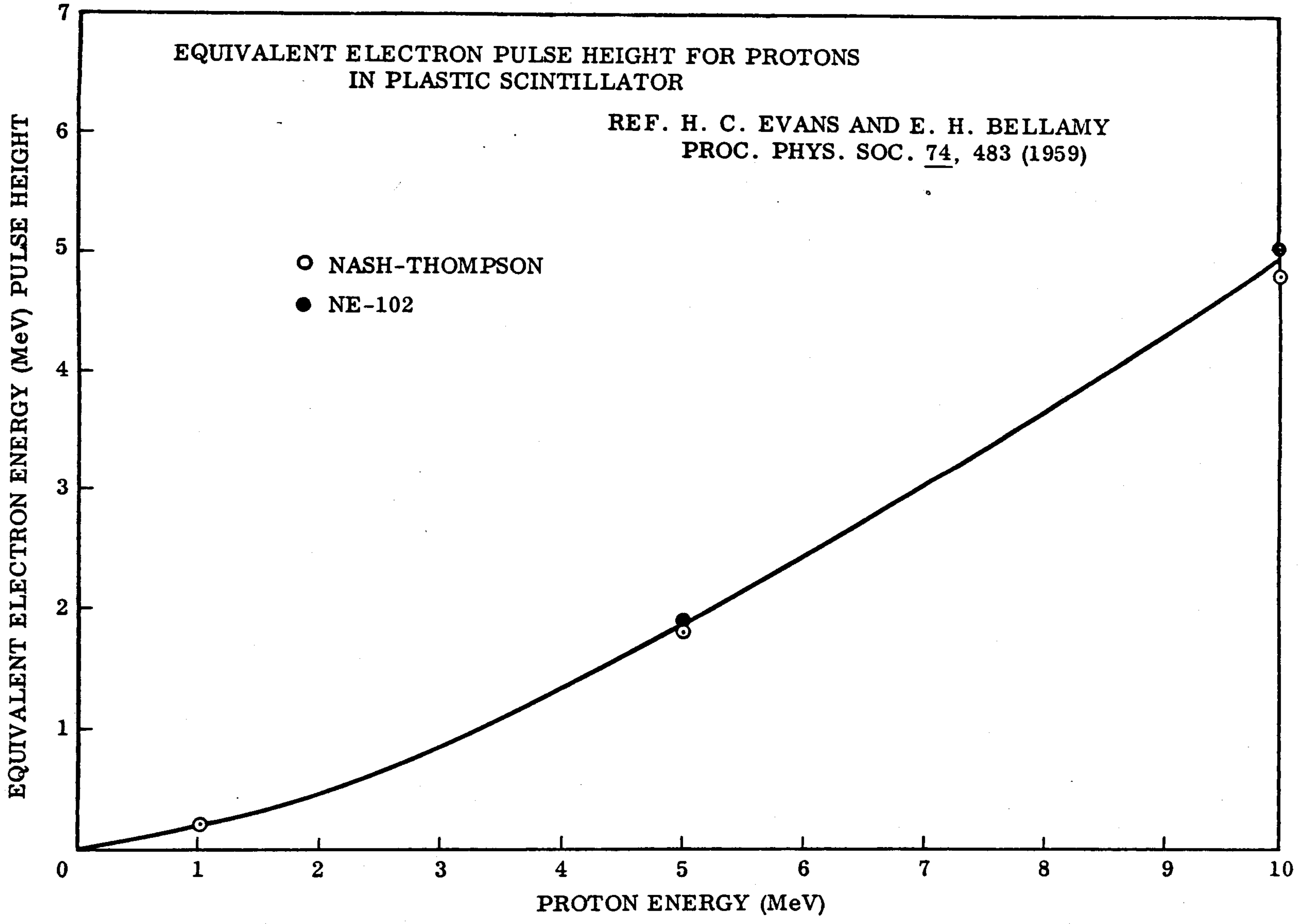

FIGURE 4. Equivalent Electron Pulse Height for Protons in Plastic Scintillator.

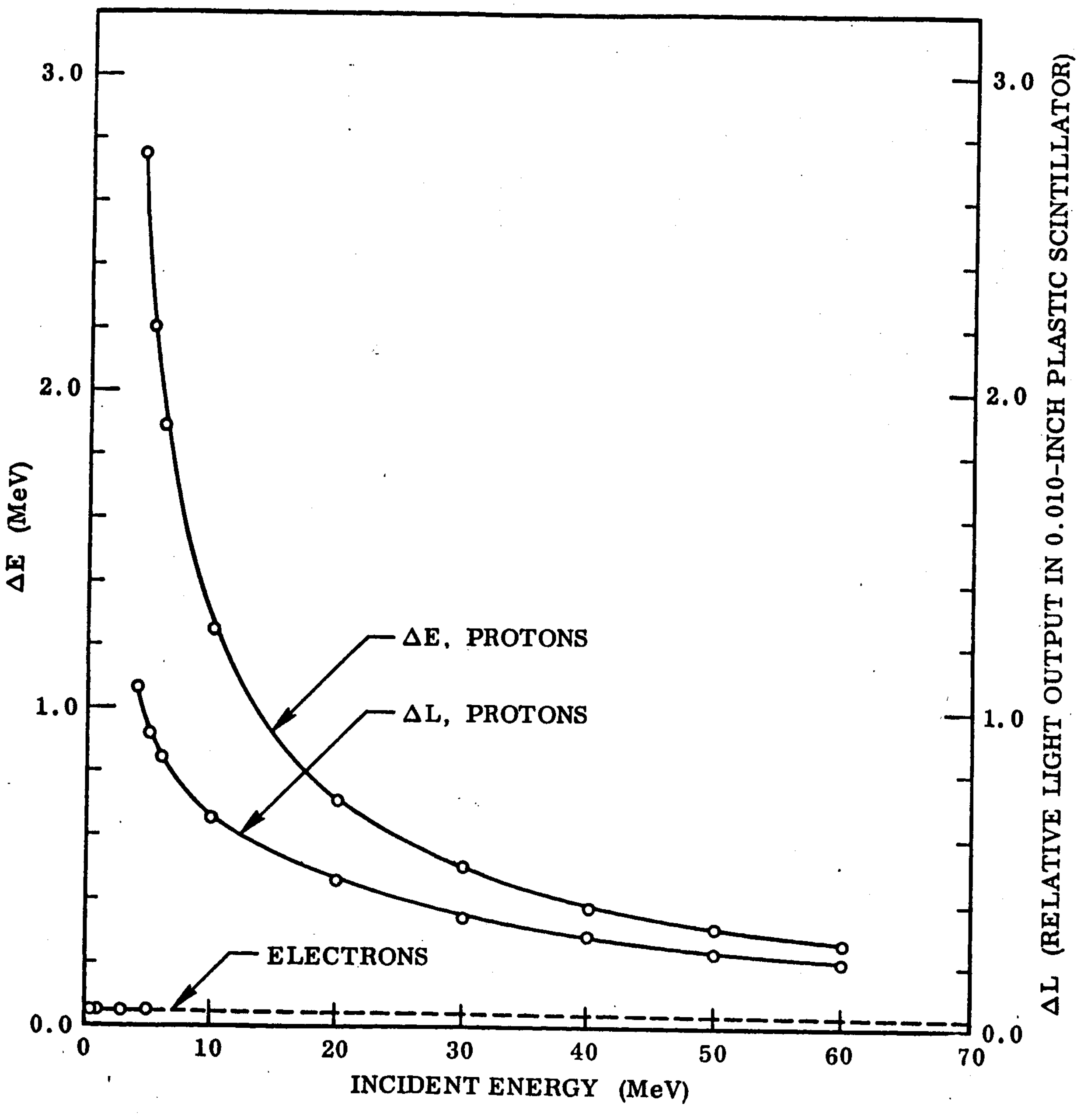

FIGURE 5. Energy Loss and Relative Light Output of Protons and Electrons in a 0.025-cm Plastic Scintillator.

approximately 100 keV. If these pulses were operated in coincidence with pulses in the main or "E" scintillator, only protons would be analyzed.

The above considerations are only valid in an ideal situation. Several phenomena associated with the large aperture and thinness of the "dE/dx" scintillator and with the high intensity electron background alter the situation somewhat. Because a large acceptance aperture is necessary in a high sensitivity omnidirectional detector, incident electrons at extreme angles can traverse path lengths as much as a factor of three greater than expected for normal incidence. In addition, energetic electrons in their travel through the scintillator are scattered into statistically random paths producing pulse heights many times greater than expected. This effect is illustrated in Figure 6 where a laboratory pulse-height spectrum of energetic electrons in a 0.025-cm scintillator is shown. On the basis of range-energy considerations, a 62-keV peak corresponding to the energy deposit of a minimum ionizing electron in the scintillator should be obtained. In addition to the peak, however, a long tail which extends to several times the peak energy is obtained. Because the electron flux in typical Gemini orbits is several decades more intense than the expected proton flux, a bias well out on this tail is required to avoid false coincidences on electrons. All of these effects demand that the effective bias on the dE/dx scintillator be raised. In practicality, one is not able to achieve the ideal separation shown in Figure 5 but is limited to a coincidence proton range of 5-20 MeV that is relatively free of electron contamination.

Those protons which are sufficiently energetic to traverse the "dE/dx" scintillator deposit their remaining energy in the main of "E" scintillator. The actual energy deposited in this scintillator as a function of incident energy is shown in Figure 7. The light output in the scintillator for the protons relative to the electron light output is also shown. For example, an incident 5-MeV electron deposits approximately 2 MeV in the "E" scintillator. From Figure 4, this energy deposit in light output units is equivalent to the energy deposit of a 0.5-MeV electron. In practice, then, one

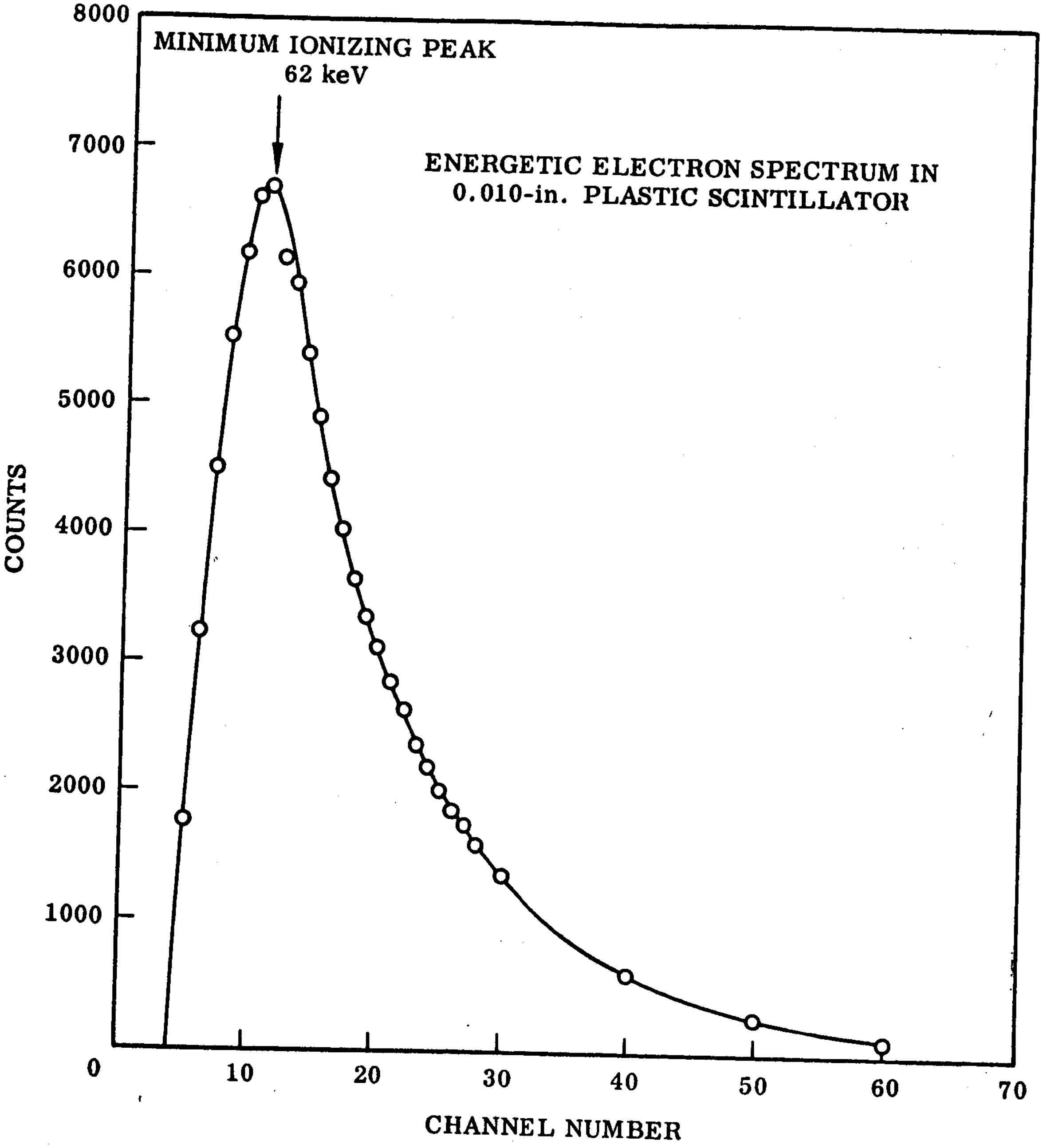

FIGURE 6. Energetic Electron Spectrum in a Thin 0.025-cm Plastic Scintillator.

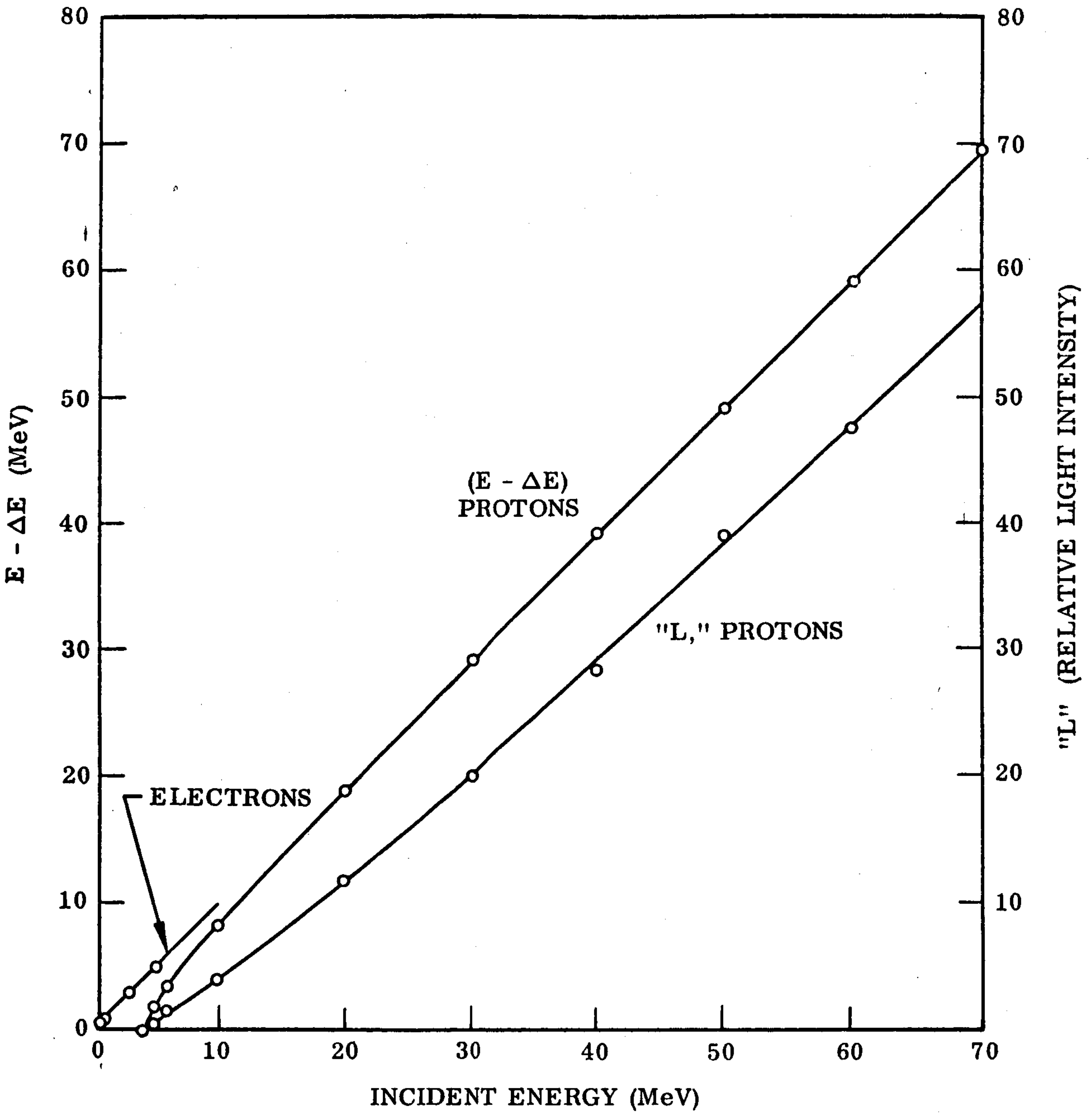

FIGURE 7. Energy Deposit and Relative Light Output of Protons and Electrons in the E-Scintillator of the Gemini-7 Spectrometer.

can analyze protons in the 5-20-MeV range in the "E" scintillator by demanding a coincidence between the "dE/dx" and "E" scintillators. If the coincidence is not demanded, all pulses in the "E" scintillator corresponding to incident protons greater than 5 MeV or electrons greater than 0.5 MeV will be analyzed. Since the intensity of electrons in most regions of the Gemini orbits are so much greater than the proton intensity, one essentially obtains an analysis of electrons above this threshold with only a very small and determinable proton contamination.

A photograph and cross-sectional view of the actual spectrometer used on the Gemini-7 flight is shown in Figures 8 and 9, respectively. The basic detector for analyzing both protons and electrons was a cylindrical plastic scintillator (Pilot-B) 5.59 cm in diameter by 2.79 cm in height. These dimensions correspond to a normal incidence energy deposit of 5.0 MeV for electrons, 60 MeV for protons, and 5.7 MeV for minimum ionizing protons. The spectrometer aperture was 2.29 cm in diameter compared to 2.54 cm diameter of the Gemini-4 spectrometer. The "dE/dx" scintillator which was 0.025 cm thick by 2.29 cm in diameter was mounted adjacent to the "E" scintillator in a lucite light pipe which coupled the light output to an Amperex XP-1011-02 photomultiplier. The shielding which surrounded the entire detector assembly was identical to that employed in the Gemini-4 spectrometer. Therefore, both scintillators were subjected only to those electrons which entered through the opening aperture. Energetic protons greater than approximately 60 MeV could also penetrate the shielding and be detected in the "E" scintillator in the electron mode of operation. Over most spatial regions, however, this background flux within the electron energy rnage of interest will be small because of the much higher flux of electrons within the acceptance aperture. The details of this penetrating background can be measured in flight as the flux and spectrum obtained when the detector is oriented along magnetic field lines where the electron flux within the acceptance angle vanishes. This flux and spectrum as a function of the magnetic shell parameter, L, can then be subtracted from the flux and spectrum obtained at other orientations.

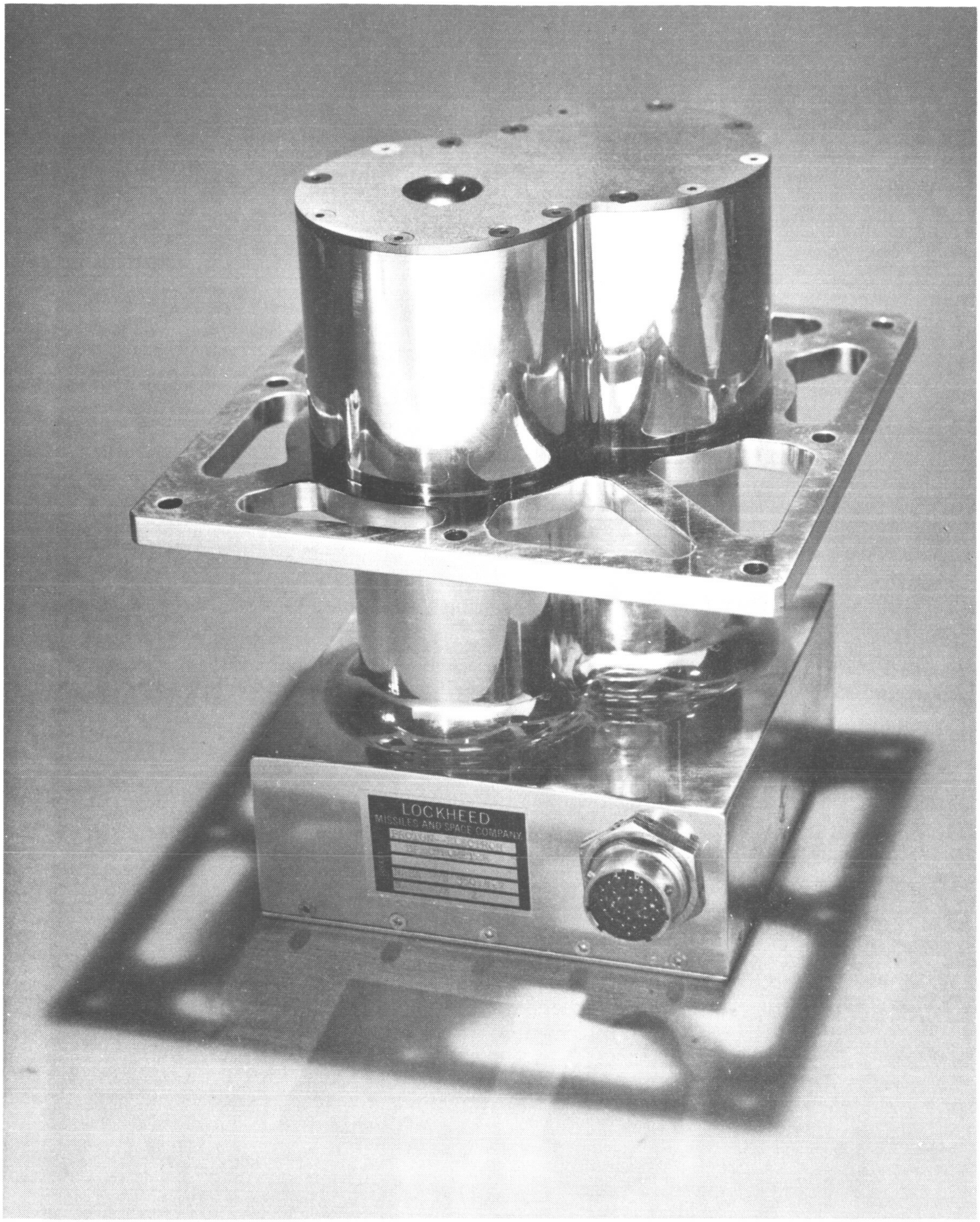

FIGURE 8. Photograph of Gemini-7 Proton-Electron Spectrometer.

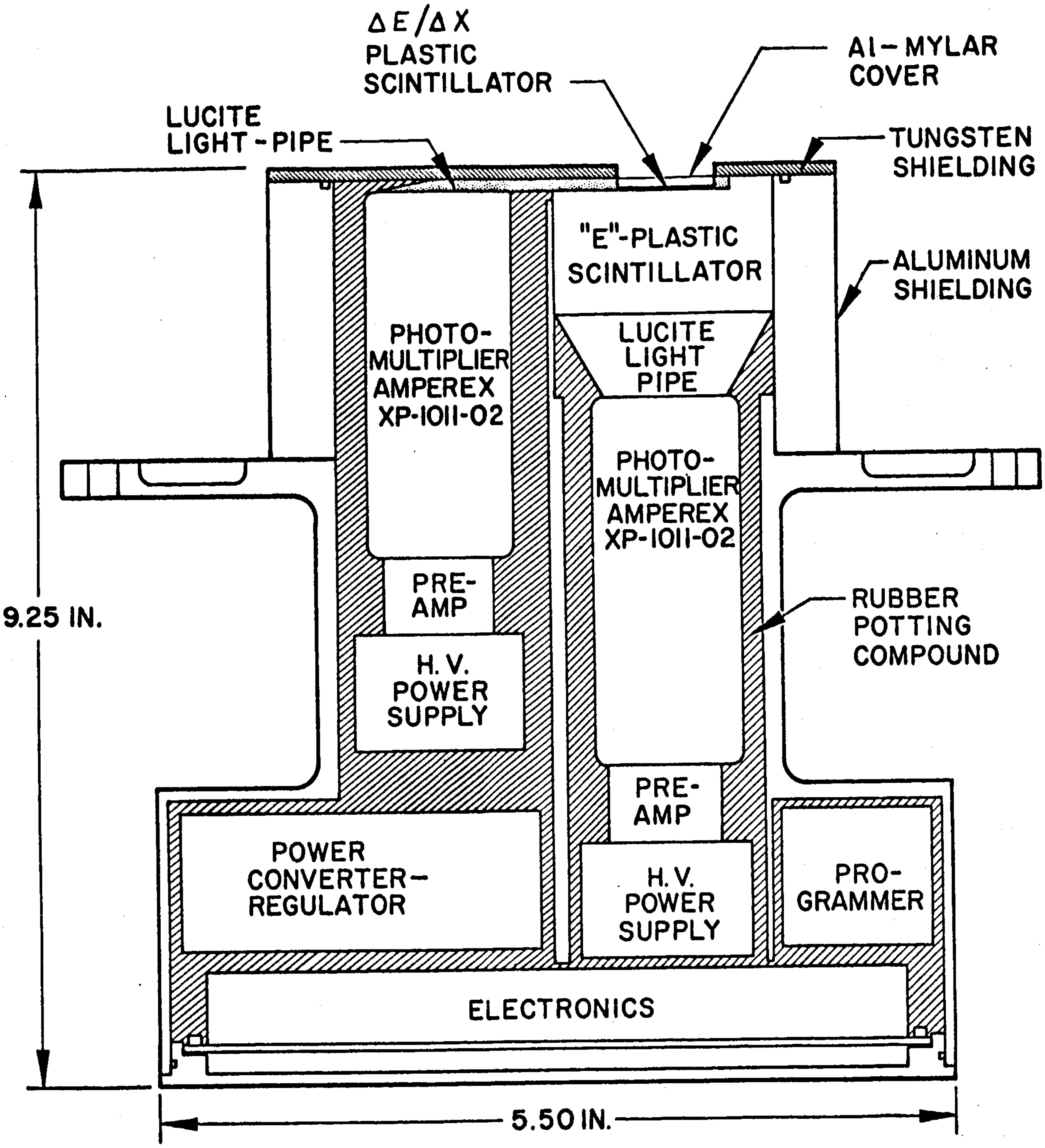

GT-7 PROTON-ELECTRON SPECTROMETER

FIGURE 9. Cross-Section Diagram of Gemini-7 Proton-Electron Spectrometer.

A block diagram of the data-handling system used to perform the measurement is shown in Figure 10. The light from the "E" and "dE/dx" scintillators was coupled to two ruggedized photomultiplier tubes, type XP-1011-02. Each of the tubes was equipped with a high-voltage power supply and preamplifier similar to those described for the Gemini-4 spectrometer. Since the spectrometer was to operate in two modes, an internal programmer was utilized to control and identify the time multiplexing of the modes. In the proton mode, a coincidence gate between the "E" and "dE/dx" signals was enabled for 18 seconds. Pulses which exceeded an integral energy level in either of the scintillators generated 50-nanosecond pulse inputs. If pulses from both the "E" and "dE/dx" scintillators were simultaneous in time within the 80-nanosecond resolution of the coincidence circuit, a gate width of 400 nanoseconds was created. This gate allowed the signal from the "E" scintillator to pass through for further analysis. In the electron mode, the programmer provided a continuous signal to one input of the coincidence circuit such that any signal from the "E" scintillator which exceeded the discrimination level would create a coincidence and open the signal gate.

The signals passing through this gate were analyzed for pulse height by a 16-channel pulse-height analyzer identical to that used in the Gemini-4 experiment. Because the sampling of these data by the telemetry was performed at only 20 samples per second, alternate methods of obtaining the absolute counting rates were utilized. To obtain the absolute coincidence rate, two linear ratemeters covering the range from 0 to 2000 counts/sec were used. In the proton mode, this range was adequate to cover the expected proton flux. In the electron mode these ratemeters functioned essentially as "singles" counters since a coincidence was not demanded. To extend the electron range to approximately 3×10^5 counts/sec a logarithmic ratemeter was used which continuously monitored the output of the "E" discriminator. A logarithmic ratemeter also continuously monitored the output of the "dE/dx" discriminator. All four ratemeters had an output voltage range of 0-5 Vdc and were sampled 1.25 times per second.

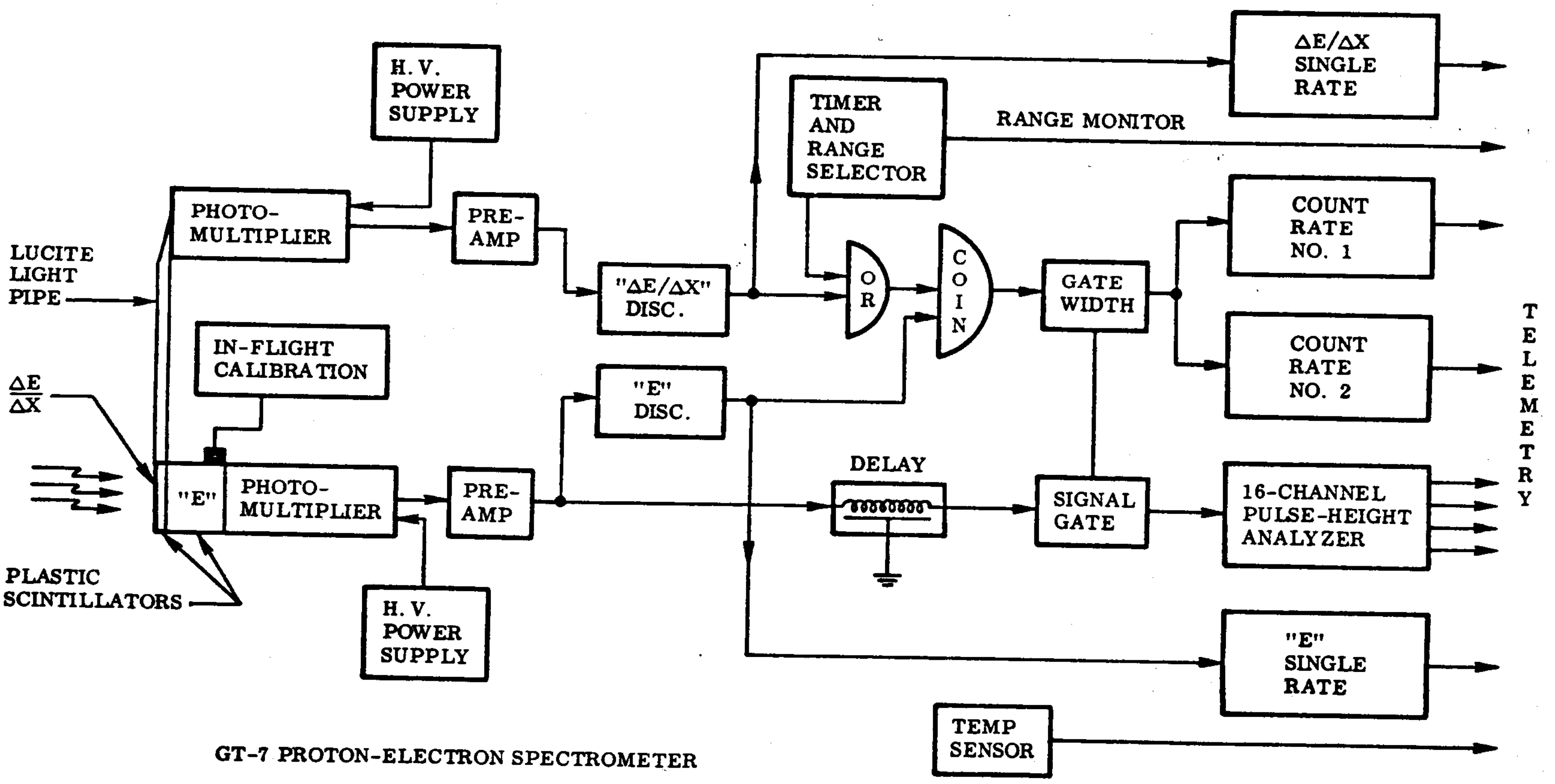

FIGURE 10. Block Diagram of Data Analysis and Handling System for the Gemini-7 Proton-Electron Spectrometer.

The Gemini-7 spectrometer contained a programmable in-flight calibration system which will be described in the next section. A temperature sensor was also included to allow corrections to be made to the data for the effects of temperature. An internal dc-dc converter provided regulated power for the instrument and isolation from the vehicle power system.

Section 3

CALIBRATION PROCEDURE

3.1 Laboratory Calibration

The spectrometers were calibrated in the laboratory to determine their response to protons and electrons over the energy and intensity range of interest. To accomplish this, a variety of calibration devices including electronic pulse generators, radioactive sources, beta-ray spectrometers, and particles obtained from reactions produced with the Lockheed 3.5-MeV Van de Graaff accelerator were used. A description of each of these techniques follows.

3.1.1 Electronic Calibration

To establish such criteria as the linearity and ranges of the pulse-height analyzers and the counting-rate ranges of the ratemeters used in the spectrometers, electronic calibration techniques were used.

Pulse generators having outputs simulating the pulses obtained from the scintillation detectors were used to measure the linearity and range of the pulse-height analyzers. An example of this is shown in Figure 11 where the amplitude of such a pulse generator is plotted against channel number of the Gemini-7 pulse-height analyzer in both the proton and electron modes. This procedure was used to match the analyzer conversion gain to the desired energy range. The gain of the scintillation detector was then adjusted to provide the proper output channel for a given energy input.

A similar technique was utilized to calibrate the ratemeters in the system. This is illustrated in Figure 12 where the output of the ratemeters used in the Gemini-4 spectrometer is plotted against the input from a variable frequency pulse generator. The ratemeter response was adjusted with this technique to provide the desired overall range and overlap between ranges. In all cases, these electronic calibrations

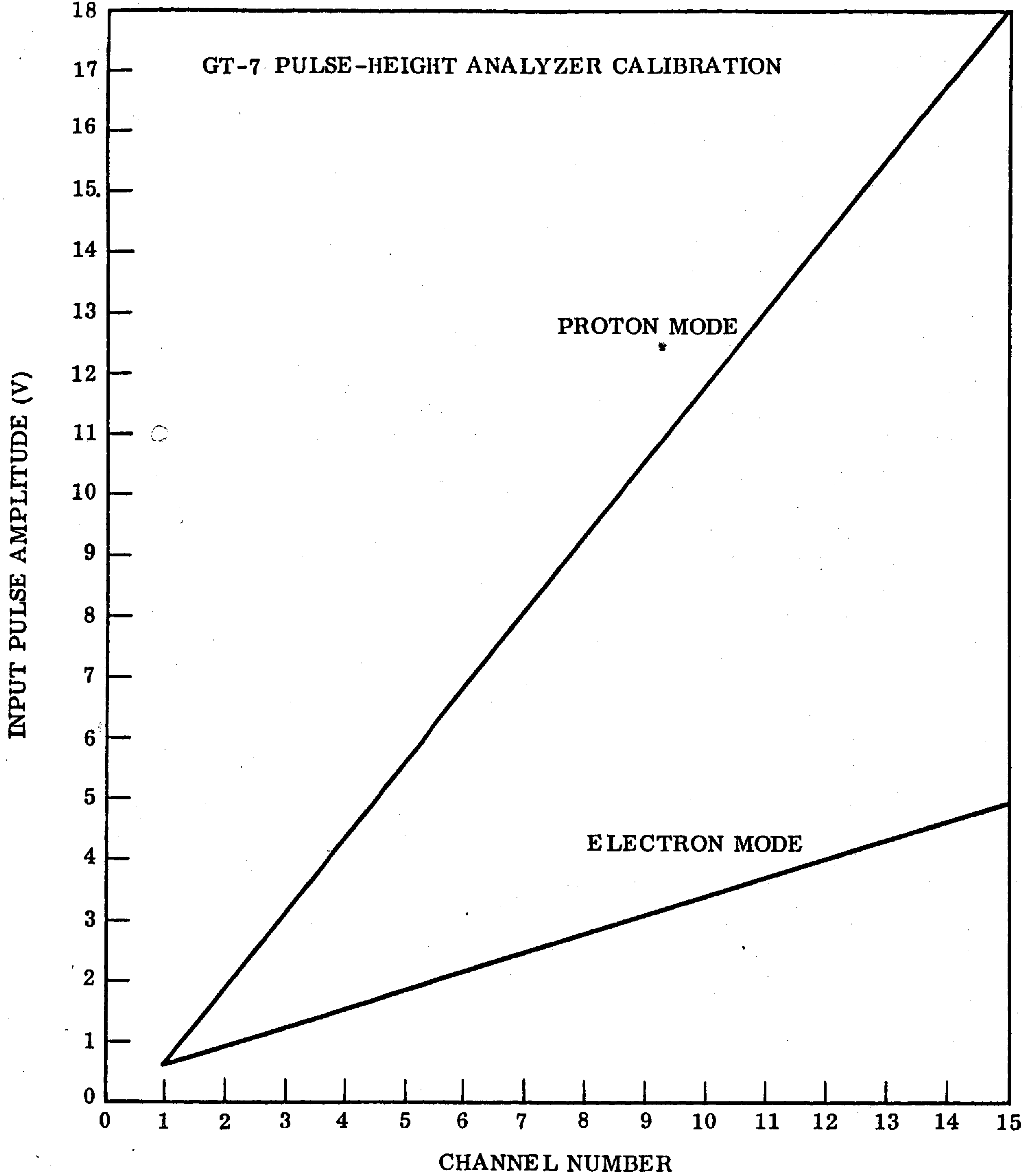

FIGURE 11. Pulse-Height Analyzer Calibration of Gemini-7 Spectrometer With Electronic Pulse Generator.

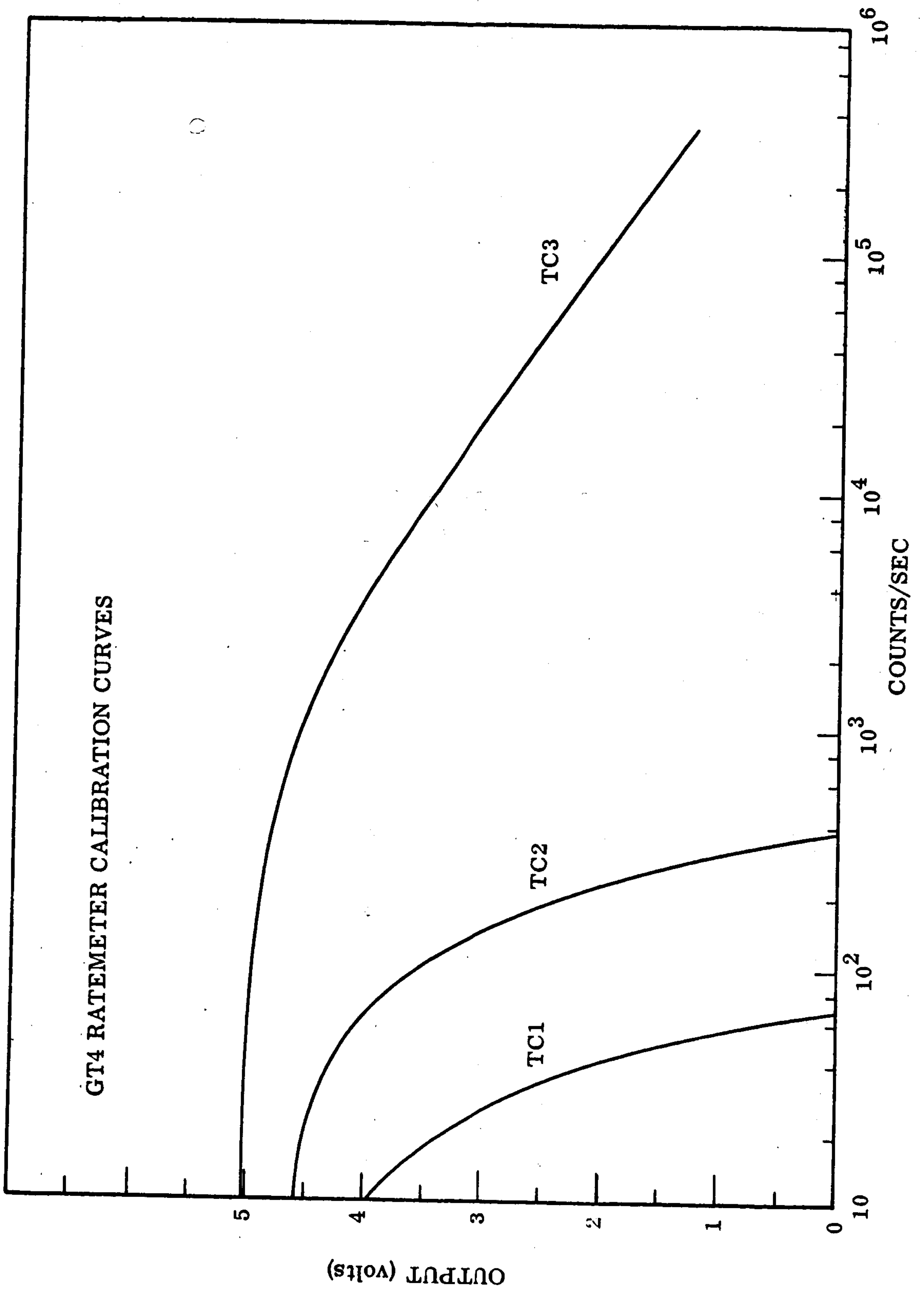

FIGURE 12. Gemini-4 Ratemeter Calibrations With Electronic Pulse Generator.

were substantiated by using one or more of the additional calibration schemes to be described.

3.1.2 Calibration With Radioactive Sources

Once the desired electronic dynamic ranges were established with the previous techniques, radioactive sources were used to set the gain of the scintillation detectors. An example of this is shown in Figure 13 where the spectra obtained for several different radioactive sources with the Gemini-7 spectrometer in the electron mode are shown. The β-ray end points of such electron sources as Sr^{90}-Y^{90} and the Compton electron edge produced by such gamma sources as Na^{22} and Th-C were used as accurate energy calibration points since photopeaks are not available in plastic scintillator. Also shown is the spectral shape of the gallium-phosphide light diode used as an in-flight calibration source. A series of Sr^{90}-Y^{90} sources having electron rates up to 10^6 electrons/sec were used in addition to establish the effects of high rates on the spectrometer.

To determine the resolution of the spectrometers and the effects of scattering in the electron mode and to substantiate the calibration performed with the radioactive sources, an additional electron calibration was performed with a 180-degree beta-ray spectrometer employing Sr^{90}-Y^{90} as a source of electrons. Monoenergetic electrons up to 2.27 MeV in energy could be selected with this technique. Figure 14 illustrates the spectrum obtained from the "E" scintillation detector in the Gemini-7 spectrometer for a monoenergetic 2-MeV electron input. The spectrum also illustrates the small backscattering effect that existed in this detector. Much more detailed investigation of the resolution and backscattering effects as a function of incident electron energy and orientation is required for a complete interpretation of the flight data. This work could be performed with the available backup instruments for each flight.

3.1.3 Accelerator Calibrations

To establish the response of the spectrometers to protons and higher

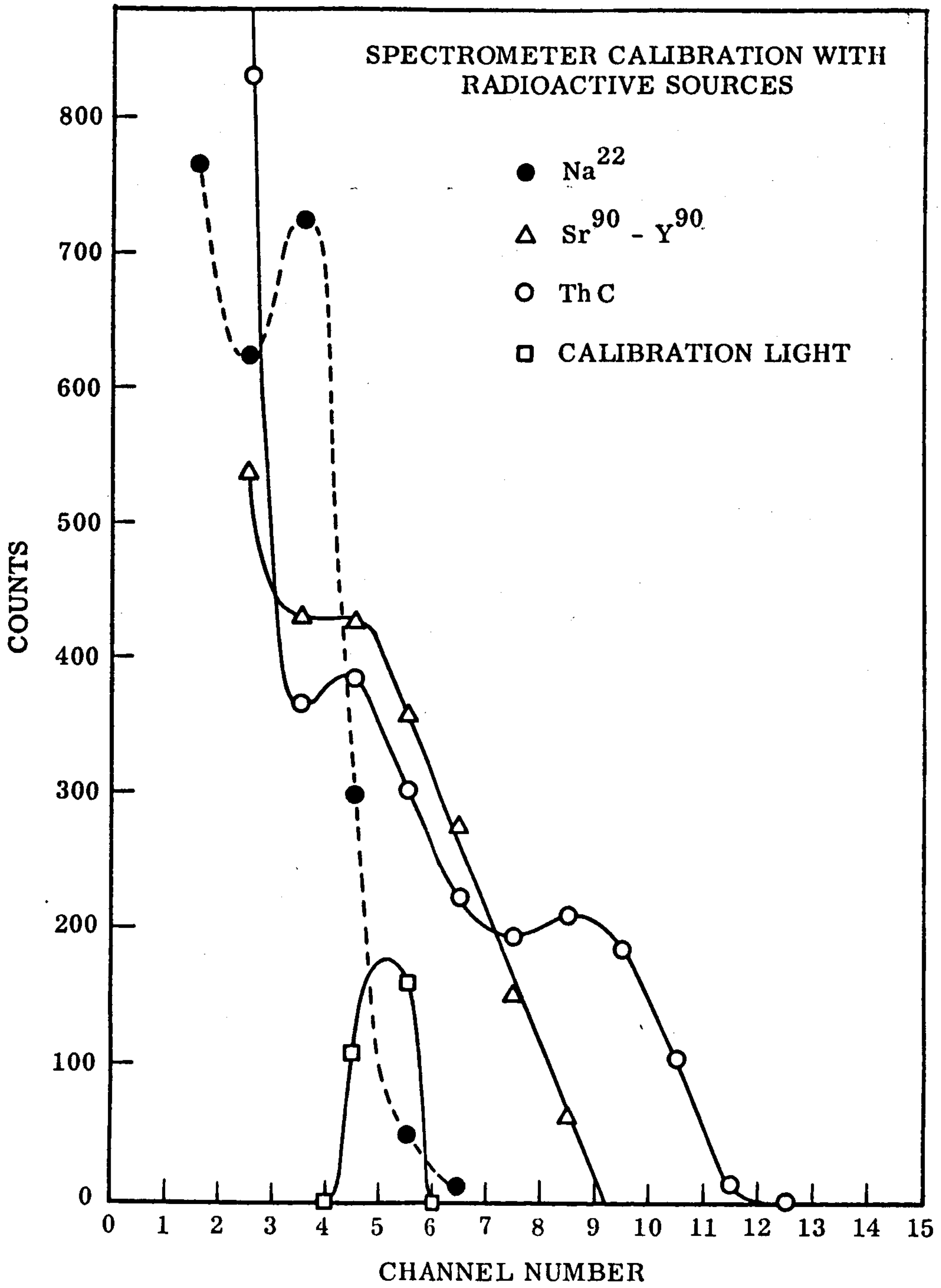

FIGURE 13. Response of the Gemini-7 Spectrometer in the Electron Mode to Several Radioactive Sources and to a Gallium-Phosphide In-Flight Calibration Light Source.

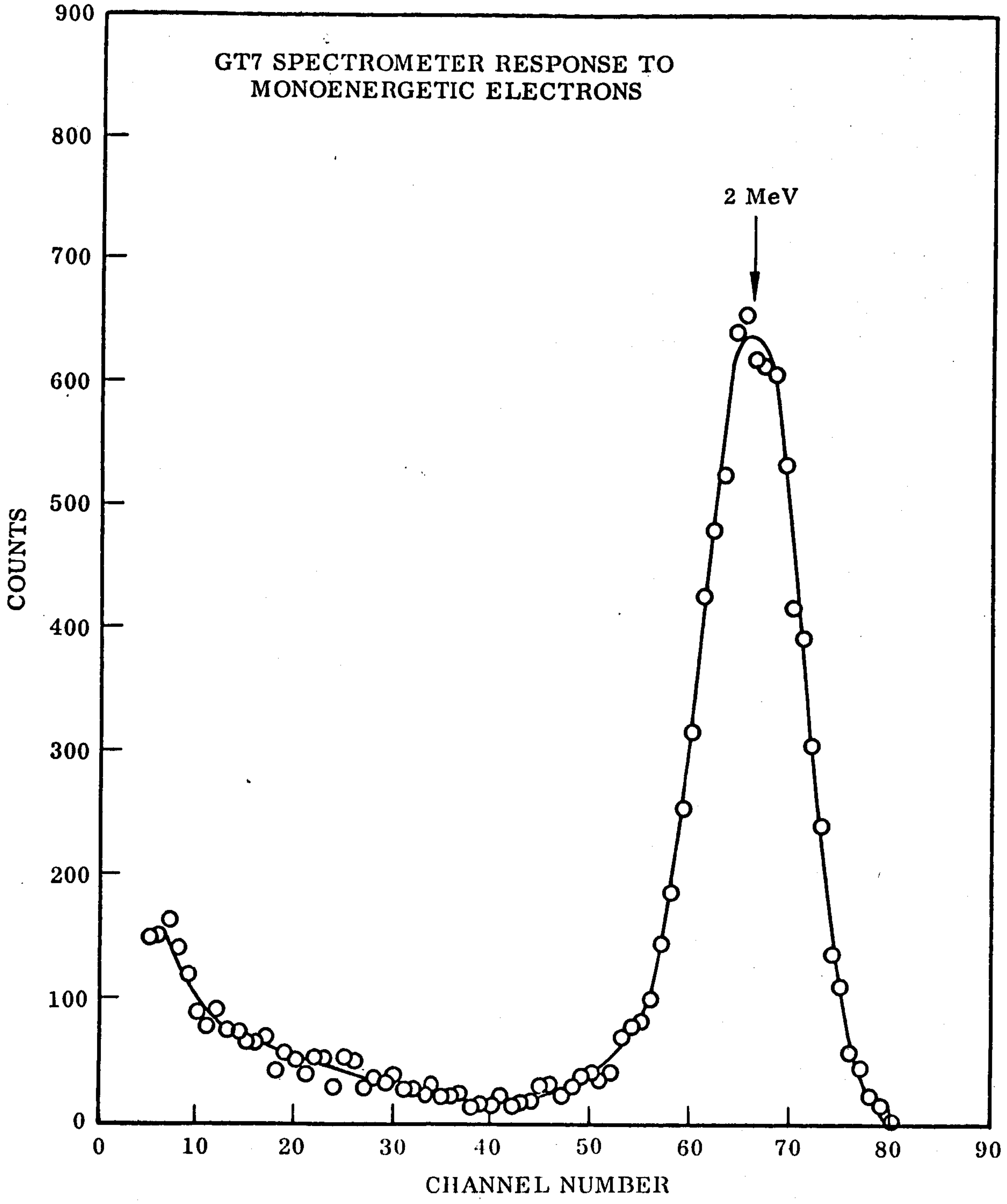

FIGURE 14. Response of the Gemini-7 Spectrometer to Monoenergetic 2-MeV Electrons.

energy electrons, the Lockheed 3.5-MeV Van de Graaff accelerator was used. Electrons with energies up to 13 MeV were obtained from the decay of Li^8 ($T_{\frac{1}{2}}$ = 0.8 sec) through the reaction $Li^7(d,p)Li^8$. The Van de Graaff beam was swept in a cyclic manner such that the Li^7 target was bombarded with deuterons for a 1-second period and after a 1-second delay the electrons from the Li^8 were counted for 1 second. A fission-like spectrum simulating that expected in flight was created by degrading the Li^8 electrons with appropriate absorbers. Figure 15 shows the response of the Gemini-4 spectrometer at L = 1.30, B = 0.220. To determine the effect of bremsstrahlung produced by these fission-type electrons, the entrance aperture was shielded and the detector was rotated 90 degrees to the incident beam. The resultant spectrum for the same bombarding period is also shown. The background spectrum obtained from the Gemini-4 spectrometer at the same B,L region in space as previous but for a detector orientation which was 90 degrees to the incident electrons is also shown. It can be seen that although the laboratory fission spectrum is somewhat harder than experienced in flight, the shape and intensity of the flight background spectrum is in reasonable agreement with the bremsstrahlung spectrum obtained in the laboratory. This small background can then be subtracted from the measured values to obtain the true electron spectrum and flux. This is another area where additional calibration as a function of incident energy and orientation is required before a detailed bremsstrahlung flux and spectrum can be established. This work can be performed with the available backup spectrometers from both flights.

Protons in the energy region of 12-20 MeV were obtained by bombarding a B^{10} target with 1.5-MeV He^3 particles from the Van de Graaff through the reaction $B^{10}(He^3,p)C^{12}$. The resultant spectrum obtained with the Gemini-4 spectrometer is shown in Figure 16. The 12.1-MeV, 14.5-MeV, and 19.2-MeV proton peaks corresponding to the second excited state, first excited state, and ground state of C^{12} are easily recognized. This spectrum was then gated with the output of the integral discriminator in the flight spectrometer to determine the proton energy threshold. This knowledge combined with the electronic calibration shown in Figure 11 and

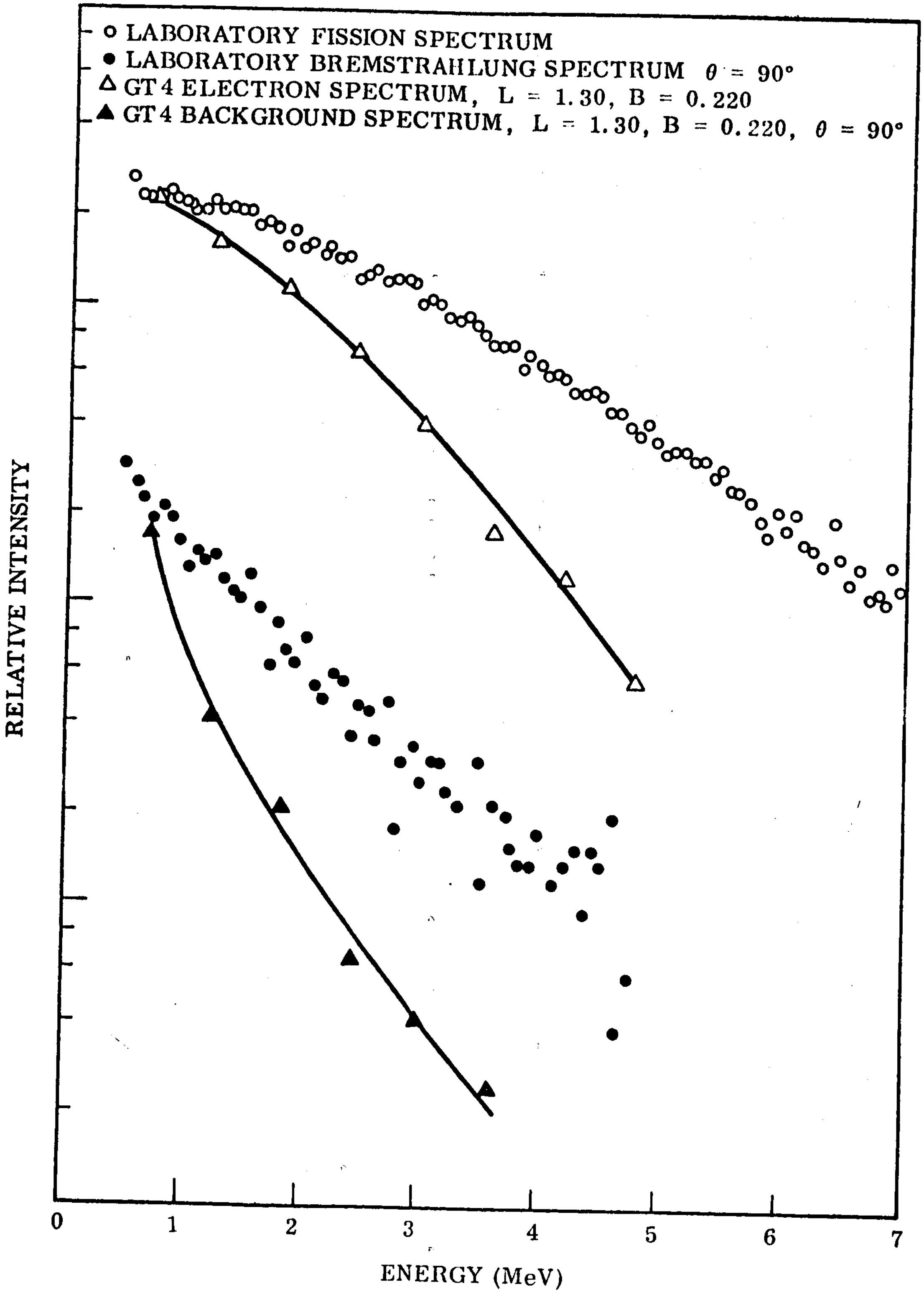

FIGURE 15. Comparison of the Electron and Bremsstrahlung Response of the Gemini-4 Spectrometer to a Laboratory Fission Spectrum and to Actual Flight Data Obtained at L = 1.30, B = 0.220.

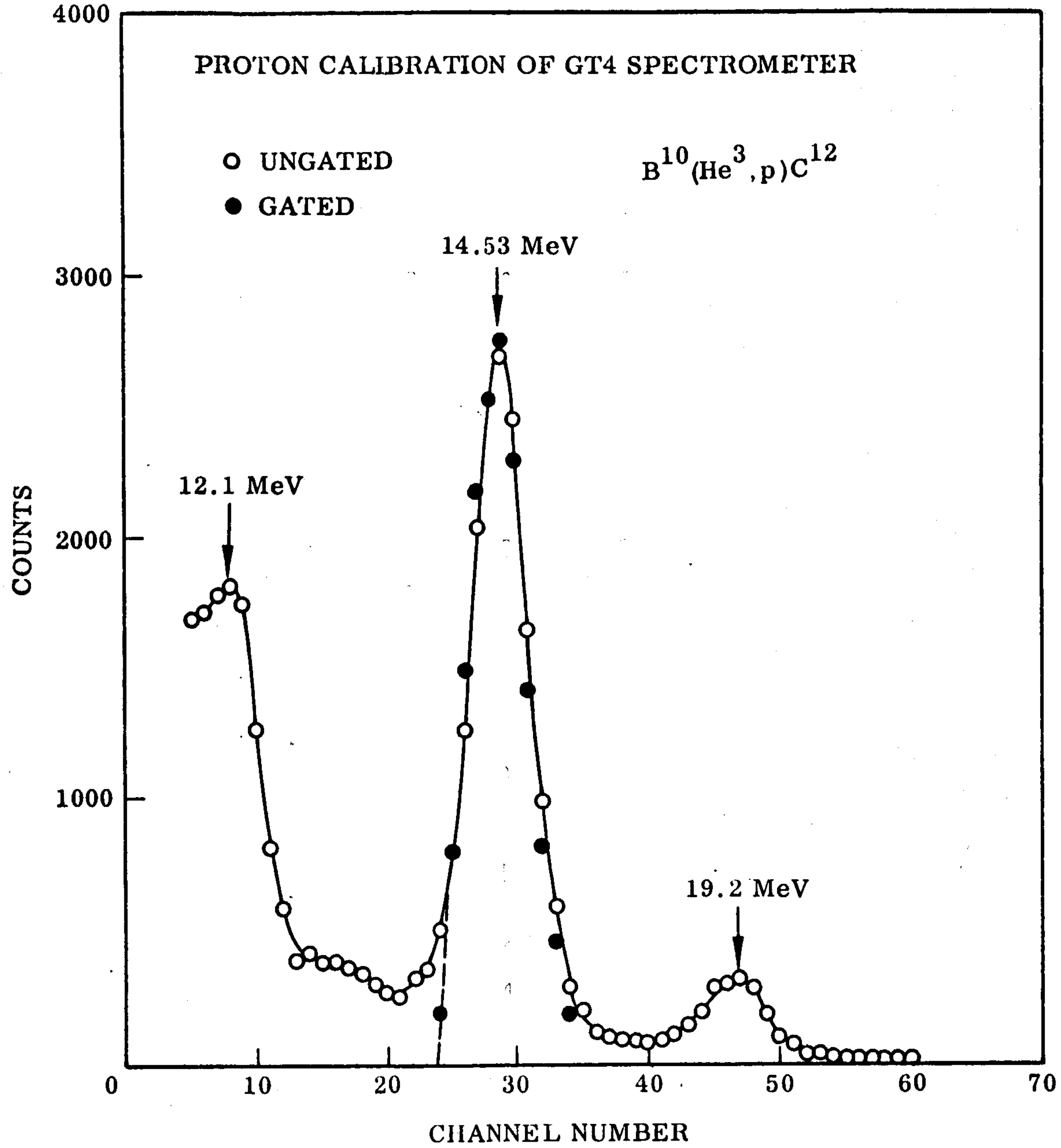

FIGURE 16. Response of the Gemini-4 Spectrometer to Protons From the Reaction $B^{10}(He^3,p)C^{12}$.

and the known non-linear response of protons in plastic scintillator [Evans and Bellamy, 1959; Gooding and Pugh, 1960] was sufficient to establish the response of the spectrometer to higher energy protons.

3.2 Field and In-Flight Calibration of the Spectrometers

To provide a monitor of the spectrometer calibration throughout the several months of field testing which preceded a launch, a combination of radioactive sources and a calibrated light source were used. In the case of the Gemini-4 spectrometer, the radioactive sources shown in Figure 13 were used for ground calibrations. In addition, the flux and spectrum obtained from the small amount of Thorium metal present in the adapter section of the spacecraft was used both as a ground and an in-flight calibration. Fortunately, this Thorium background was not intense enough to seriously degrade the experiment and, by compiling the spectrum over regions where other particle fluxes were not present, a statistically significant flux and spectrum was available as an absolute gain monitor. Compilation of this background on an orbit-by-orbit basis showed that the Gemini-4 spectrometer exhibited no measurable gain shift throughout the flight. In addition to this Thorium calibration source, the Gemini-7 spectrometer contained a programmable calibrated light source. When power was applied to the instrument, the 18-second proton mode was initiated by the internal programmer. Following this period, the programmer enabled a calibration circuit consisting of a pulsating gallium-phosphide light-emitting diode for the normal 13-second electron mode. The light pulses from this diode simulated the scintillation pulses in the "E" detector with enough stability and resolution to be analyzed into a single channel of the pulse-height analyzer. This provided an excellent monitor of small gain shifts in the overall "E" system. The stable 900 Hertz rate of the light pulses also provided an in-flight monitor on the calibration of the "E" ratemeter circuits. The calibration circuit incorporated a lockout feature such that after the initial 13-second period it was disabled until power was disrupted and reapplied to the instrument. Figure 17 shows both the typical Thorium and calibration light spectra that were obtained from the Gemini-7 spectrometer. During ground checkouts of the spectrometer, an electronic decoder which accepted the spacecraft PCM telemetry signals and interfaced the spectral information with a laboratory-type multichannel analyzer was used. This provided a rapid and accurate assessment of the overall system.

A preliminary evaluation of the in-flight calibration sources on the Gemini-7 flight indicate that the gain of the system did not remain constant throughout the flight. In order to perform the low-energy proton measurement, it was necessary to mount the spectrometer outside the thermal curtain and centrally located at the rear of the spacecraft, as shown in Figure 18. As a result, the thermal excursions experienced by the instrument were much more severe than during the Gemini-4 flight. Measurements of the temperature at a location in the potted electronics section of the spectrometer as a function of systems time after launch show a continuous increase to about a maximum internal temperature of +50°C. Temperatures at the scintillators and photomultipliers which quite often were in full sun exposure probably exceeded this level. The calibration sources show that the system experienced a slow increase in gain as the temperature increased. By following the calibration edge, however, appropriate gain compensation can be applied to the data. Without this calibration source, serious error would exist in the resulting data.

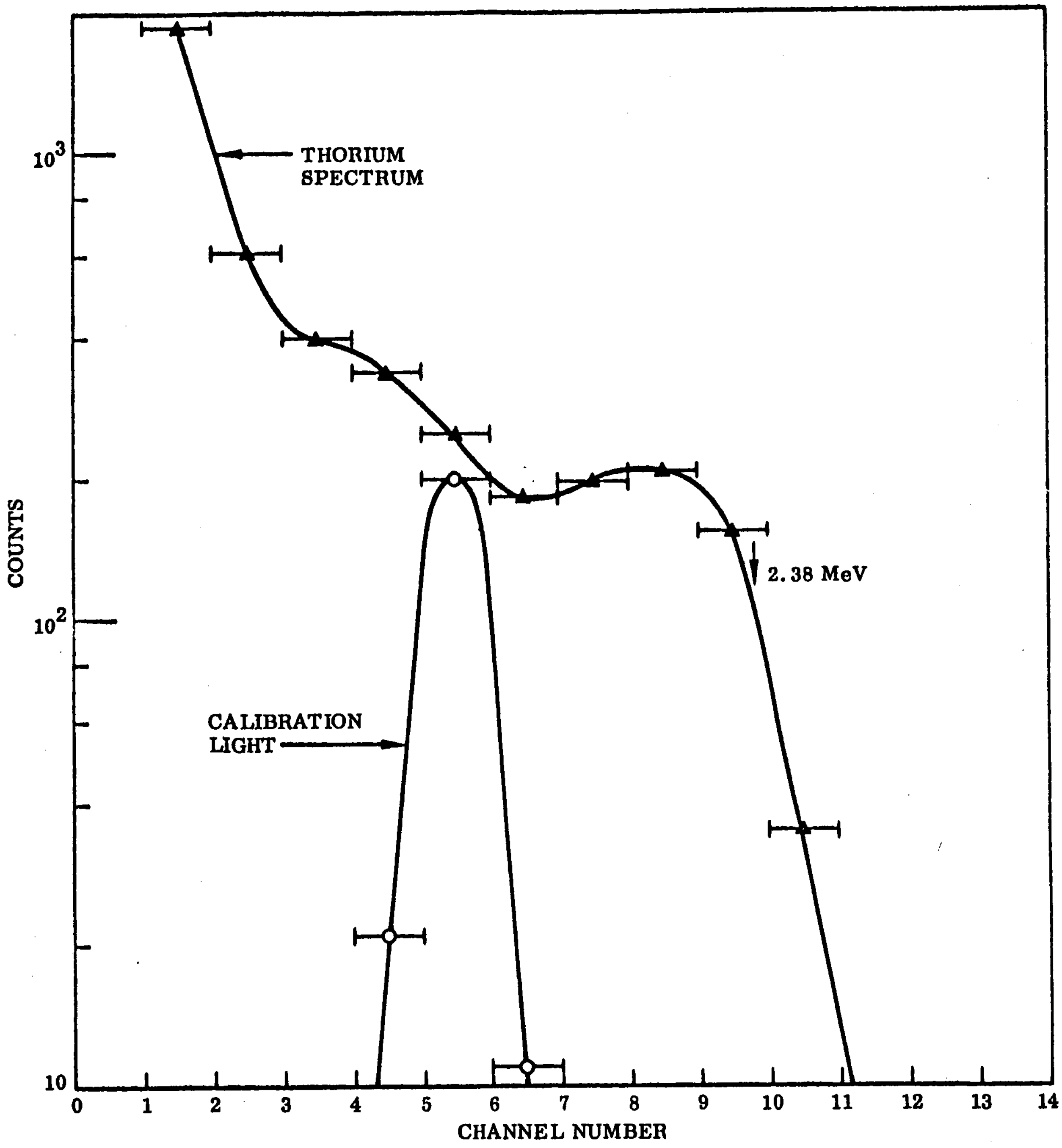

FIGURE 17. Response of the Gemini-7 Spectrometer to the In-Flight Thorium and Ga-P Light Calibration Sources.

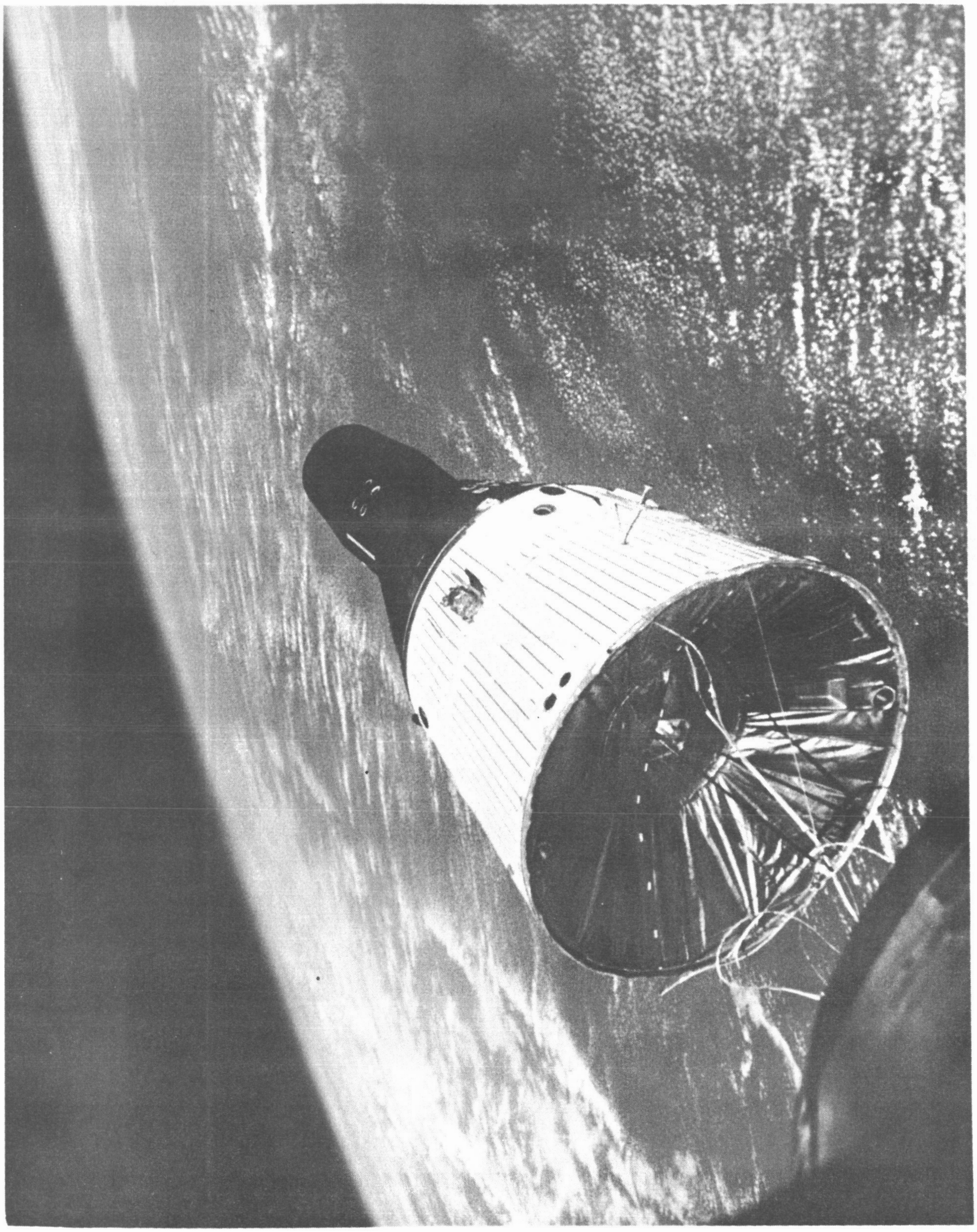

FIGURE 18. Location of the Proton-Electron Spectrometer on the Gemini-7 Spacecraft as Photographed in Flight by the Gemini-6 Spacecraft.

Section 4

DATA PROCESSING

4.1 Data Quantity and Quality

Data were obtained from the spectrometer throughout the Gemini-4 flight period of 3-7 June, 1965. Of the total of twelve orbits which were programmed for turn-on, nine orbits of good data were obtained. The remaining data were lost because of poor signal quality on the flight magnetic tapes. Data were obtained from the Gemini-7 spectrometer for the first seven-day period of the 4-18 December, 1965, flight. Twenty-four orbits of useful data have been obtained to date from this flight. Twenty-two additional orbits of data may be potentially available.

The raw data were provided by the NASA-MSC Computation and Analysis Group and presented both as tabular listings and on magnetic tape for subsequent utilization. The analog voltage outputs of the spectrometer were listed at each sampling of the telemetry; i.e., every 0.8 second. The sixteen samples of the pulse-height analyzer output obtained during this time period were decoded, sorted, and listed by channel number in the digital computer output. At the end of each energy-range period, the totalized content of each channel was printed. The data from the MSC-3 magnetometer experiment were also supplied on magnetic tape. Pertinent spacecraft ephemeris data were provided for the entire flight in thirty-second intervals. In areas of particular interest, ephemeris data were generated every five seconds and merged with the "B,L" program of McIlwain [1961] to provide the spectrometer data in terms of the earth's magnetic field strength, B, and the magnetic shell parameter, L.

4.2 Orbit Coverage in B,L Space

Because of the low-altitude, circular nature of the Gemini orbits, significant radiation fluxes were encountered only in the vicinity of the Brazilian anomaly. In this region, which is located between South America and Africa, the magnetic field of the earth departs drastically from a dipole field representation and both trapped and precipitated particles are observed at low altitudes. Figure 19 shows the regions of each orbit of Gemini-4 in geographic coordinates where significant particle fluxes above background were observed. Figure 20 shows the orbital paths for the same region in B,L space. The orbital paths in B,L space for the Gemini-7 flight are shown in Figure 21. On both flights, the region of $1.1 < L < 1.7$ and $0.213 < B < 0.260$ was reasonably well covered by the orbital trajectories through the anomaly. The magnetic equator is plotted on Figures 20 and 21 as well as the locus of B,L points corresponding to particles which in their longitudinal drift around the earth encounter a minimum altitude of 100 kilometers. Particles encountering minimum altitudes less than this value are presumably lost in a very short time due to atmospheric collisions. Therefore, one can expect to encounter particle fluxes with significant lifetimes on these flights only in the B,L region below the $h_{min} = 100$ km curve. Spacecraft altitudes in this region varied between 274 and 293 kilometers.

4.3 Telemetry Outputs

Figure 22 contains plots of the analog voltage outputs of the spectrometer for orbit 7 of the Gemini-4 flight as a function of system time. The parameters, TC1, TC2, and TC3, refer to the total-flux count-rate meter outputs in order of increasing dynamic range. Some overlap existed between these ranges so that cross-calibration with the flight data was possible. The output of the anticoincidence detector is also shown. Background condition for all four ratemeters was approximately 5.0 Vdc. Increasing flux deflected the ratemeters toward 0.0 Vdc in an approximately linear manner for parameters TC1 and TC2 and in approximately a logarithmic manner for parameters TC3 and Anti-Coinc. Figure 22 is illustrative of the data quality throughout the flight. The data are in

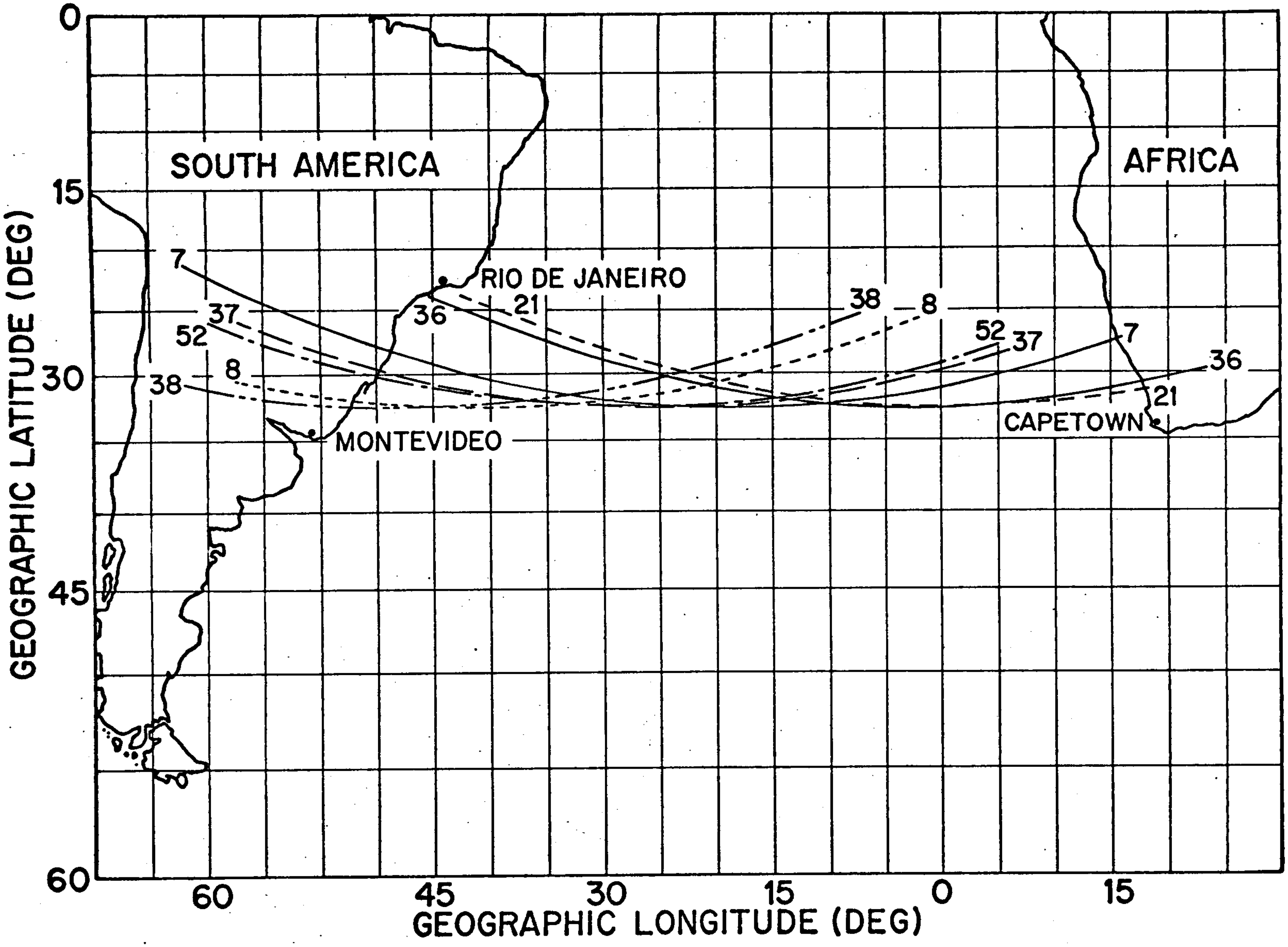

FIGURE 19. Geographic Location of Significant Particle Fluxes on Gemini-IV Flight.

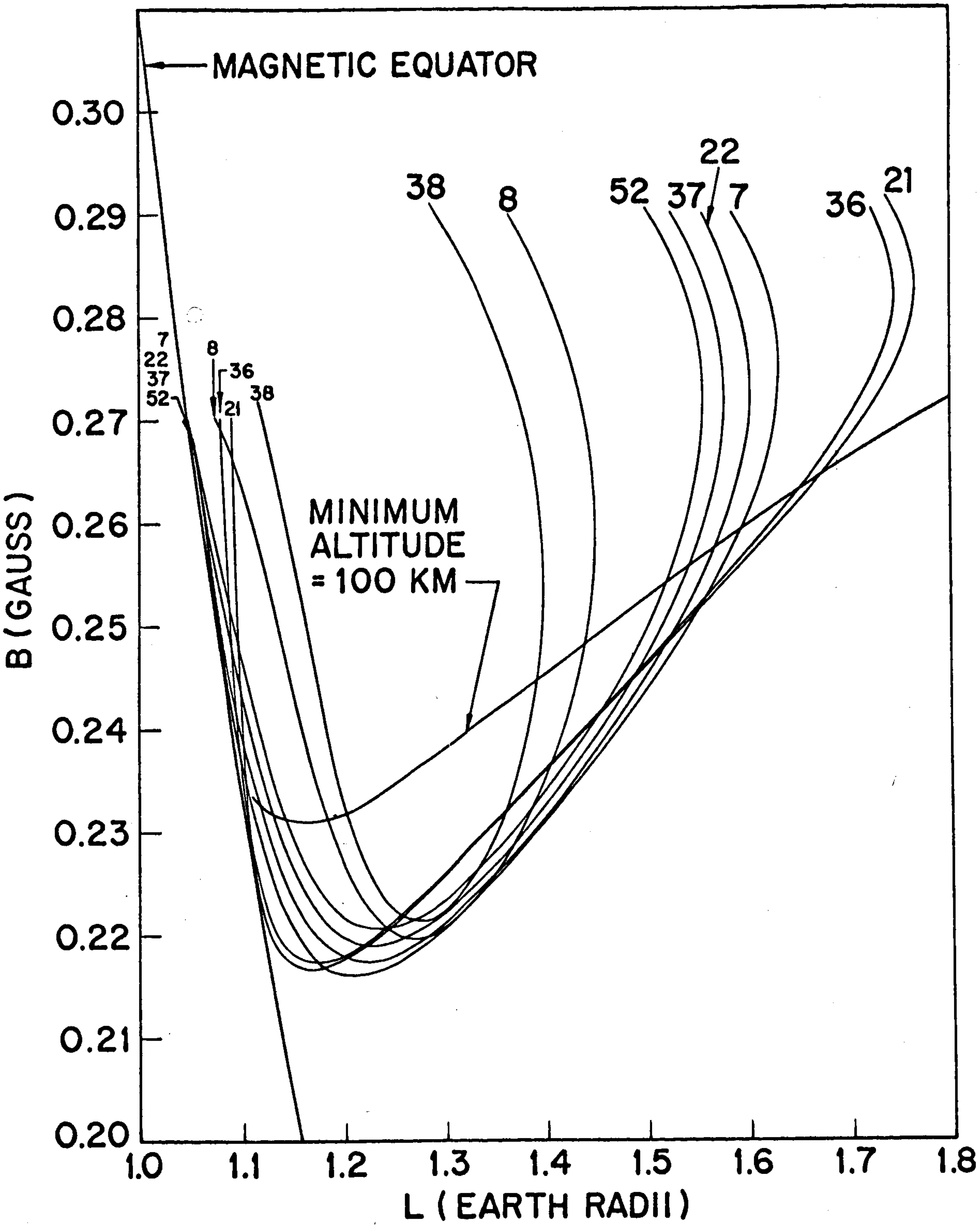

FIGURE 20. Regions of B,L Space Covered by the Gemini-4 Flight.

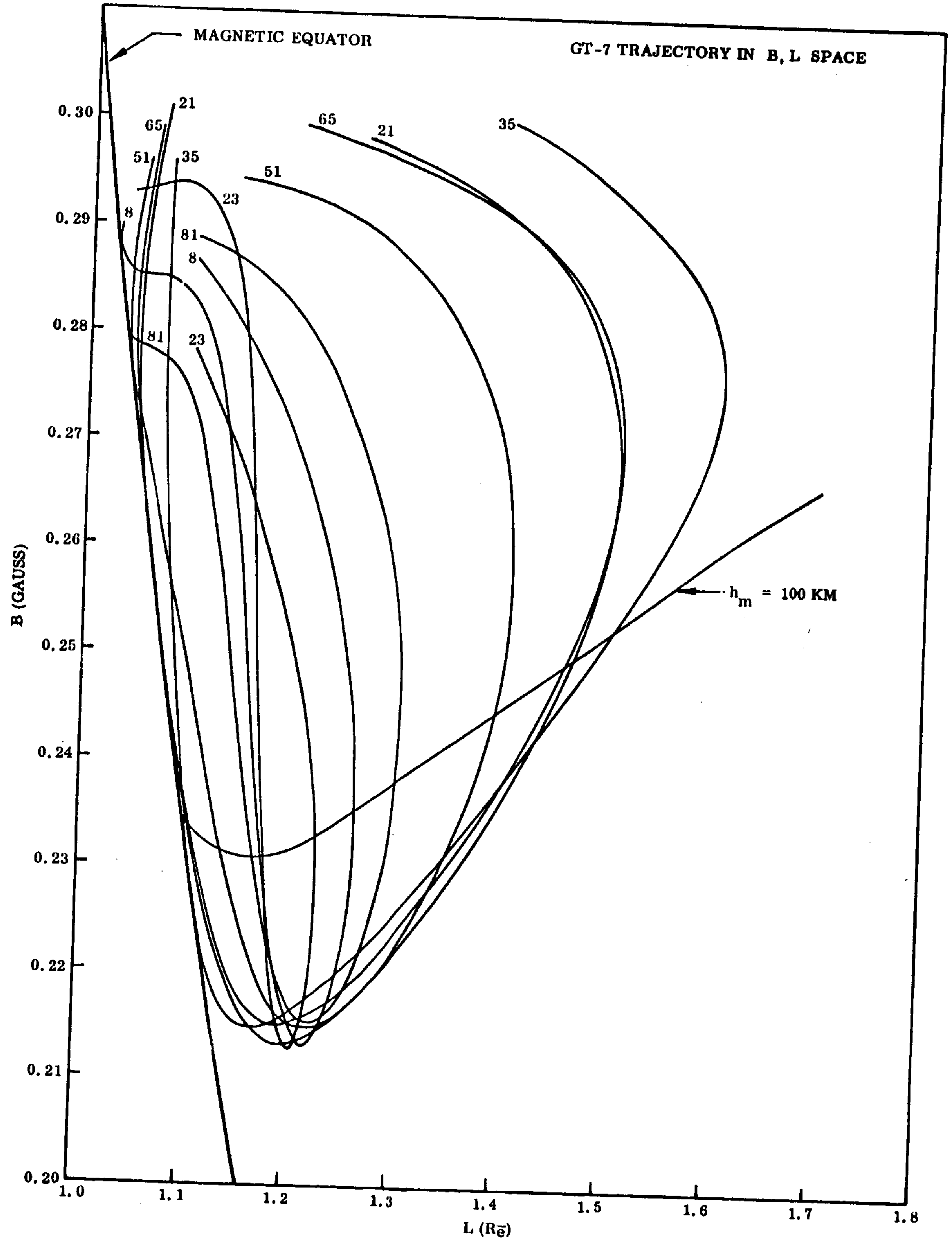

FIGURE 21. Regions of B,L Space Covered by the Gemini-7 Flight.

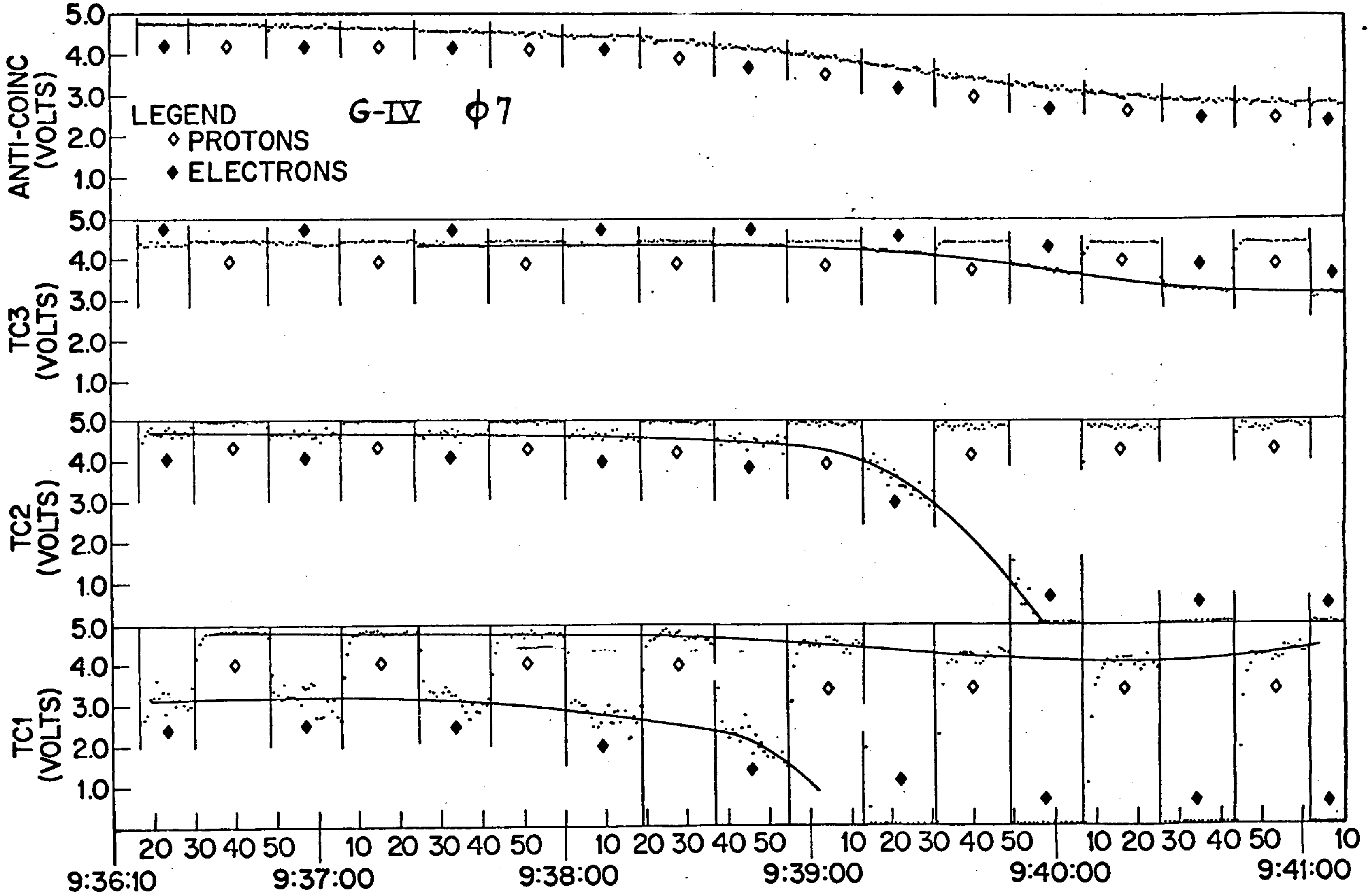

FIGURE 22. Analog Count-Rate Outputs Versus System Time for Orbit 7 of the Gemini-4 Flight Through the Anomaly Region.

general smooth and virtually free from noise and dropouts. The fluctuations observed are statistical in nature and are consistent with the observed counting rates and the ratemeter time constants. These figures also illustrate the manner in which the spectrometer alternated between the proton and electron range every 18 seconds. The counting rates indicated on TC1 and TC2 at the beginning of Figure 22 were due to the small amount of radioactive Thorium metal present in the equipment-adapter structure of this spacecraft. This radiation created a low background in the electron range of the spectrometer which reduced its capability of measuring very low electron fluxes. This background did not exist in the proton range, however.

Section 5

PRELIMINARY DATA ANALYSIS AND RESULTS

5.1 Flux Counting-Rate Contours

A preliminary analysis of both the Gemini-4 and Gemini-7 flight data has been performed under this contract. Flux counting-rate contours as a function of system time have been generated for all of the available Gemini-4 data and for five orbits of the Gemini-7 data. Best fit smooth curves were made to the ratemeter analog voltage plots for each orbit. Voltages were read every 10 seconds and converted to counting rates by using the appropriate calibration curves. Dead-time corrections resulting from the random nature of the flux and from the finite resolving times of the coincidence and anticoincidence circuits have been applied to the calibration curves. Vehicle background in the electron range of the spectrometer was also subtracted.

Figures 23, 24, 25, 26, 27, 28, 29, and 30 show the counting-rate profiles of the measured proton and electron radiation on the Gemini-4 flight. The counting rates observed in the anticoincidence detector are also shown for each orbit. Several general characteristics of the data are observable in these plots. Data obtained from the ratemeters in regions where overlapping response occurred are in good agreement, thereby substantiating the calibrations performed in the laboratory. At any given time the electron counting rate is from 300 to 2000 times greater than the proton counting rate. Thus, the proton flux within the energy range measured constitutes a maximum background to the electron measurement of only 0.3 percent. Since protons of energy below 7 MeV were shielded from the detector scintillator by the entrance window, only protons in the energy range 7-25 MeV and greater than 80 MeV could contribute any additional contamination. The data of Freden and Paulikas [1964] in the same region of space indicate that the proton flux between 5 and 20

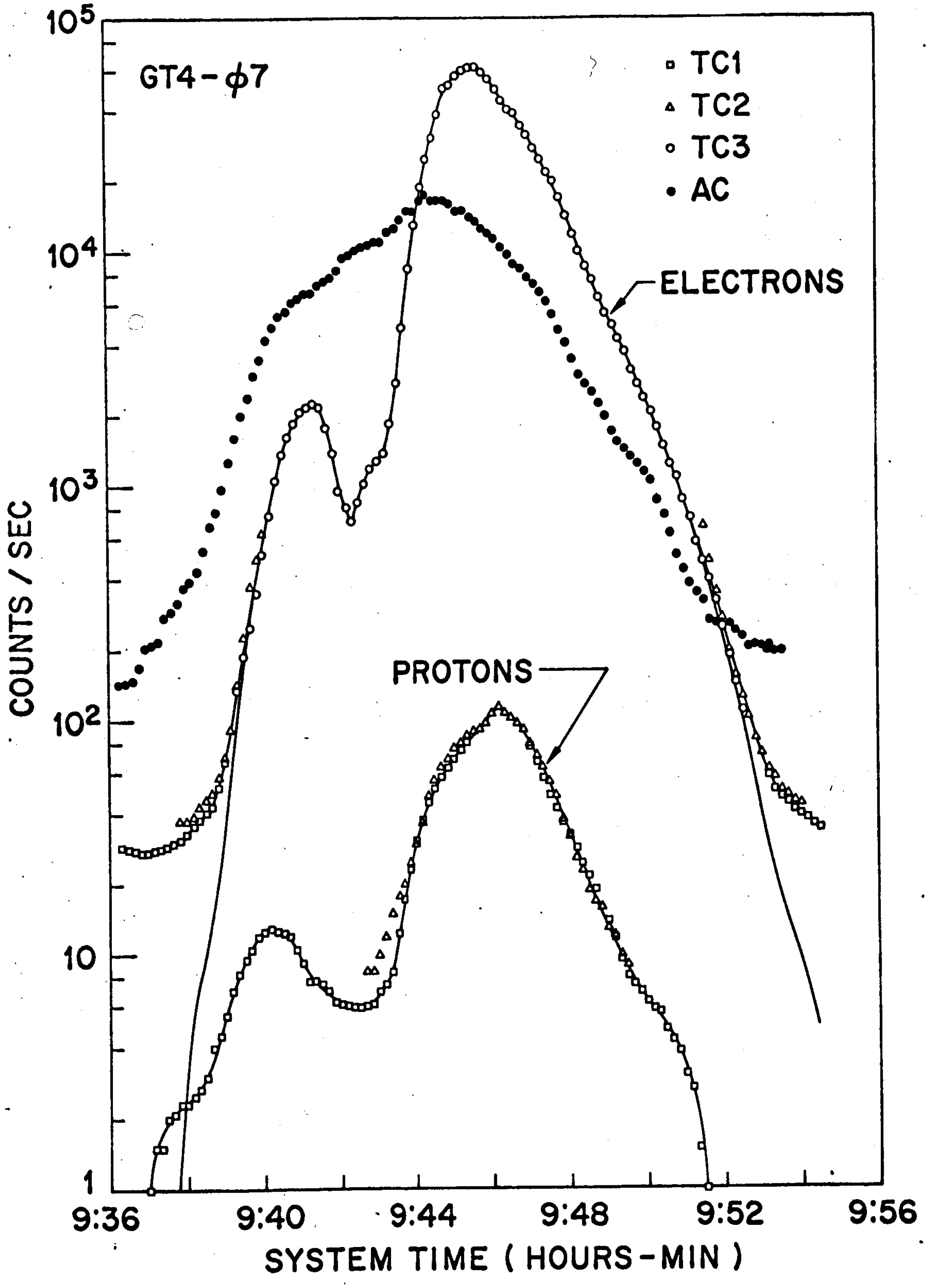

FIGURE 23. Gemini-4 Counting-Rate Profiles Versus System Time—Φ 7.

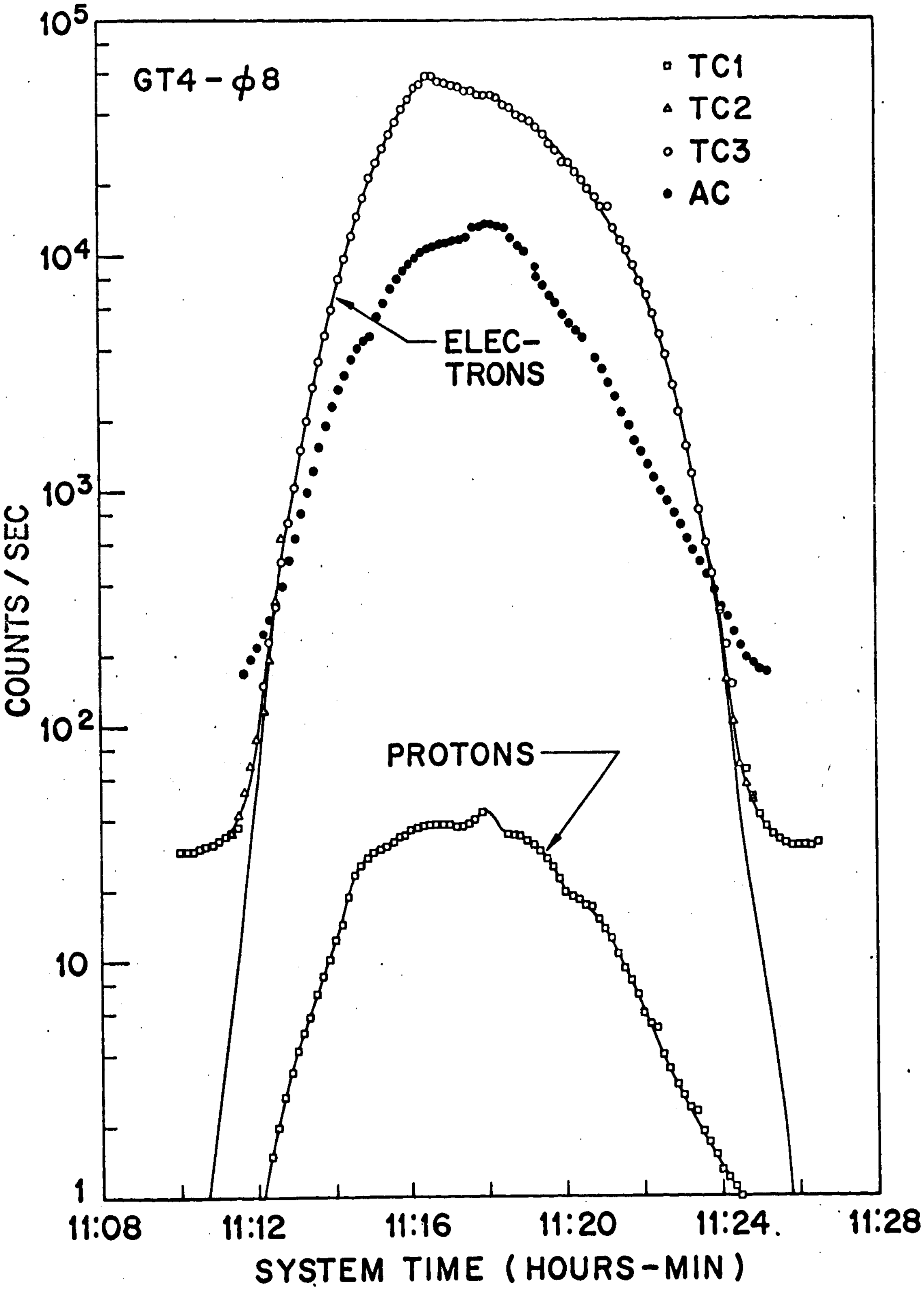

FIGURE 24. Gemini-4 Counting-Rate Profiles Versus System Time—Φ 8.

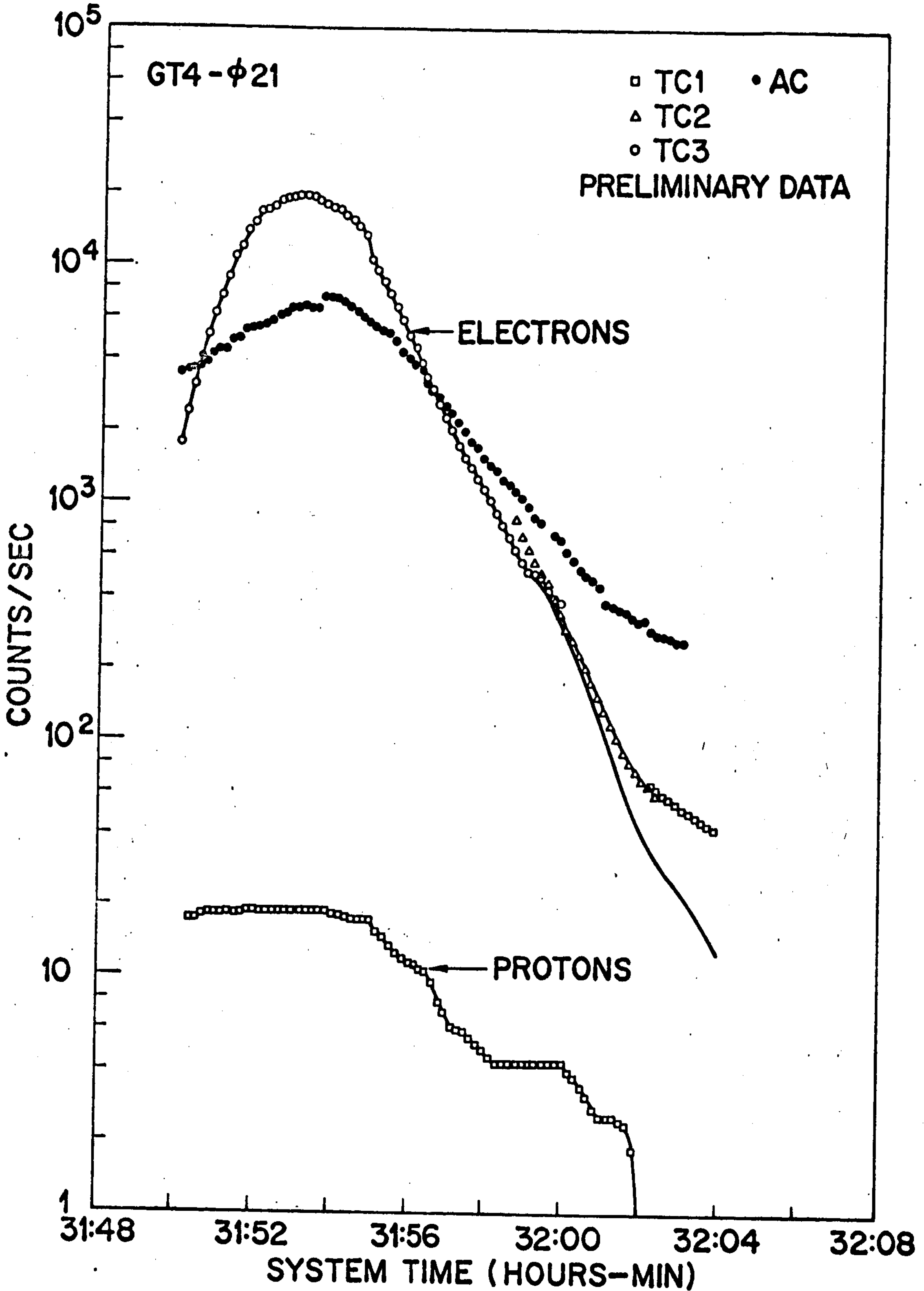

FIGURE 25. Gemini-4 Counting-Rate Profiles Versus System Time—Φ 21.

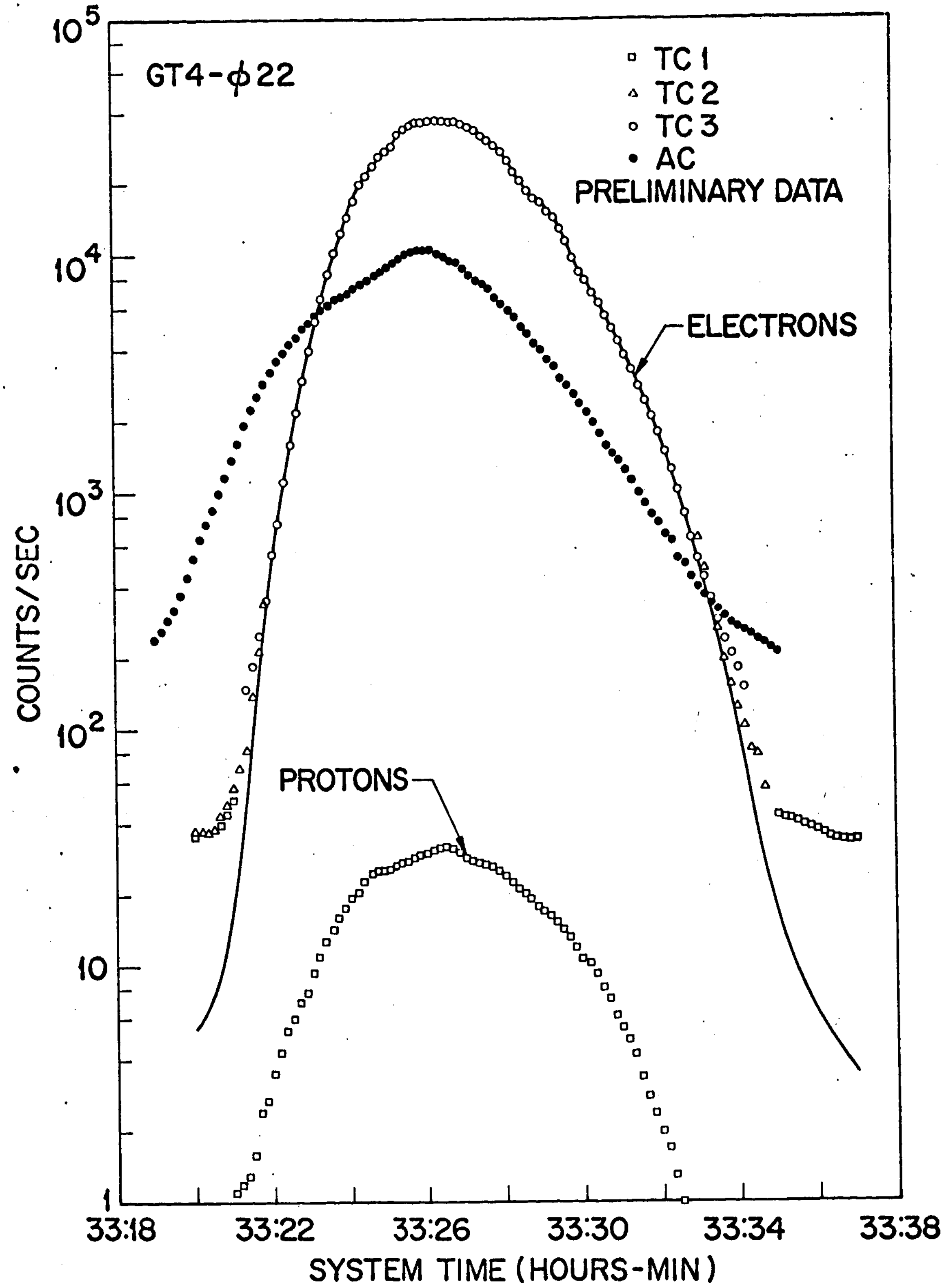

FIGURE 26. Gemini-4 Counting-Rate Profiles Versus System Time—Φ 22.

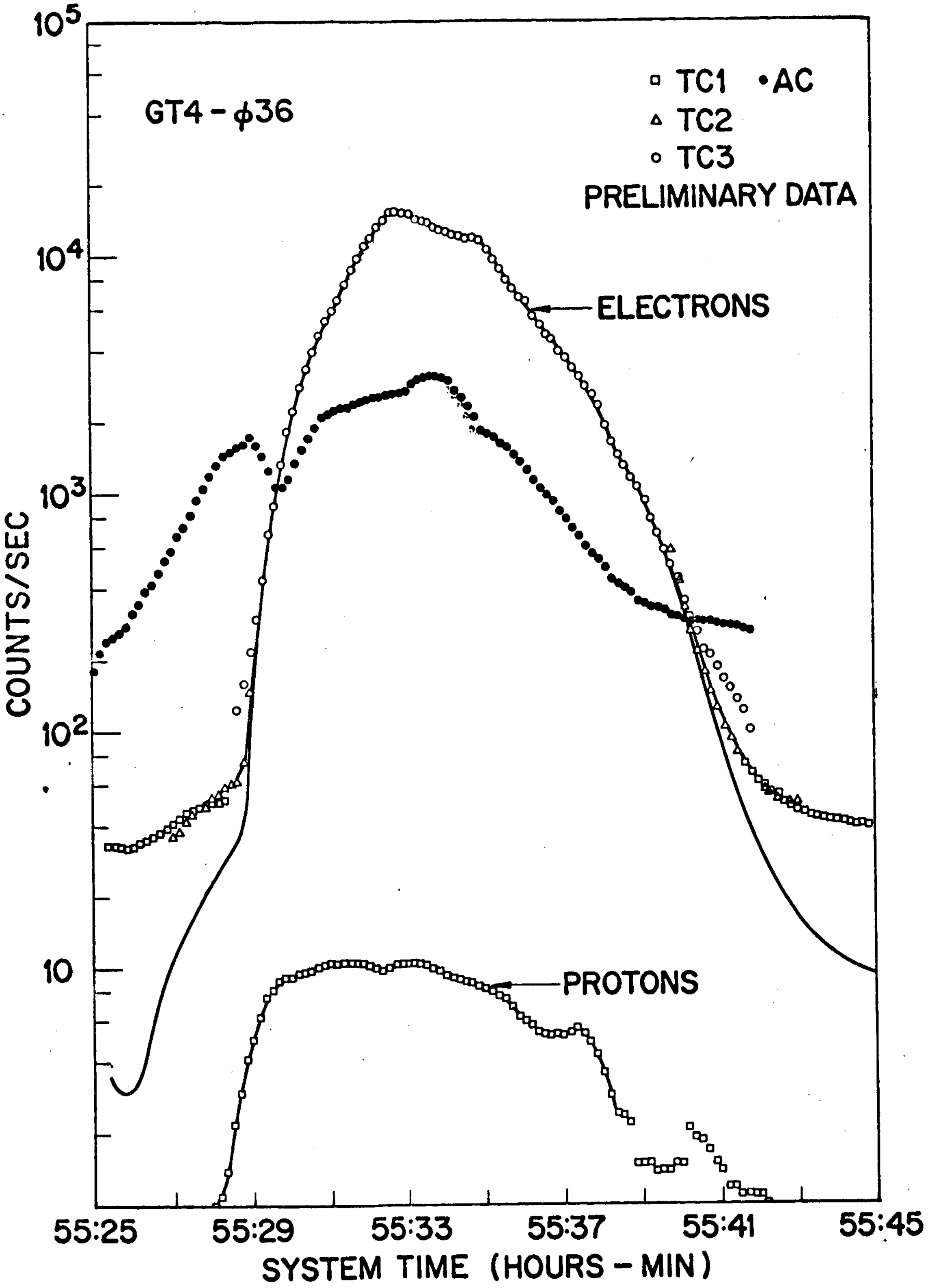

FIGURE 27. Gemini-4 Counting-Rate Profiles Versus System Time—Φ 36.

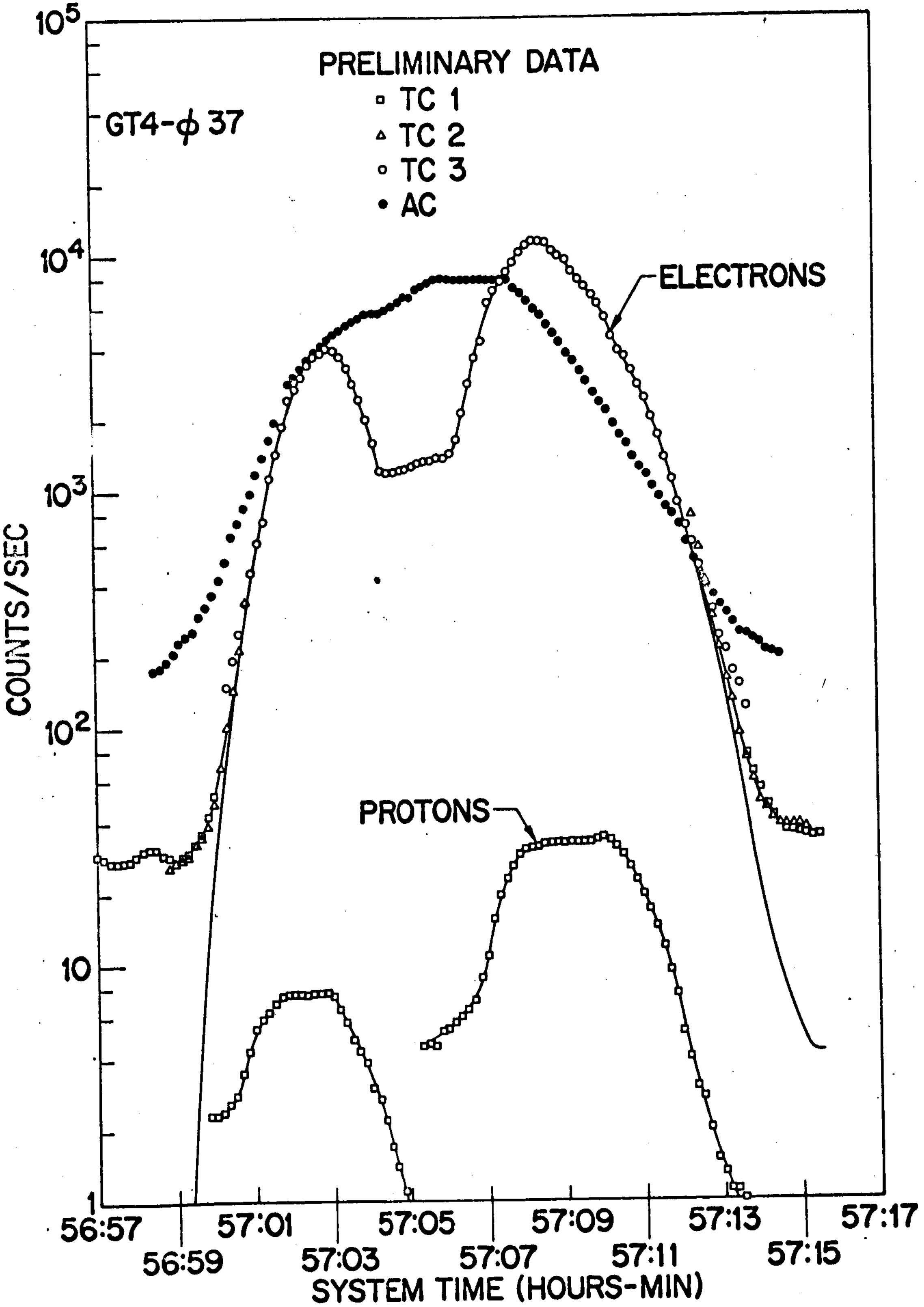

FIGURE 28. Gemini-4 Counting-Rate Profiles Versus System Time—Φ 37.

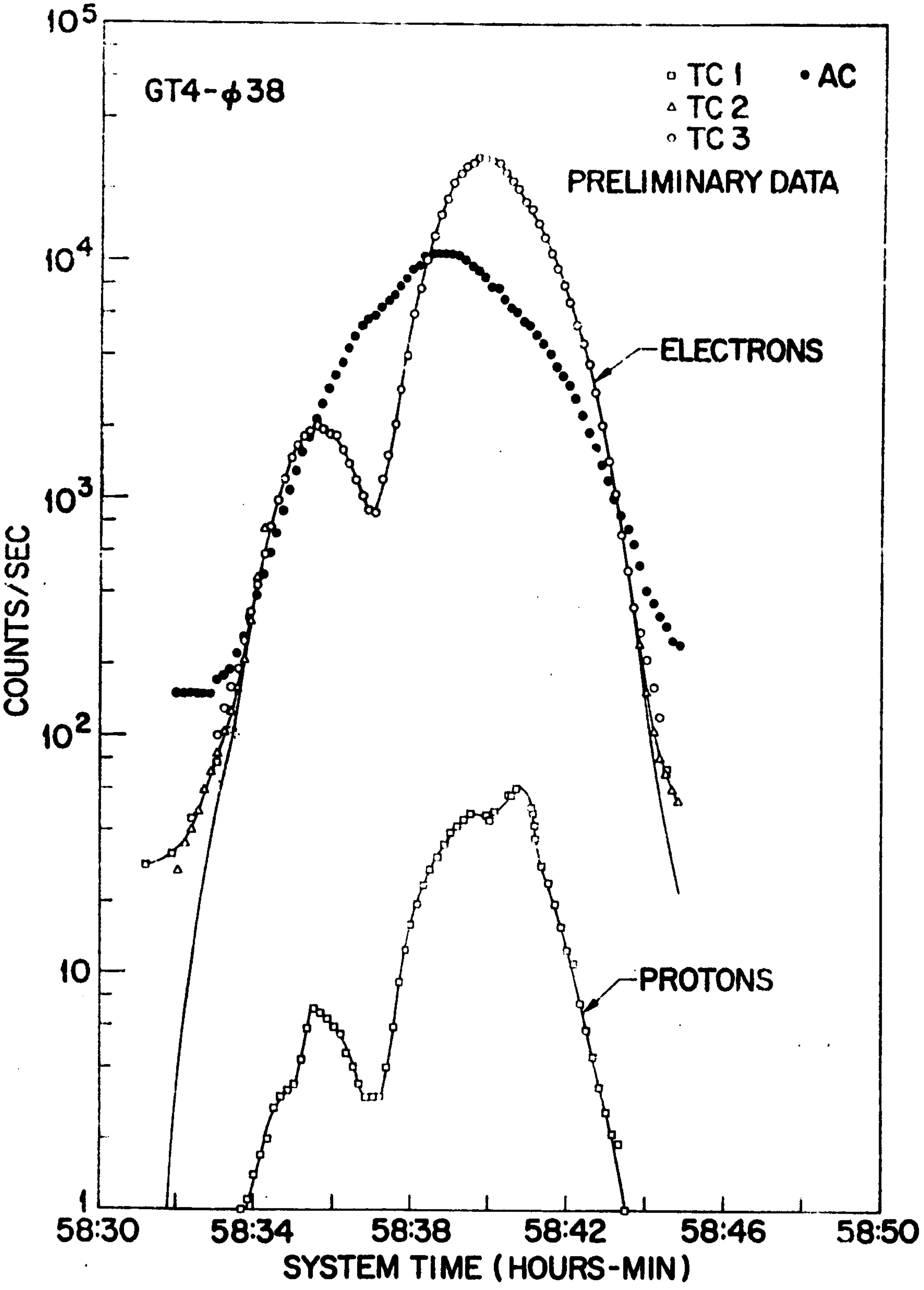

FIGURE 29. Gemini-4 Counting-Rate Profiles Versus System Time—Φ 38.

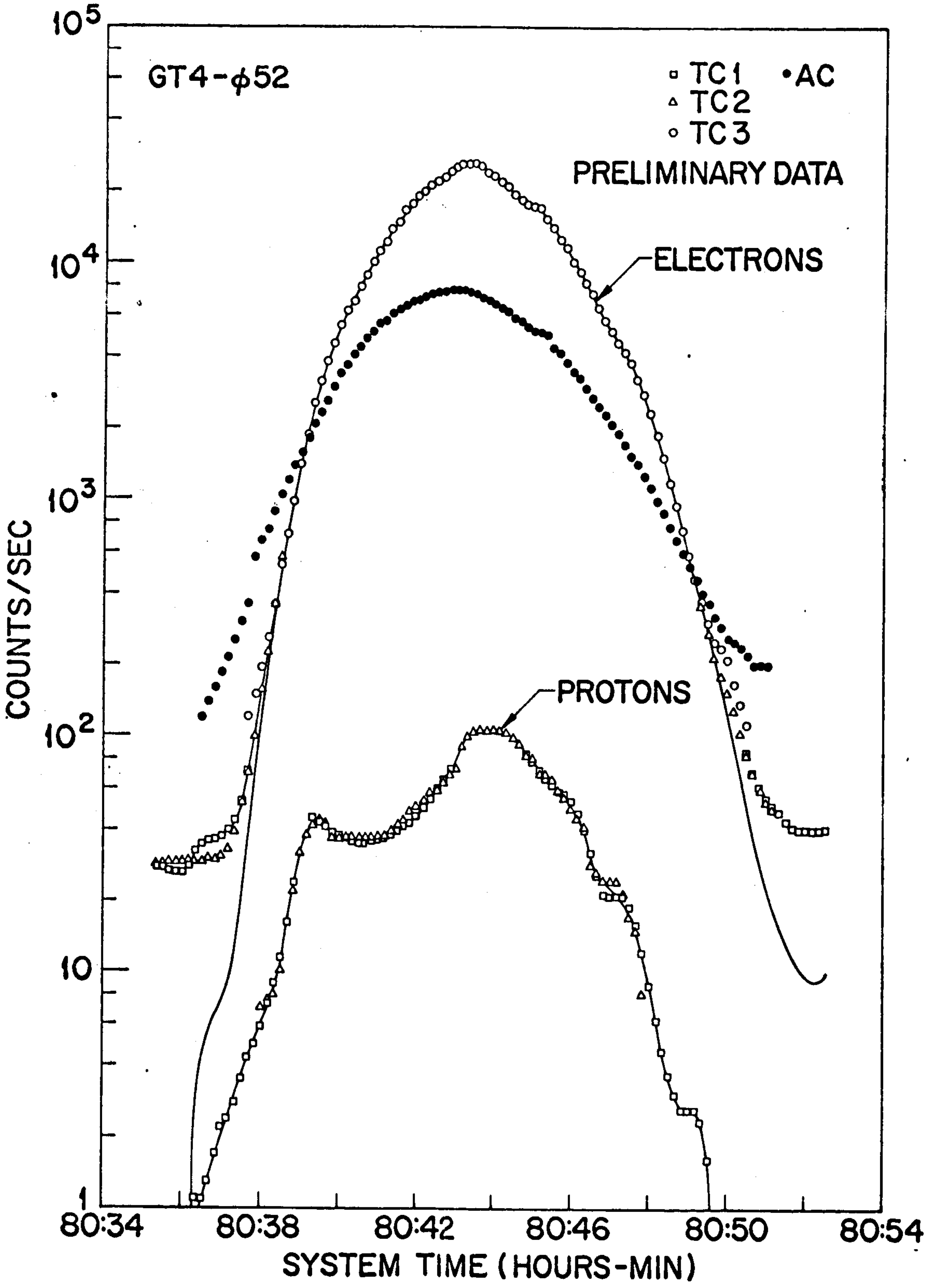

FIGURE 30. Gemini-4 Counting-Rate Profiles Versus System Time—Φ 52.

MeV is about equal to the flux between 60 and 120 MeV. Therefore, we can conclude that the overall proton contamination to the electron measurement may be neglected. It is also assumed that the electron flux does not contribute any contamination to the proton measurement merely on the basis of energy range and scintillator efficiency. To be detected in the proton mode, electrons would have to produce at least 12 MeV of energy deposit. Electrons in this energy range have not been observed in the anomaly region, and the rates are such that the probability of pile-up is negligibly small.

Another feature of the Gemini-4 data is the occurrence of sharp peaks and valleys in both the electron and proton profiles on certain orbits, particularly on orbits 7, 37, and 38. In all three cases, these perturbations were not observed in the anticoincidence detector. The effect in each case has been associated with the orientation of the spacecraft with respect to the incoming flux. Figure 31 is a plot of θ_Z, the angle between the spectrometer axis and the direction of the local magnetic field vector as obtained from the MSC-3 magnetometer for orbit 7. It can be seen by comparison of Figure 23 with Figure 31 that the valley in the flux profiles coincides approximately in time with the minimum reading of 22 degrees on the magnetometer. More detailed analysis indicated that the apparent time displacement could be explained by the presence of residual magnetic fields in varying amounts in the three axes of the magnetometer. A discussion of the technique utilized to determine these residual offsets is given in the next section.

Iso-counting rate contours in B,L space for the anticoincidence detector in the Gemini-4 spectrometer have been made and are shown in Figure 32. These count-rate data correspond to energetic protons greater than approximately 60 MeV which penetrated the shielding in an isotropic manner. Because of its large geometric factor, the anticoincidence detector functioned as a very sensitive proton threshold detector. Since the geometry was relatively complex, further analysis will be required before an omnidirectional proton flux above this energy threshold can be determined.

The total counting rates obtained from the Gemini-7 spectrometer

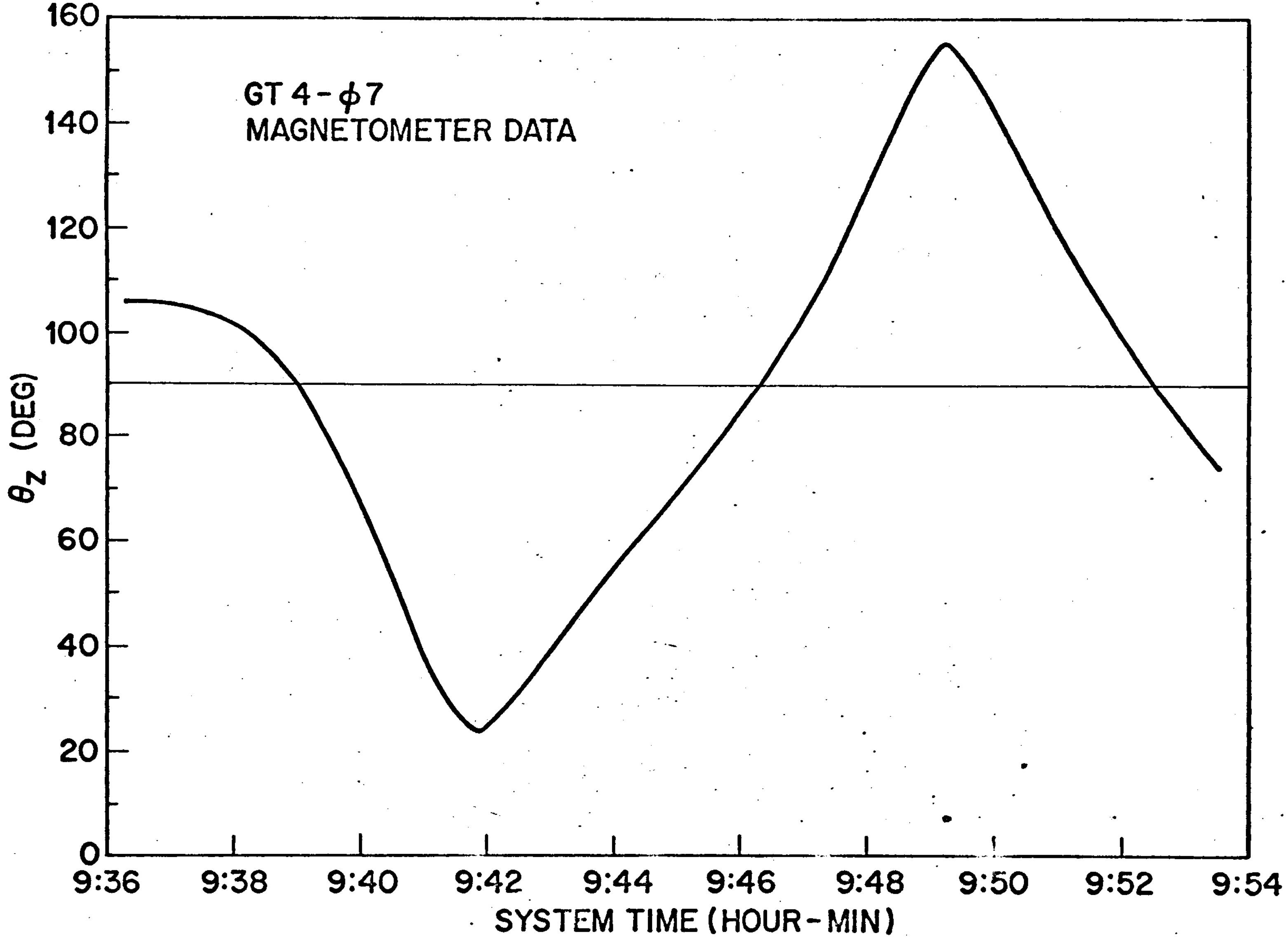

FIGURE 31. Orientation of the Gemini-4 Spectrometer With the Magnetic Field Vector Versus System Time During Orbit 7.

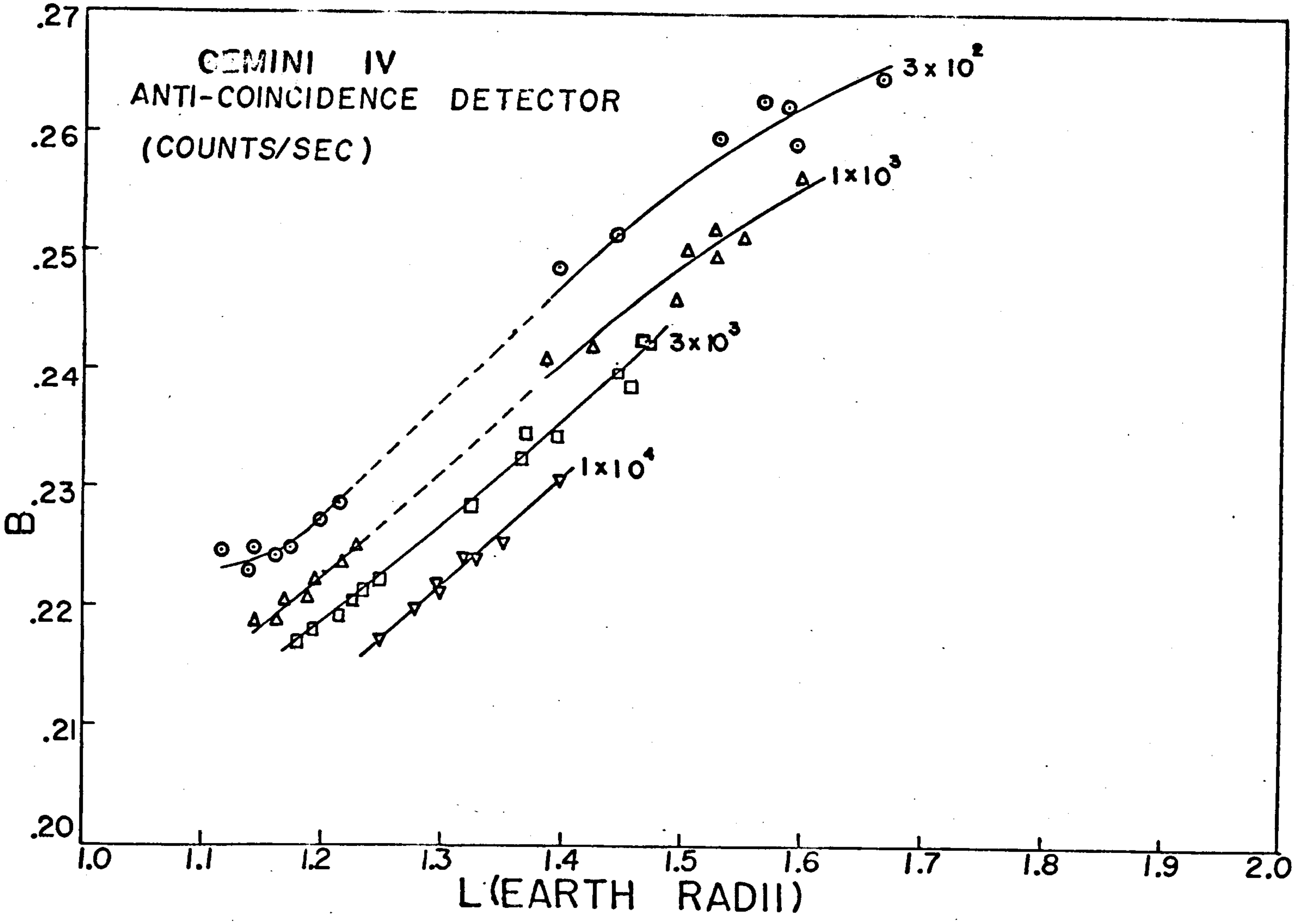

FIGURE 32. Isocounting-rate Contours in $\bar{B}$,L Space for the Anticoincidence Detector of the Gemini-4 Spectrometer.

in the electron mode of operation for the five orbits of data which have been processed are shown in Figures 33, 34, 35, 36, and 37. A light leak in the aluminized-mylar entrance window of the spectrometer created a high light background in the "dE/dx" detector. As a result, useful data obtained in the proton mode of operation is minimal. This problem did not exist in the electron mode as the "E" scintillator was sufficiently shielded from the entrance aperture. Some proton data were obtained in the electron mode of operation, however. Figure 38 shows a typical spectrum obtained from the pulse-height analyzer in this mode of operation. The first fourteen channels of the analyzer were assigned to covering the electron energy range of 0.5-4.0 MeV. It can be seen that the electron flux is down in intensity over an order of magnitude between the first and fourteenth channels. There is however a significant counting rate in the fifteenth or overload channel. This channel represents all energy deposits in the "E" scintillator which exceed approximately 4.0 MeV for electrons and 8.5 MeV for protons. From the available electron spectrum below 4 MeV in the lower channels, it can be seen that any higher energy electron contribution to this overload channel is negligible. The observed counting rate in this channel must then be due to a combination of cosmic rays, protons within the acceptance aperture, and high energy protons which penetrate the shielding. The cosmic ray contribution can easily be ascertained by observing the counting rate in this channel for those portions of the flight where particle fluxes cannot remain trapped. Since the geometric factor available for penetrating protons is approximately fifteen times greater than the geometric factor for protons within the acceptance aperture, this overload channel functions as a very sensitive detector of protons greater than approximately 80 MeV. This threshold includes the effect of both shielding and electronic bias. Thus, by using the spectral information, the total counting rate contours can be separated into omnidirectional electron and proton fluxes above 0.5 MeV and 80 MeV, respectively.

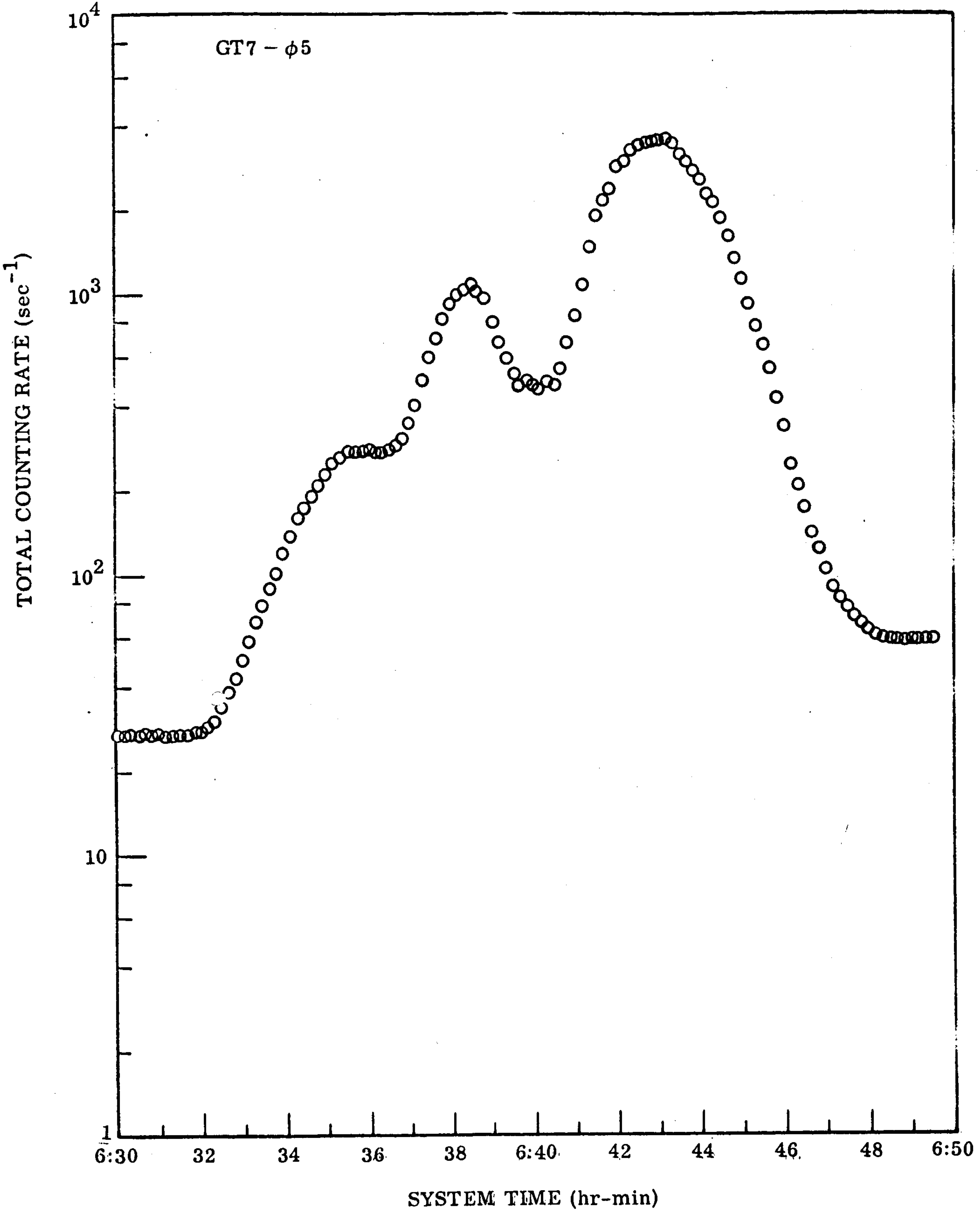

FIGURE 33. Gemini-7 Counting-Rate Profiles Versus System Time—Φ 5.

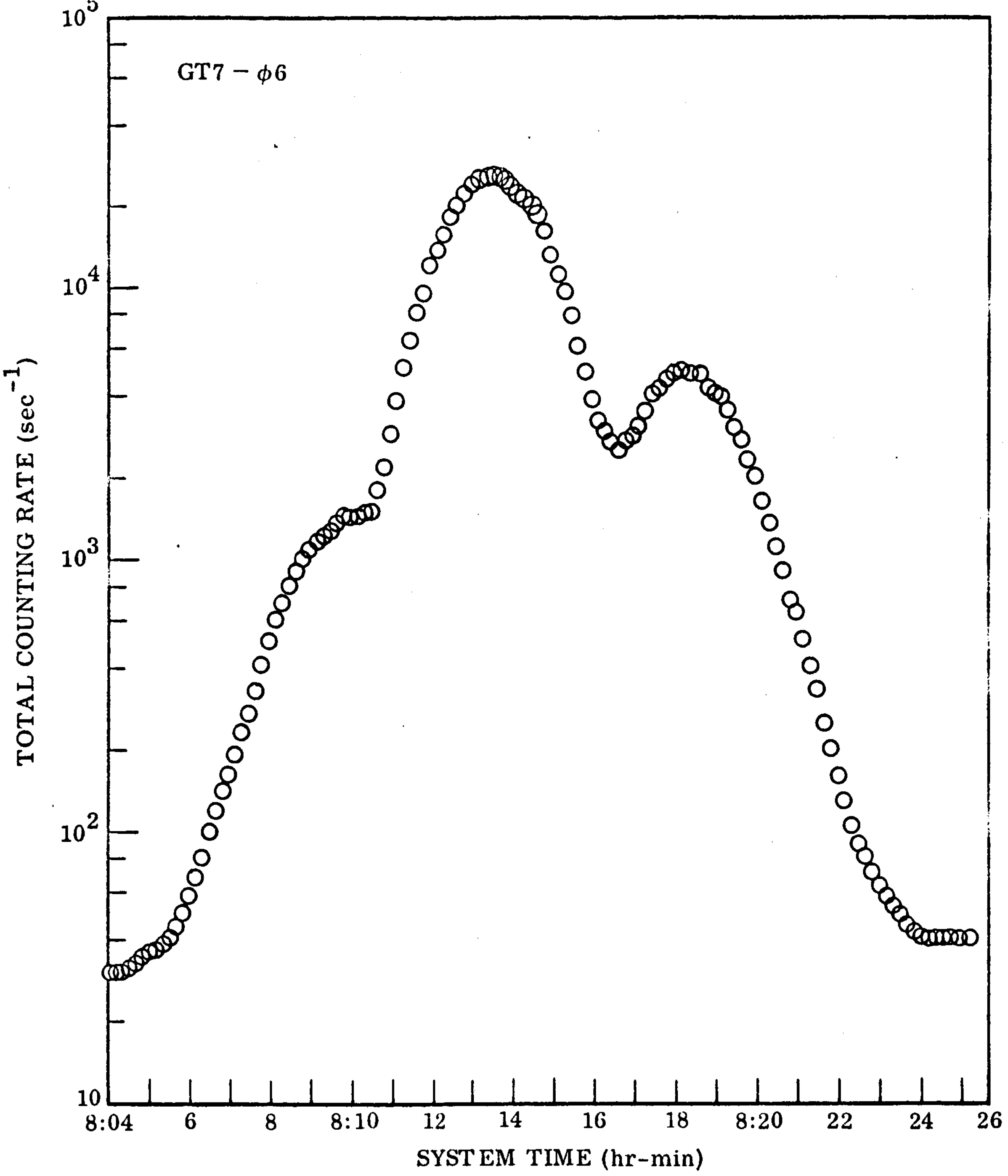

FIGURE 34. Gemini-7 Counting-Rate Profiles Versus System Time—Φ 6.

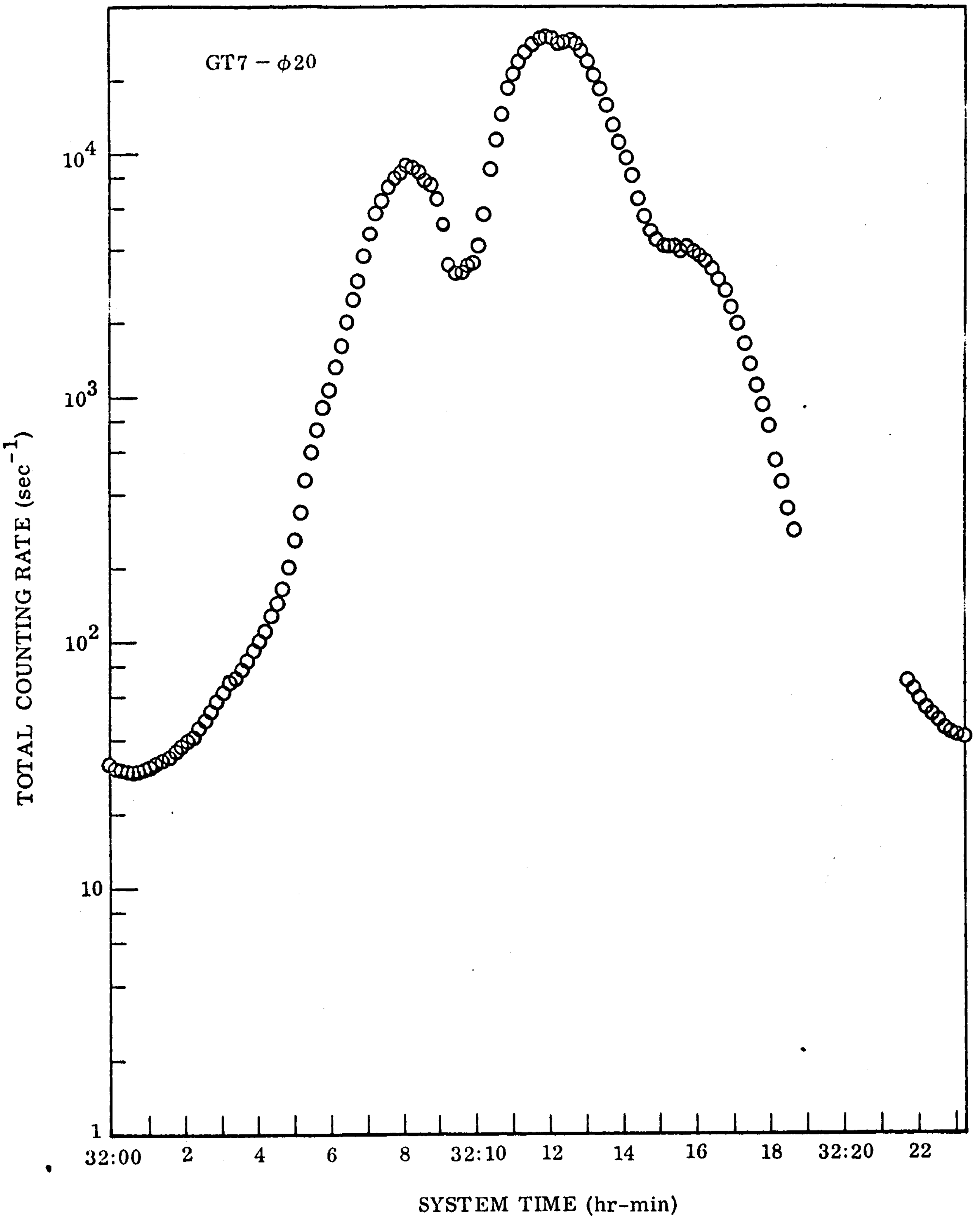

FIGURE 35. Gemini-7 Counting-Rate Profiles Versus System Time—Φ 20.

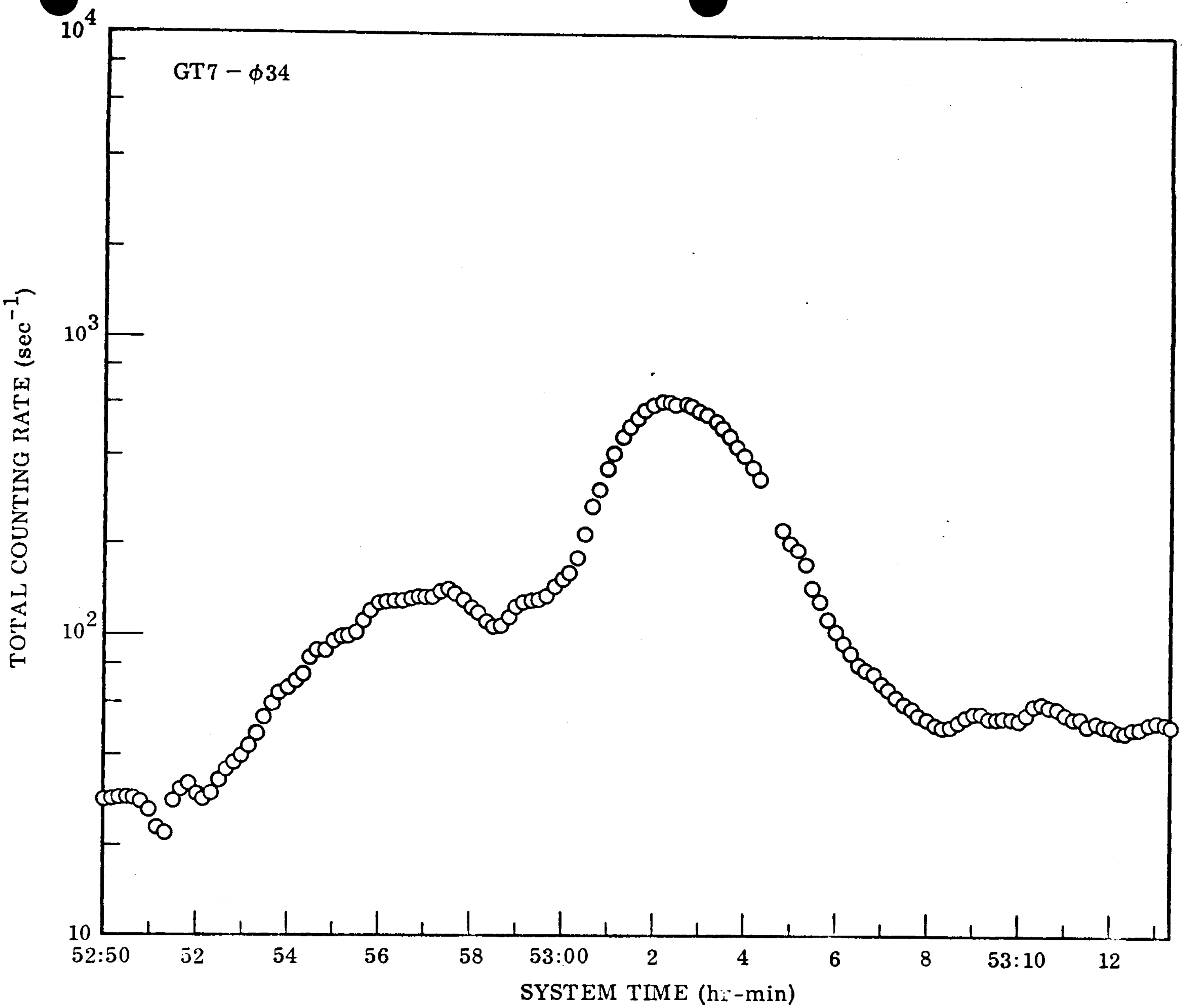

FIGURE 36. Gemini-7 Counting-Rate Profiles Versus System Time—Φ 34.

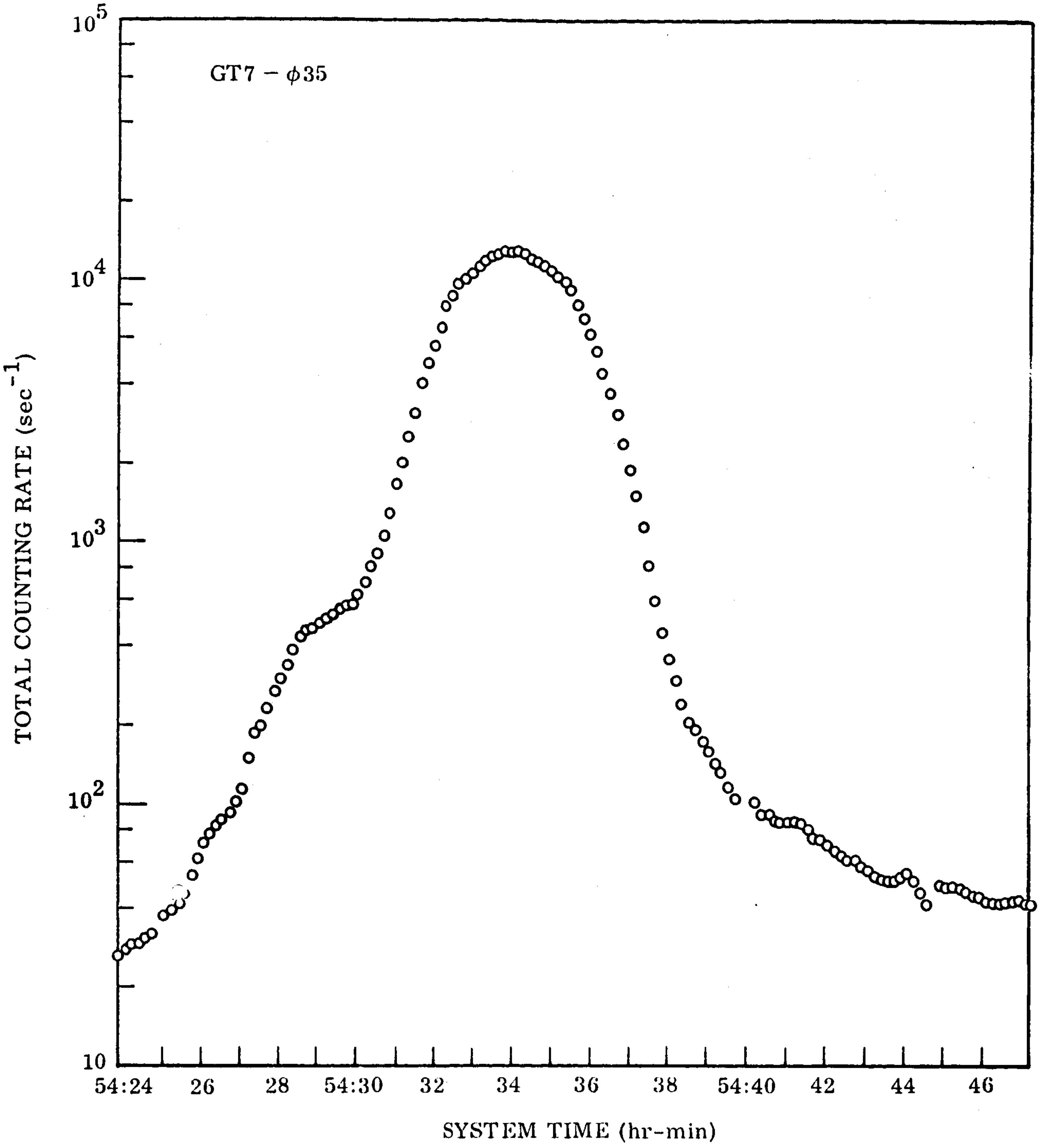

FIGURE 37. Gemini-7 Counting-Rate Profiles Versus System Time—Φ 35.

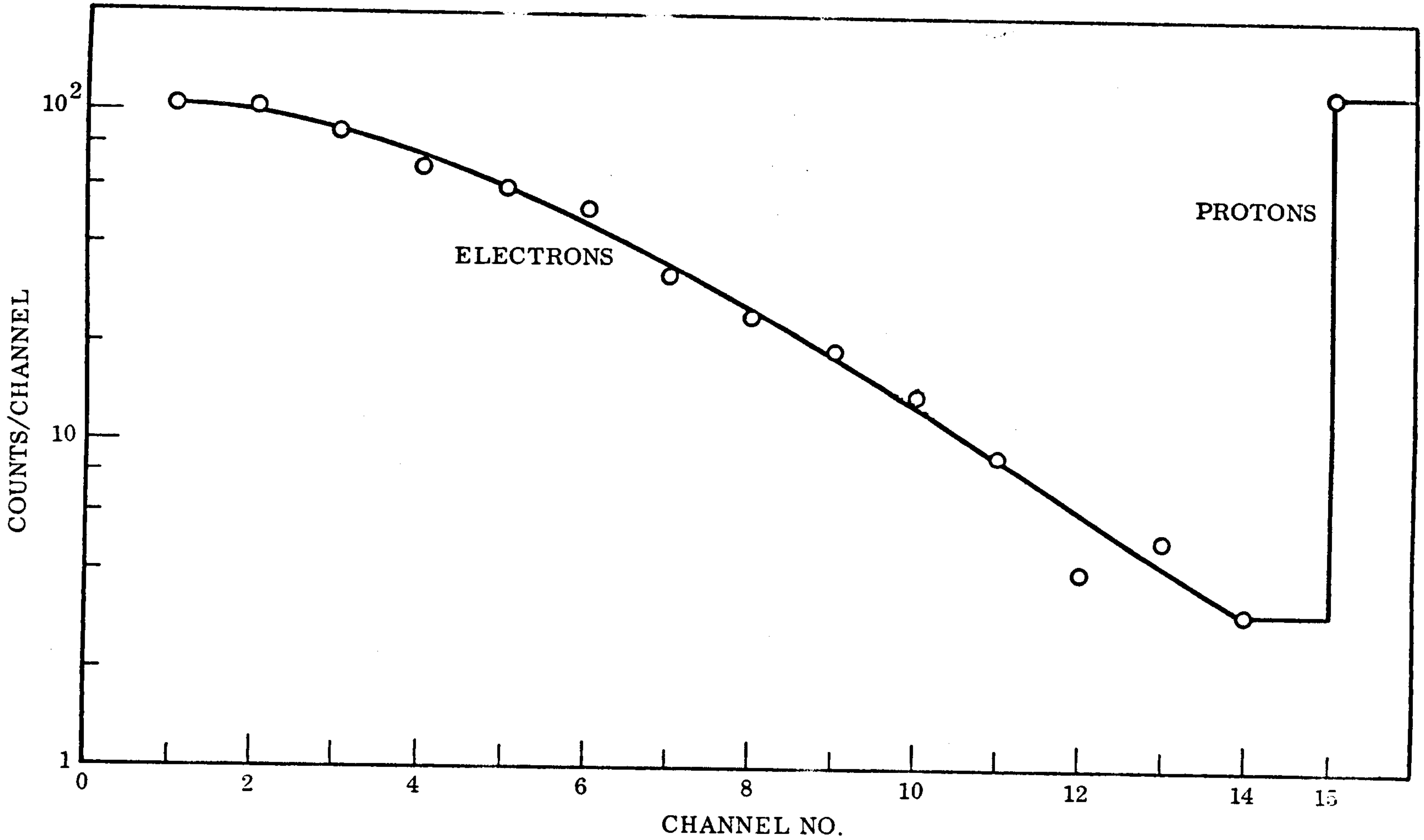

FIGURE 38. Typical Pulse Height Spectrum Obtained In Flight From the Gemini-7 Spectrometer in the Electron Mode.

5.2 Magnetometer Data

To determine the orientation of the spectrometer at any time with respect to the magnetic field, the data from a tri-axis magnetometer provided by the NASA-MSC-3 experiment was used on both flights. On the Gemini-4 experiment, a rather large residual magnetic field existed on one axis of the magnetometer due to the presence of some magnetic material in the mounting structure. Before this magnetometer data could be used to determine orientation, the magnitude of these offsets needed to be determined. To accomplish this, it was first assumed that the offsets could be both additive and multiplicative in each of the three axes. The known value of the scalar magnetic field at any time obtained from the Jensen and Cain 48-term magnetic field model [Jensen and Cain, 1962] using the spacecraft ephemeris data was used as an additional input. The following equation was used to determine the residual offsets a_j:

$$a_1(Hx_i+a_2)^2 + a_3(Hy_i+a_4)^2 + a_5(Hz_i+a_6)^2 = B_i^2 - \delta_i \tag{1}$$

where the subscript i indicates time, B is the scalar value of the magnetic field from the Jensen and Cain code, δ is the margin of error between the value of B and the scalar field calculated from the three magnetometer components, H_x, H_y, and H_z. By minimizing the six partial derivatives

$$\frac{\partial}{\partial a_j}\left[\sum_i \delta_i^2 - n\left(\frac{\Sigma_i \delta_i}{n}\right)^2\right] \tag{2}$$

where the term in brackets is the standard error of estimate, six equations with six unknowns were obtained. The six solutions were then substituted in equation (1) to generate a measured value of the total field H_T and a value of the angle between the instrument axis and the field vector by the expression:

$$\theta_{z_i} = \cos^{-1}\left[\frac{\sqrt{a_5}(Hz_i+a_6)}{B_i}\right] \tag{3}$$

A plot of both the raw magnetometer data and a corrected version utilizing this technique is shown in Figure 39. The largest deviations of H_{T_i} from B_i using this technique are on the order of 5 percent. The values of θ_{z_i} in conjunction with the calculated values of the angular dependent geometric factor described in the next section provide a very consistent explanation of the flux data in B,L space throughout the flight. This technique should be examined in greater detail to determine if even better agreement can be reached.

On the Gemini-7 flight, only two axes of magnetometer data were available. Therefore, it had to be initially assumed that any offsets which existed were small and that the calculated value of B_i was an accurate representation of the scalar magnetic field. With these assumptions, the magnitude of the missing component could be calculated from the equation

$$H_{z_i} = [B_i^2 - H_{x_i}^2 - H_{y_i}^2]^{\frac{1}{2}} \tag{4}$$

and the orientation could be obtained from the relation

$$\theta_{z_i} = \cos^{-1} \frac{H_{zi}}{B_i} \tag{5}$$

If these assumptions were correct, the quantity

$$B_i^2 - H_{x_i}^2 - H_{y_i}^2 \tag{6}$$

should never be less than zero by more than would be indicated by the scatter of the data. The raw Gemini-7 data, however, showed that this quantity assumed negative values of fairly large absolute value. The method of correcting these data was as follows:

An equation of the form

$$H_{z_i} = B_i^2 - \left[(H_{xi} + a_2)^2 - (H_{y_i} + a_4)^2\right]^{\frac{1}{2}} \tag{7}$$

was assumed. The constants a_2 and a_4 were assumed to be small so that by choosing data points for which, for example, $H_{y_i} = 0$, no significant error

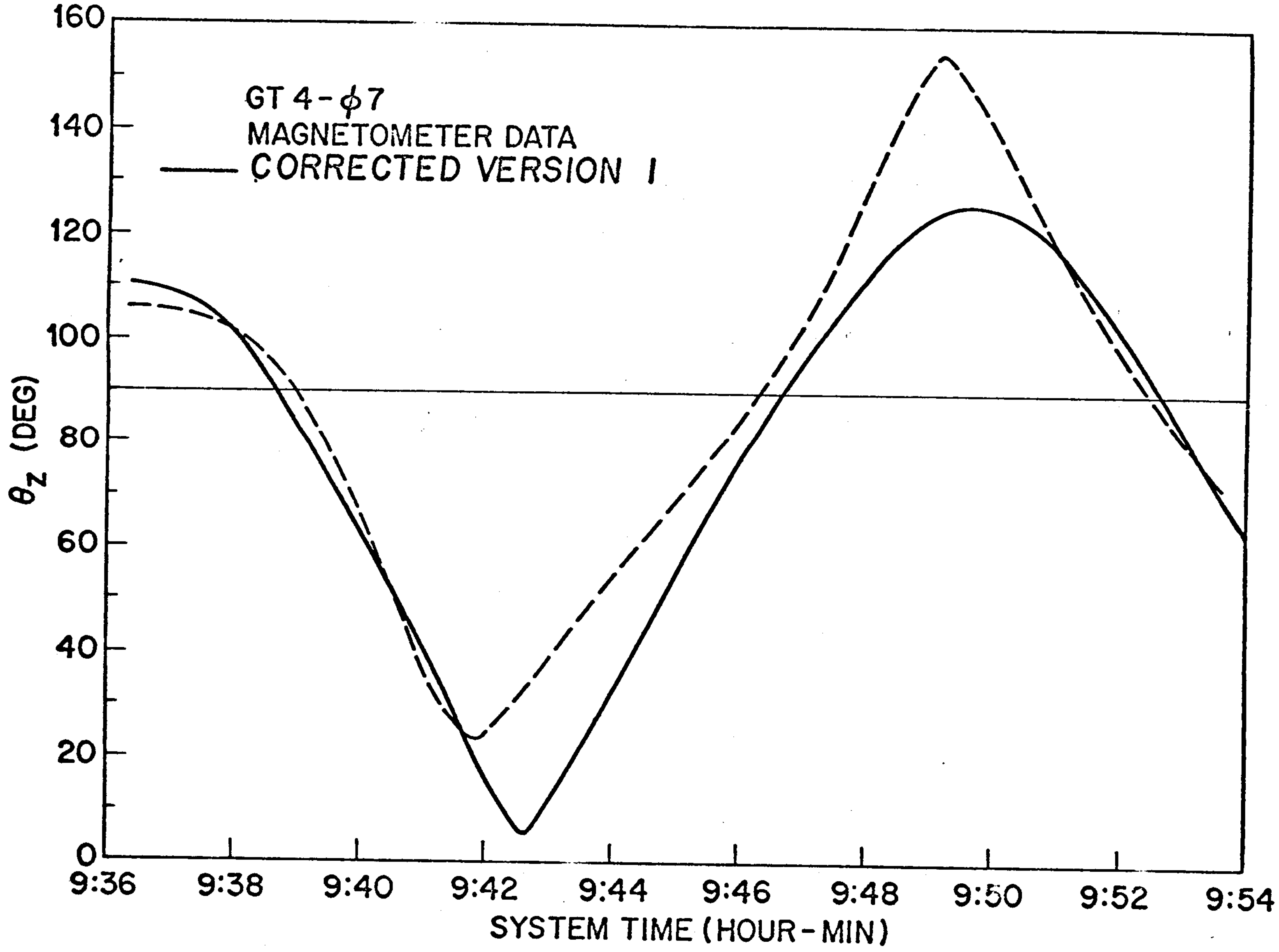

FIGURE 39. Gemini-4 Raw and Corrected Magnetometer Data.

would be introduced by dropping a_4 in equation (7). Therefore, we obtain the equation

$$H_{z_i} = \left[B_i^2 - (H_{x_i} + a_2)^2\right]^{\frac{1}{2}} \tag{8}$$

By examining a large quantity of the data for which $H_{y_i} = 0$, it was possible to calculate a_2 such that $B_i^2 - (H_{x_i} + a_2)^2$ never assumed large negative values. The same method was used to correct H_{y_i}.

There is no method of calculating the error after the data have been corrected in this manner other than examining most of the data keeping in mind the last assumption in addition to the requirement that the value

$$\theta_{z_i} = \cos^{-1} \frac{\sqrt{B_i^2 - (H_{z_i} + a_2)^2 - (H_{y_i} + a_4)^2}}{B_i} \tag{9}$$

must be continuous at values close to $\theta_{z_i} = 90^\circ$. An example of the results of this technique is shown in Figure 40 where the raw and corrected magnetometer data for a region of the anomaly on the Gemini-7 flight is presented. As can be seen, the corrected data exhibit a smooth transition through ninety degrees, in contrast to the discontinuities which existed in the raw data.

The accuracy of this analysis, which has been based exclusively on the magnetometer data and the calculated value of the scalar magnetic field, must ultimately be tested by observing the consistency it produces in the radiation data over a wide variety of orientations in B,L space. Such an analysis has not yet been performed.

5.3 Geometric Factors

The counting rates observed by the detectors are related to the omnidirectional particle fluxes by the expression

$$G = \frac{C}{J_o} \tag{1}$$

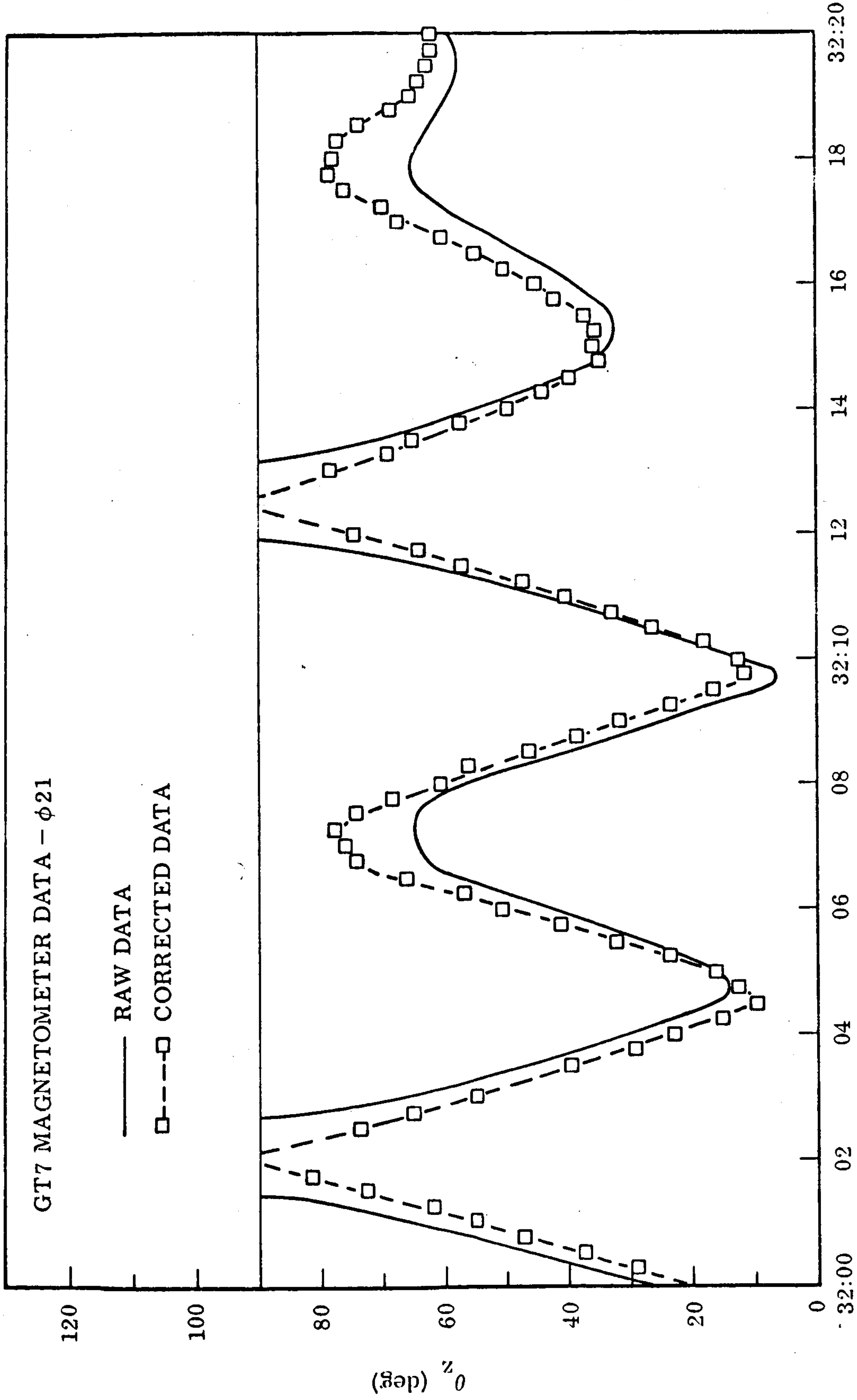

FIGURE 40. Gemini-7 Raw and Corrected Magnetometer Data.

where C is the detector counting rate, J_o is the omnidirectional flux, and G is the geometric factor of the instrument. Since the counting rate observed for a given aperture of area A in a unidirectional particle flux j is $C = jA$, the total counting rate is given by the sum over solid angle $C = \int jA d\Omega$, while the omnidirectional flux is defined by $j_o = \int j d\Omega$ so that

$$G = \frac{\int jA d\Omega}{\int j d\Omega} \tag{2}$$

As can be seen from Figure 9, the radiation incident on the plane of the detector was collimated by the finite tungsten shielding and the thickness of the anticoincidence scintillator in the vicinity of the aperture. The effective area A of the detector is then the area available for the passage of particles through the ends of an open-ended cylinder, as shown in Figure 41.

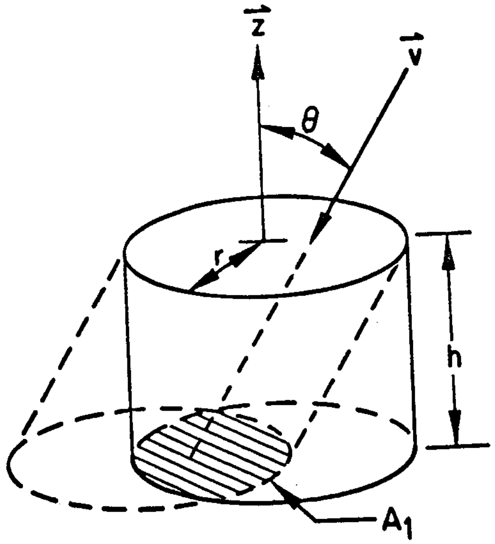

FIGURE 41. Effective Area of the Spectrometers Available to Particles as a Function of the Incident Angle θ.

This area can be expressed by the relation

$$\begin{aligned} A &= A_1 \cos\theta \\ &= \pi r^2 \cos\theta \left\{ 1 - \frac{2}{\pi}\left[\sin^{-1}(\delta \tan\theta) + \delta \tan\theta \sqrt{1-(\delta \tan\theta)^2} \right] \right\} \end{aligned} \tag{3}$$

where $\delta = h/2r$.

The spatial distribution of the particle flux must be taken into account before this last equation may be used to integrate equation 2. Heckman and Nakano [1963] have shown that in the anomaly region at these altitudes the particle fluxes are near their mirror points and are therefore confined to a plane or "pancake" distribution normal to the local magnetic field. The relationships between the particle flux, the longitudinal axis of the detector, and the magnetic field vector can then be described as shown in Figure 42.

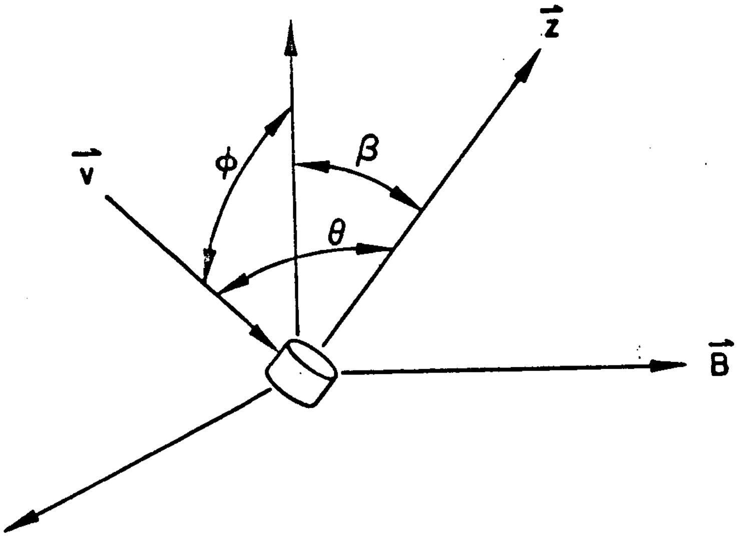

FIGURE 42. Angular Relationships Between the Incident Particle Flux $\vec{v}$, the Longitudinal Axis of the Spectrometer Z, and the Magnetic Field Vector, $\vec{B}$.

The assumptions that the flux distribution parallel to $\vec{B}$ is constant over the dimension of the aperture and that the angular distribution of j can be expressed completely by $j(\varphi)$ = constant leads to the expression

$$G = \frac{1}{2\pi} \int A\ [\theta(\varphi)] d\varphi \tag{4}$$

If β is defined as the minimum angle θbetween the Z axis and the plane of the particle flux, as shown in Figure 43, the relation between θ and φ is

$$\cos\ \theta = \cos\ \beta \cos\ \varphi \tag{5}$$

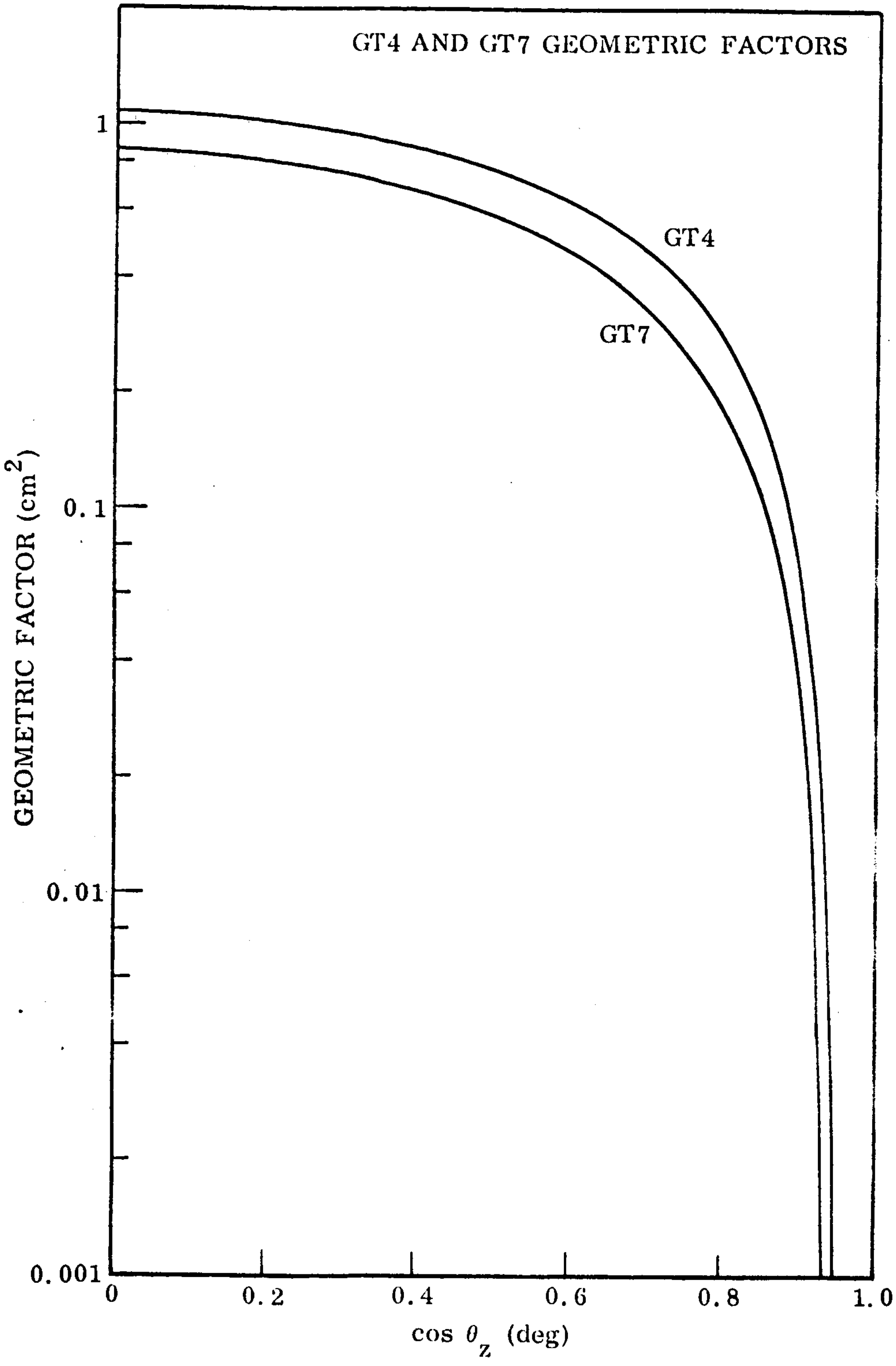

FIGURE 43. Geometric Factors of the Gemini-4 and -7 Spectrometers as a Function of the Angle Between the Z-Axis and the Magnetic Field.

and $$\frac{d\varphi}{d\theta} = \frac{\sin\theta}{\sqrt{\sin^2\theta - \sin^2\beta}} .$$

Substitution of this expression into equation 4 yields

$$G(\beta) = \frac{1}{\pi} \int_{\theta_{min}=\beta}^{\theta_{max}} \frac{A(\theta)\sin\theta\, d\theta}{\sqrt{\sin^2\theta - \sin^2\beta}} \tag{6}$$

where θ_{max} is the angle at which $A(\theta)$ goes to zero and is determined by the geometry of the detector and its location in the spacecraft.

The above expression has been solved by numerical integration for fixed values of β. The resulting relationship of geometric factor as a function of the cosine of the angle between the z axis of the detectors and the magnetic field is shown for both spectrometers in Figure 43. This mathematical analysis of the geometric factors should be verified by experimental determinations involving the backup spectrometers. In addition, this preliminary analysis has not included energy dependent effects on the geometric factor.

5.4 Omnidirectional Particle Fluxes

Omnidirectional fluxes of electrons and protons measured during the Gemini-4 flight have been generated by combining the counting rate contours, the corrected orientation data, and the appropriate geometric factor as determined from Figure 43. The resultant flux contours in B,L space for electrons greater than 0.5 MeV are shown in Figure 44. A similar flux contour for protons in the 25-80-MeV energy range is shown in Figure 45. These fluxes should not be considered as the final results of the experiment since more detailed analysis of each of the above items, including a more comprehensive investigation of backgrounds, is required. It is felt, however, that the present flux values are accurate within a factor of two.

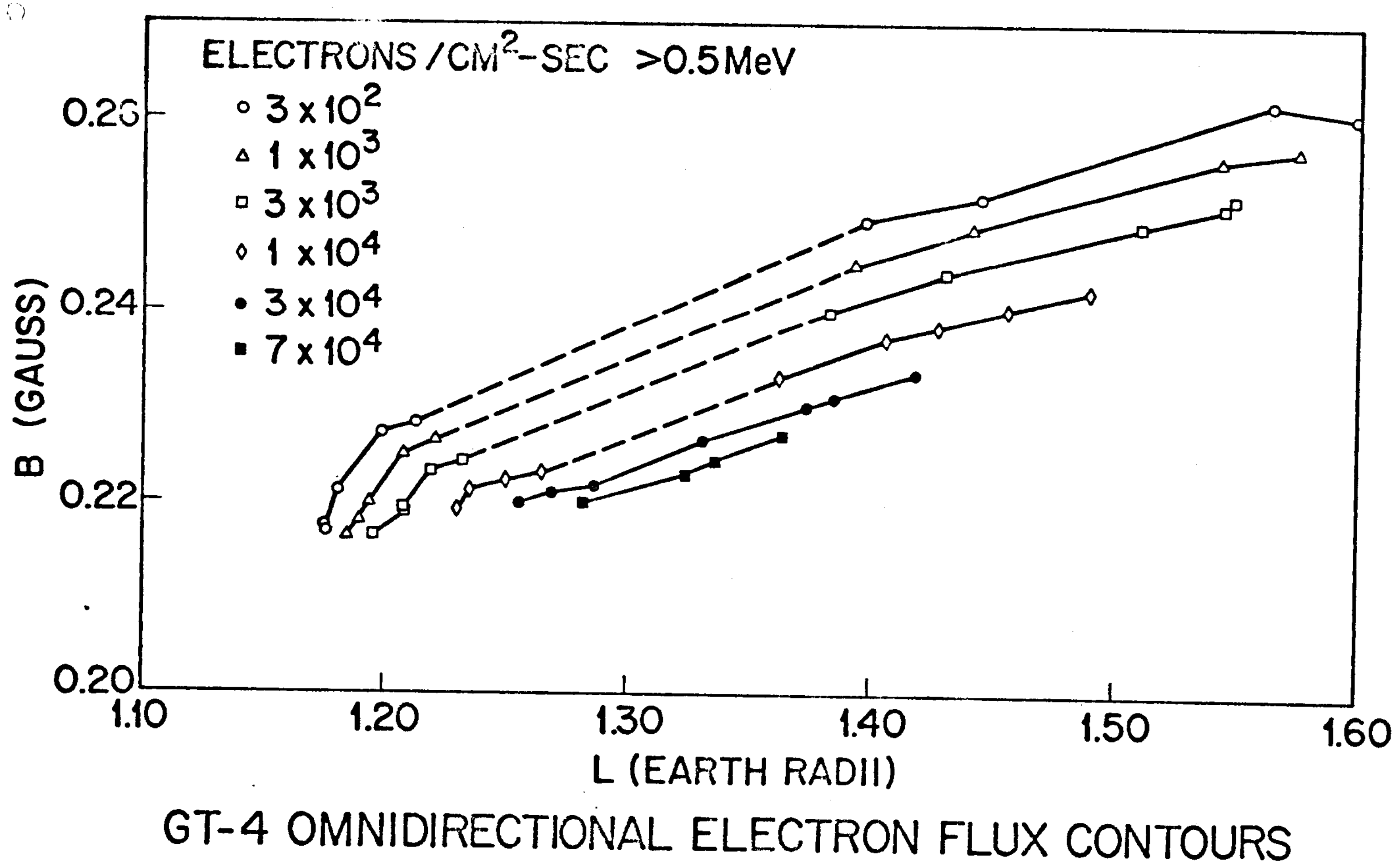

FIGURE 44. Gemini-4 Omnidirectional Electron Flux Contours in B,L Space for $E_e > 0.5$ MeV.

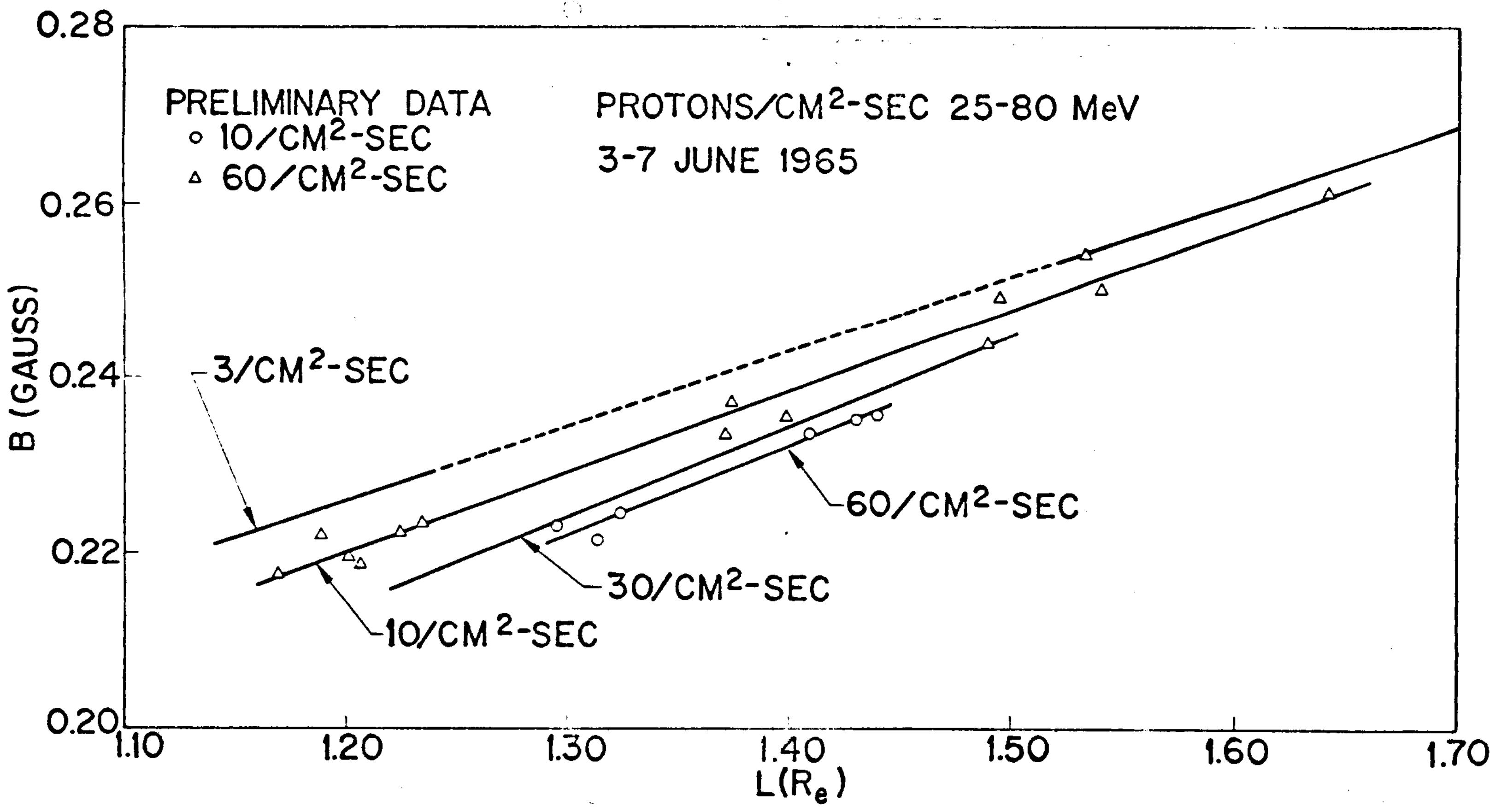

FIGURE 45. Gemini-4 Omnidirectional Proton Flux Contours in B,L Space for 25 MeV < E_p < 80 MeV.

Only a small percentage of the Gemini-7 data has been processed to date. A presentation of the preliminary results of the analysis of two orbits of data is shown in Figures 46 and 47. Omnidirectional particle fluxes for electrons greater than 0.5 MeV and for protons greater than approximately 80 MeV are shown. The latter data were obtained from an analysis of the overload channel in the pulse-height analyzer as described in Section 5.1. Vehicle background and cosmic-ray background have been subtracted from the data shown. The contribution from penetrating protons to the electron data, particularly at low L values, has not yet been analyzed, however. This background can be determined and subtracted by investigating the flux and spectrum within the electron range at times when the spectrometer is oriented normal to the electron flux.

5.5 Energy Spectrum Data

The information obtained from the pulse-height analyzer on the Gemini-4 experiment has been catalogued to form characteristic electron and proton spectra for regions in B,L space covered by the flight. Figure 48 shows the electron spectrum obtained for three different B,L regions of space. It can be seen that the typical spectrum is essentially hard and fission-like reflecting the remains of the artificial radiation belt created by the Starfish high-altitude nuclear test of 9 July, 1962. The effect of a four-year decay of this radiation can be seen as the spectrum softens significantly for both increasing and decreasing L regions about $L \simeq 1.30$. This probably indicates the contribution of a softer spectrum of naturally-trapped electrons on L shells removed from the center of the artificial belt. The actual spectrum in this region is a complex merging of an inadequately defined flux and spectrum and naturally-occurring electrons with a flux of decaying artificially injected fission-type electrons. Figure 49 shows the characteristic electron spectrum obtained from several orbits of Gemini-7 data. The spectral shape, particularly at higher energies, is quite similar to the Gemini-4 data in the same B,L regions.

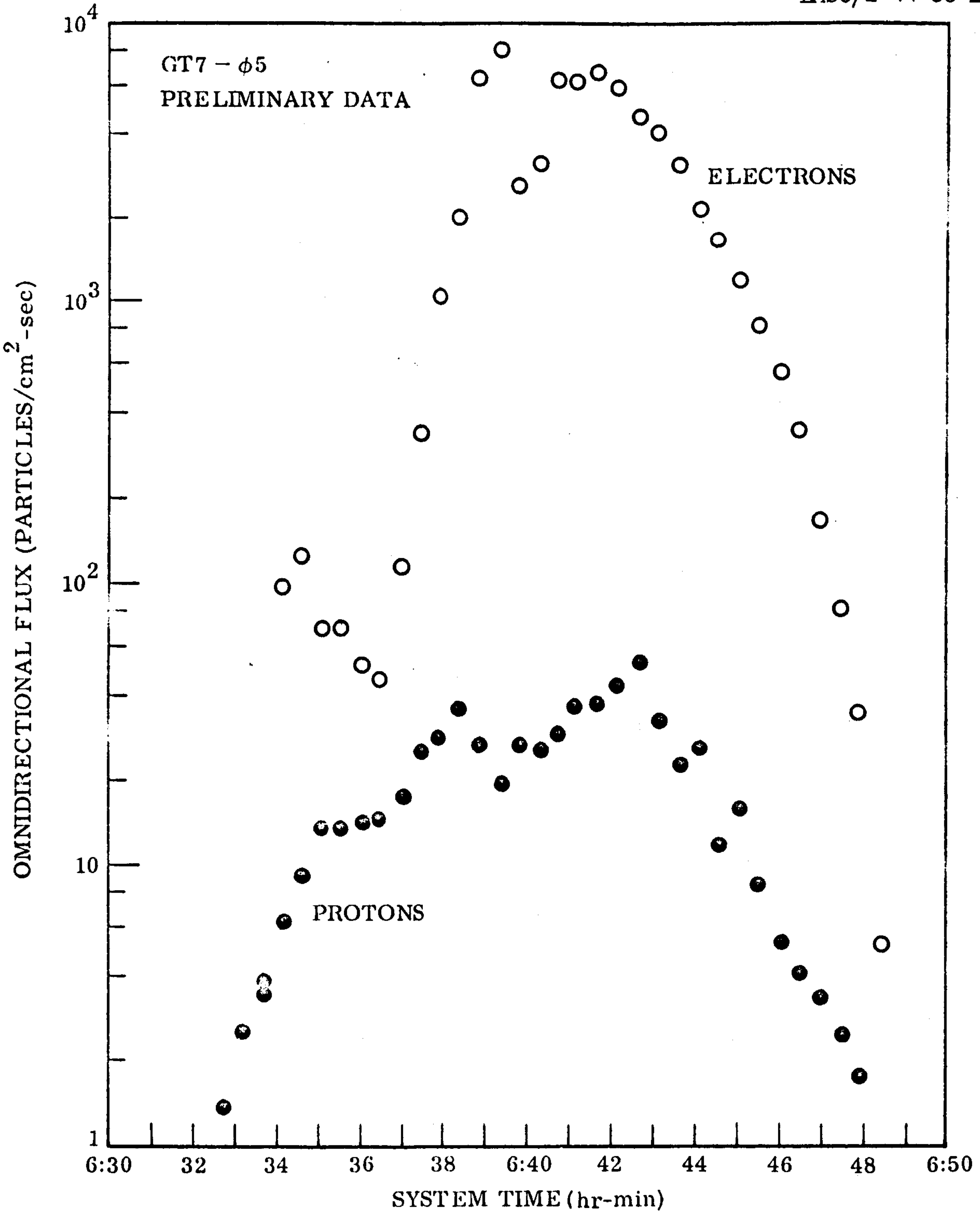

FIGURE 46. Gemini-7 Omnidirectional Electron Flux > 0.5 MeV and Proton Flux > 80 MeV as a Function of Systems Time—Orbit 5.

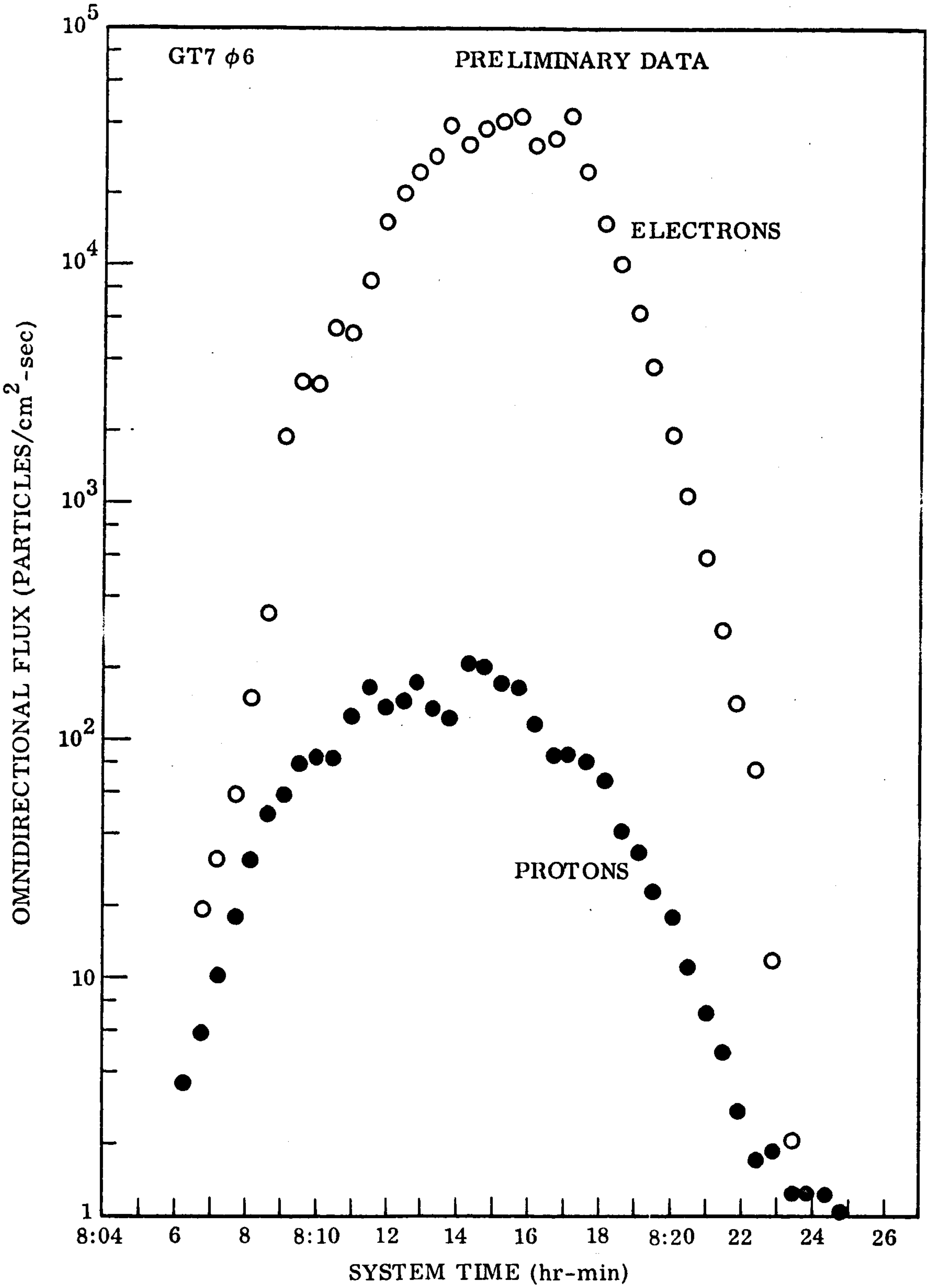

FIGURE 47. Gemini-7 Omnidirectional Electron Flux > 0.5 MeV and Proton Flux > 80 MeV as a Function of Systems Time—Orbit 6.

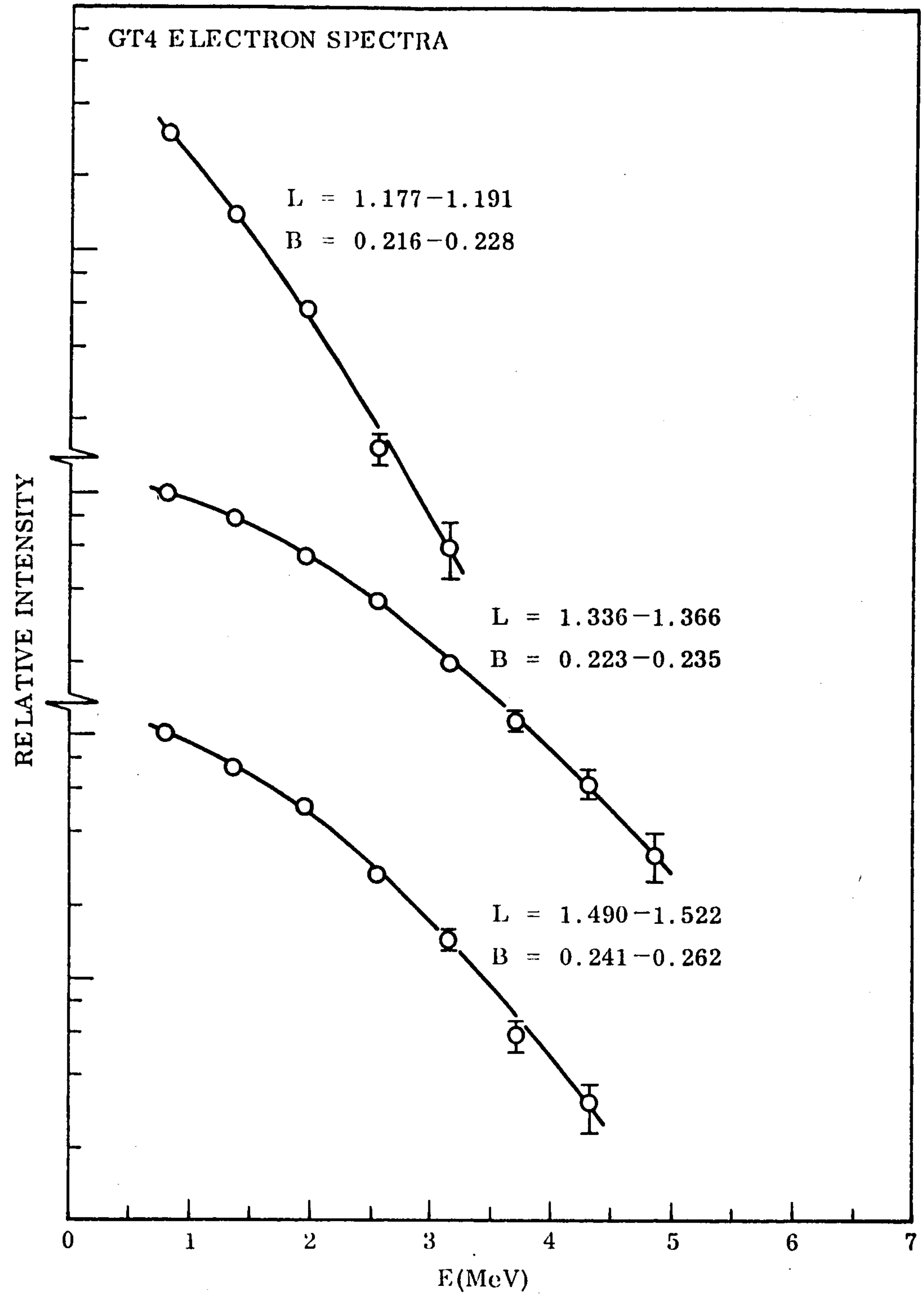

FIGURE 48. Gemini-4 Characteristic Electron Spectra as a Function of B,L Location.

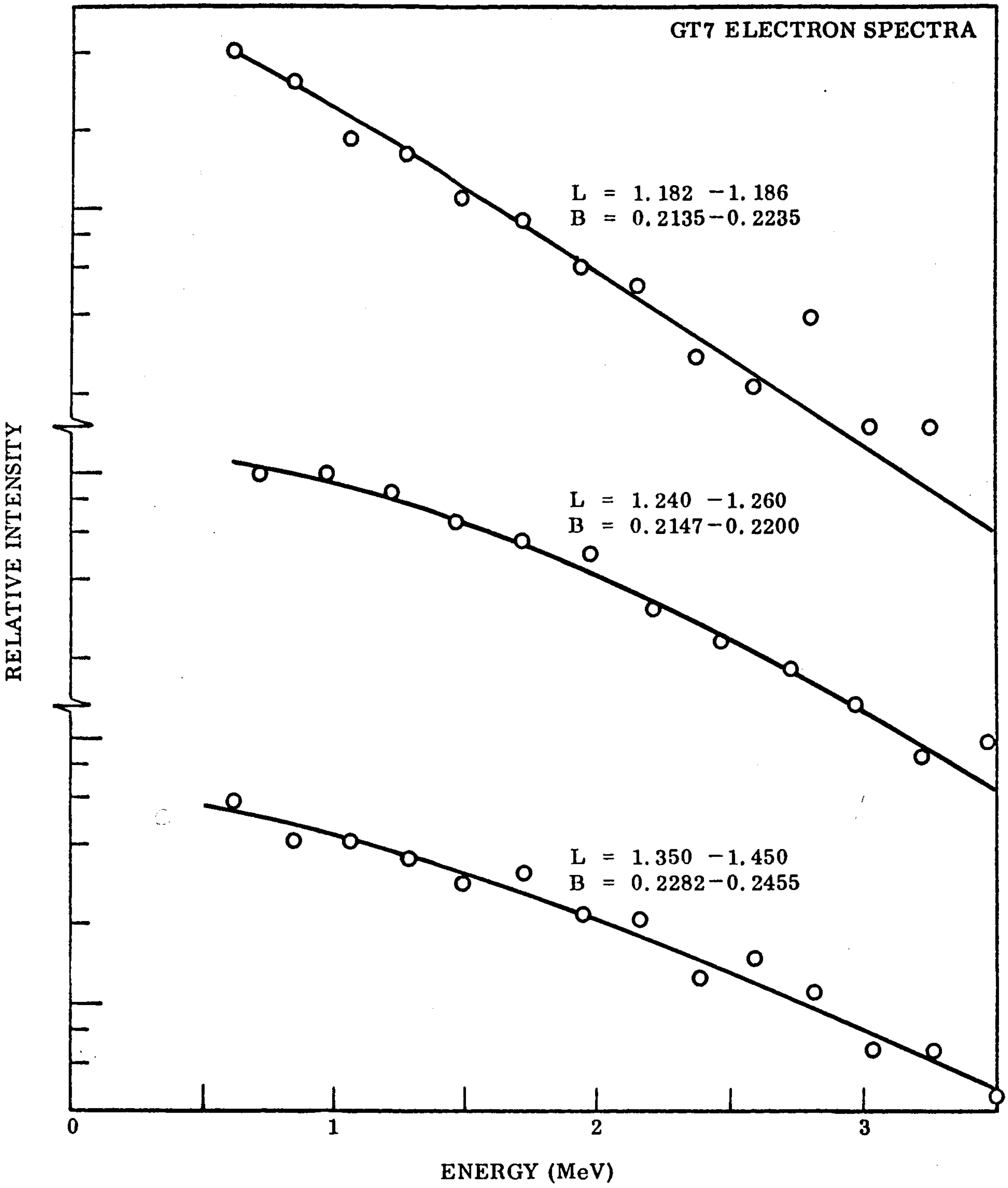

FIGURE 49. Gemini-7 Characteristic Electron Spectra as a Function of B,L Location.

Figure 50 shows the characteristic proton spectrum obtained for the 25-80-MeV region. As can be seen, the proton spectrum is relatively hard and flat over the entire B,L region of the flight. A characteristic small peak which appears on a wide range of L values can also be seen at approximately 50 MeV.

5.6 Comparison With Previous Results

The electron data obtained from the Gemini-4 and -7 experiments have been compared at specific B,L regions with the previous experimental results of Imhof and Smith [1965c] and with the theoretical calculations of Walt [1964b] based on the decay of the Starfish electrons due to atmospheric scattering. Figure 51 shows the omnidirectional electron flux > 1.2 MeV obtained from the experimental data as a function of days after the Starfish event. The data have been selected for L shells of 1.185 and 1.25 and for a B value of 0.220 in order to make a comparison with existing theoretical calculations at these values. The first two sets of data points were obtained from 2π-scintillation detectors, with integral electron energy thresholds of 1.2 MeV at a time of 56 and 93 days, respectively, after the Starfish event. The next set of data points were obtained from an electron spectrometer in October-November, 1963, some 470 days after the Starfish event. These data points were obtained by integrating the measured spectrum above 1.2 MeV. The Gemini-4 data [Reagan, et al., 1965] obtained at 1050 days are shown as the next set of points. These data were also obtained by integrating the measured spectrum above 1.2 MeV. Data obtained from a spectrometer on a satellite flight in November, 1965 [Imhof, et al., 1966], and the Gemini-7 data are shown as the last sets of points. The solid lines represent the electron flux above 1.2 MeV that would be predicted as a function of time if all of the initial electrons were fission-produced and if their decay were controlled only by atmospheric scattering [Walt, 1964b]. The theoretical curves have been arbitrarily normalized in both cases to the early-time

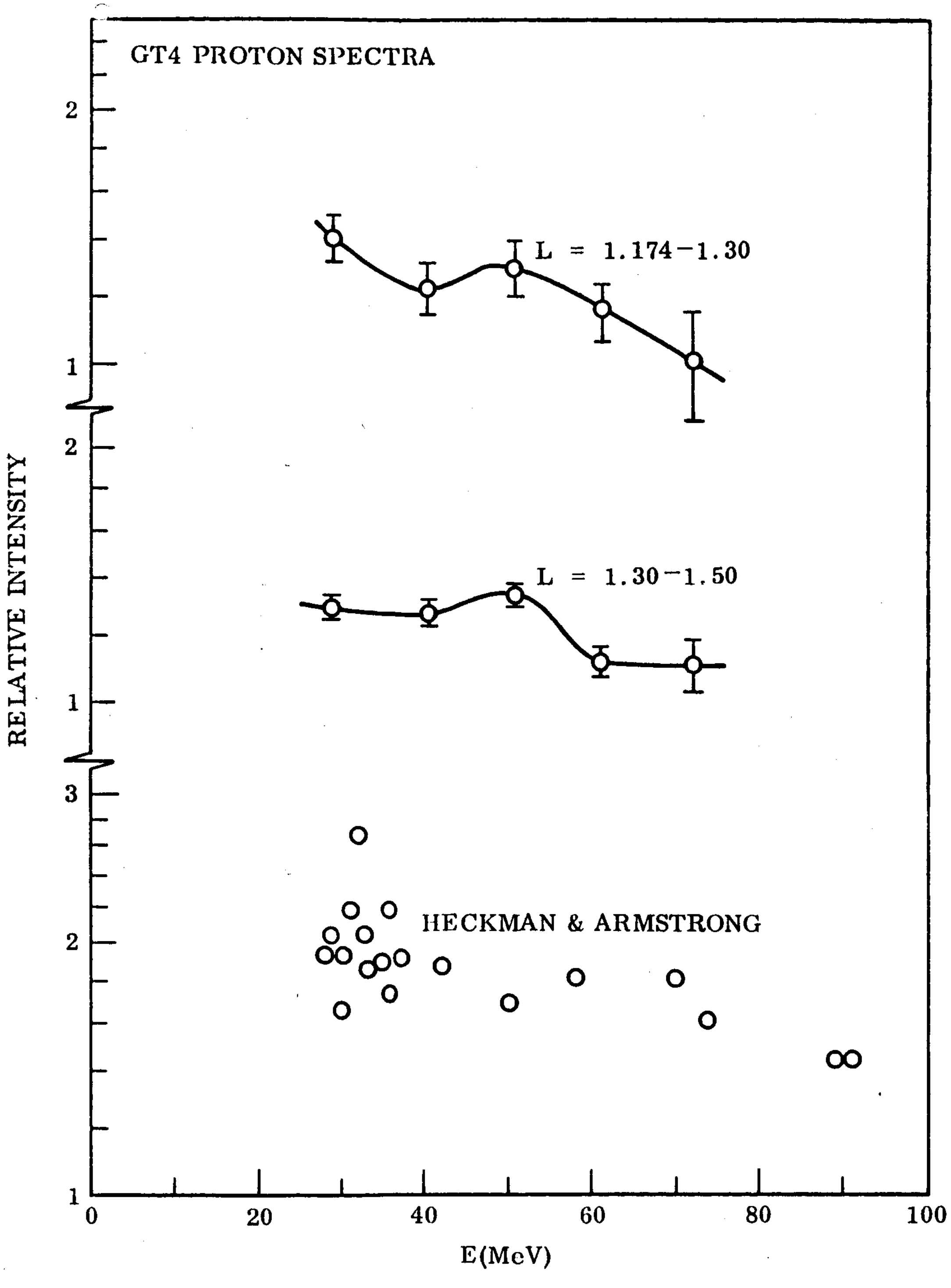

FIGURE 50. Gemini-4 Characteristic Proton Spectra as a Function of B,L Location.

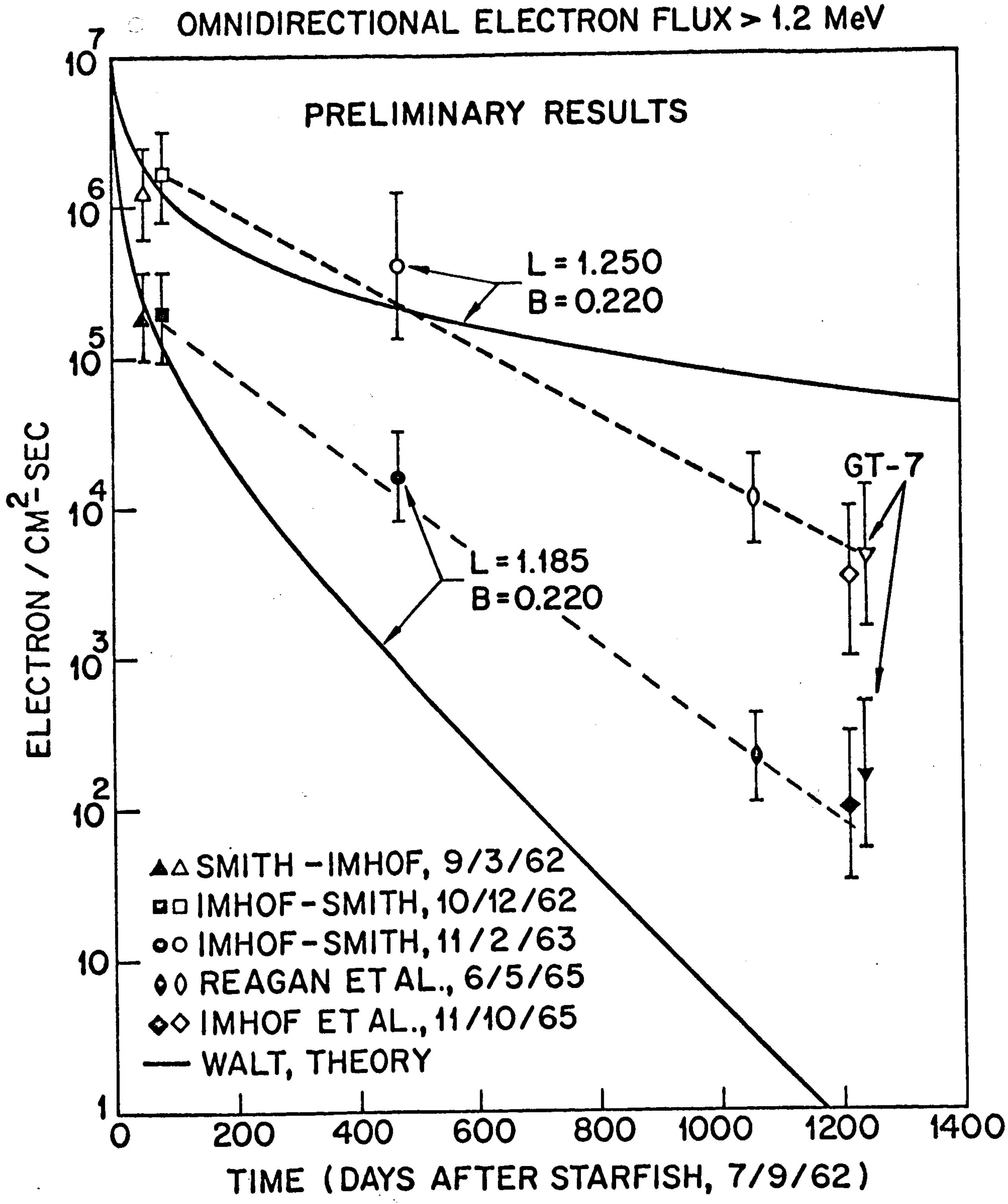

FIGURE 51. Omnidirectional Electron Flux > 1.2 MeV as a Function of Time After the Starfish Event of 9 July, 1962, for L = 1.25, B = 0.22.

data at 56 and 93 days. The dashed lines illustrated the fit to the experimental data of a single exponential decay function of the form

$$\Phi(t_o) = \Phi(t_o)e^{\overline{\tau}}^{t-t_o}.$$

The decay constant τ associated with the flux on $L = 1.25$ is 190 ± 40 days and with the flux on $L = 1.185$ is 140 ± 40 days. For comparison, the data of Bostrom and Williams [1965] obtained with a threshold solid-state detector above 1.2 MeV for a period of 151 days commencing in October, 1963, yield a mean lifetime for electrons at $L = 1.30$ and $0.160 < B < 0.230$ of 235 ± 20 days.

At $L = 1.25$, the theory would predict a slower decay rate than the experimental data show. Whether different atmospheric models and variations of the atmospheric density with solar cycle can explain the observed differences or whether other loss mechanisms are involved needs to be investigated. At $L = 1.185$ the theory predicts that virtually all of the Starfish electron flux would have decayed away by the time of the Gemini experiments. The data show, however, that a significant electron flux still exists on this L shell. The observed flux may well represent the natural existing flux on this L shell which, unfortunately, was not adequately measured prior to 1962. A singular phenomenon which can perhaps explain the behavior of the flux on both of these L shells is that of a redistribution of the Starfish electrons from higher to lower L shells. It has been shown [Imhof and Smith, 1965d] that the third adiabatic invariant can be violated at the time of magnetic storms with a resultant redistribution of trapped particles to lower L shells.

Figure 52 shows the absolute differential flux spectrum of the electrons measured at $L = 1.250$ and $B = 0.220$. The upper data were obtained with a sintillation spectrometer in October, 1963, by Imhof and Smith [1965c]. The two lower spectra were obtained with the Gemini-4 and -7 spectrometers. The theoretical spectrum shapes of Walt [1964b] for the appropriate epoch have been normalized individually to the data at about 2 MeV. At energies greater than this value, the theory and data are in excellent agreement. At lower energies the difference between the

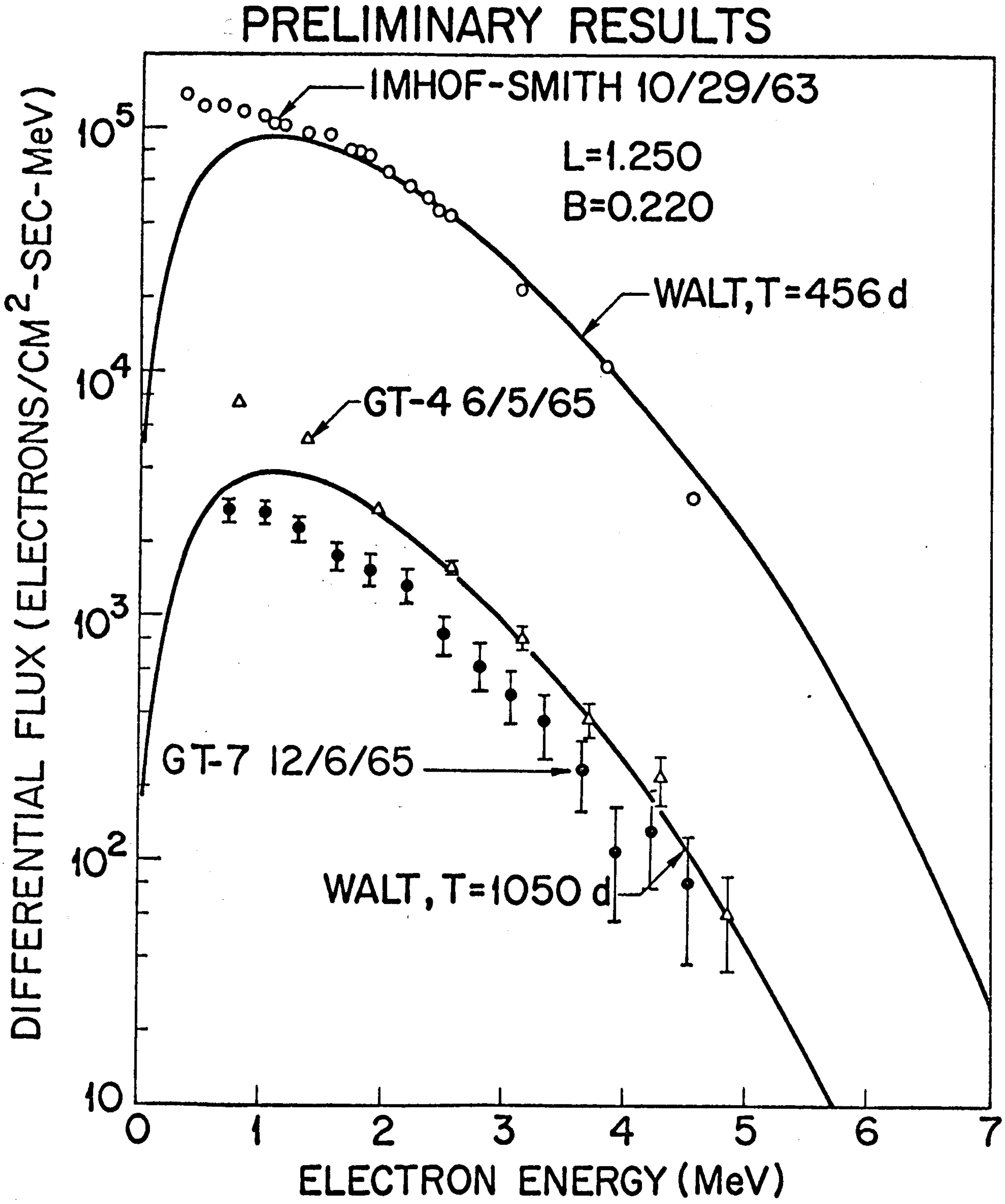

FIGURE 52. Gemini-4 and -7 Differential Electron Flux Compared to Atmospheric Scattering Predictions and Earlier Data at L = 1.25, B = 0.22.

theory and the Gemini data is more pronounced than observed in 1963. The difference spectrum between the Gemini-4 data and the theoretical curve can be described by a simple exponential shape with an E_0 of 450 keV. This difference spectrum could be that of the naturally-occurring electrons, but the analysis is too preliminary to substantiate this. Since the differential flux shown is in absolute units, this difference, if due to naturally-occurring electrons, would indicate that a significant decay has also occurred in that flux over the two-year period of these measurements.

While the Gemini-4 proton data have not been analyzed in depth, a comparison of the present spectral data with that of Heckman and Armstrong [1962] shown in Figure 51 indicates excellent agreement.

Section 6

CONCLUSIONS

The Gemini-4 and Gemini-7 spectrometer experiments have provided detailed flux and spectrum measurements on electrons and protons at low altitudes in the South Atlantic anomaly where the population, lifetime, and behavior of particles trapped on low magnetic shells are greatly influenced by the earth's atmosphere. The Gemini data, when completely analyzed and combined with the data obtained from earlier experiments performed by our laboratory, will constitute some of the best available experimental data on the Starfish electron belt. Through comparison of the experimental data with atmospheric scattering theories, much can be learned regarding loss and redistribution effects, as well as source terms for both protons and electrons in the inner radiation belts. In addition to the foregoing scientific interest, the Gemini data can greatly enhance the limited information currently available for updating models of the inner radiation belt in this region of operational importance.

A great deal of processing and post calibration remains to be accomplished, however, before the final results will be obtained. The preliminary results presented in this report were obtained from the data processed to date and reflect only a fraction of the available information. Of the fifty-five orbits of potential data, only fourteen orbits or 25 percent have been processed. If only the anomaly and adjacent background region of an orbit are considered, approximately twelve full hours of data remain to be processed. A final analysis will also require a much more thorough investigation of such items as scattering, bremsstrahlung, orientation, energy-dependent effects on the geometric factor, and background contributions. Because the preliminary analysis indicates that valuable scientific data will be obtained, every effort should be expended to analyze all of the available data beyond the scope of this contract.

Section 7

REFERENCES

Blanchard, R. C., and W. H. Heaa, "Solar Cycle Changes in Inner-Zone Protons", *J. Geophys. Res. 69*, 3927, 1964.

Bostrom, C. O., and D. J. Williams, "Time Decay of the Artificial Radiation Belt", *J. Geophys. Res. 70*, 240, 1965.

Evans, H. C., and E. H. Bellamy, "The Response of Plastic Scintillators to Protons", *Phys. Soc. Proc. 74*, 483, 1959.

Freden, S. C., and G. A. Paulikas, "Trapped Protons at Low Altitudes in the South Atlantic Magnetic Anomaly", *J. Geophys. Res. 69*, 1257, 1964.

Gooding, T. J., and H. G. Pugh, "The Response of Plastic Scintillators to High-Energy Particles", *Nucl. Instr. and Methods 7*, 189, 1960.

Imhof, W. L., R. V. Smith, and P. C. Fisher, "Particle Flux Measurements From an Atlas Pod in the Lower Van Allen Belt", *Space Res. III*, 438, 1963.

Imhof, W. L., and R. V. Smith, "Variation of Electron Spectrum and Intensity at Low Altitudes", *Space Res. V*, 360, 1965a.

Imhof, W. L., and R. V. Smith, "Longitudinal Variations of High Energy Electrons at Low Altitudes", *J. Geophys. Res. 70*, 569, 1965b.

Imhof, W. L., and R. V. Smith, "Energy Spectrum of Electrons at Low Altitudes", *J. Geophys. Res. 70*, 2129, 1965c.

Imhof, W. L., and R. V. Smith, "Observation of Nearly Monoenergetic High-Energy Electrons in the Inner Radiation Belt", *Phys. Rev. Letters 14*, 885, 1965d.

Imhof, W. L., J. C. Bakke, E. E. Gaines, J. H. Rowland, and R. V. Smith, "High Resolution Electron Measurements in the Outer Radiation Belt", *Trans. Am. Geophys. U. 47*, 135, 1966.

Jensen, D. C., and J. C. Cain, "An Interim Geomagnetic Field", *J. Geophys. Res. 67*, 3568, 1962.

Lenchek, A. M., and S. F. Singer, "The Albedo Neutron Theory of Geomagnetically Trapped Protons", *Planet. Space Sci. 11*, 1151, 1963.

Mann, L. G., S. D. Bloom, and H. I. West, Jr., "The Electron Spectrum From 90 to 1200 keV as Observed on Discoverer Satellites 29 and 31", *Space Res. III*, 447, 1963.

McIlwain, C. E., "Coordinates For Mapping the Distribution of Magnetically Trapped Particles", *J. Geophys. Res. 66*, 3681, 1961.

Mozer, F. S., D. D. Elliott, J. D. Mihalov, G. A. Paulikas, A. L. Vampola, and S. C. Freden, "Preliminary Analysis of the Fluxes and Spectrums of Trapped Particles After the Nuclear Test of July 9, 1962", *J. Geophys. Res.* *68*, 641, 1963.

Nelms, A. T., "Energy Loss and Range of Electrons and Positrons", National Bureau of Standards Circular 577, July, 1956.

Paulikas, G. A., and S. C. Freden, "Precipitation of Energetic Electrons into the Atmosphere", *J. Geophys. Res.* *69*, 1239, 1964.

Reagan, J. B., J. C. Bakke, W. L. Imhof, and R. V. Smith, "Multichannel Spectrometer for the Measurement of Trapped Particles", *IEEE Trans. NS-12*, 83, 1965.

Reagan, J. B.,J. C. Bakke, M. A. Heinemann, W. L. Imhof, and R. V. Smith, "Measurements of Trapped Particle Fluxes and Spectra at Low Altitudes From Gemini-IV", *Trans. Am. Geophys. U.* *47*, 130, 1966.

Rich, M., and R. Madey, "Range-Energy Tables", University of California Radiation Laboratory Report 2301, March, 1954.

Rowland, J. H., J. C. Bakke, W. L. Imhof, and R. V. Smith, "Instrumentation for Space Radiation Measurements", *IEEE Trans. NS-10*, 178, 1963.

Vernov, S. N., V. E. Nesterov, N. F. Pisarenko, I. A. Savenko, O. I. Savun, P. I. Shavrin, and K. N. Sharvina, "Investigation of the Earth's Radiation Belts in the Vicinity of the Brazilian Magnetic Anomaly at Altitudes of 235-345 km", *Planet. Space Sci.* *13*, 347, 1965.

Vette, J. I., "Models of the Trapped Radiation Environment. Vol. I: Inner Zone Protons and Electrons", NASA SP-3024, 1966. "Vol. II: Inner and Outer Zone Electrons", NASA SP-3024, 1966.

Walt, M., and W. M. MacDonald, "The Influence of the Earth's Atmosphere on Geomagnetically Trapped Particles", *Rev. Geophys.* *2*, 543, 1964a.

Walt, M., "The Effects of Atmospheric Collisions on Geomagnetically-Trapped Electrons", *J. Geophys. Res.* *69*, 3947, 1964b.

Welch, J. A., Jr., R. L. Kaufmann, and W. H. Hess, "Trapped Electron Time History for L = 1.18 to L = 1.30", *J. Geophys. Res.* *68*, 685, 1963.

West, H. I., Jr., L. G. Mann, and S. D. Bloom, "Some Electron Spectra in the Radiation Belts in the Fall of 1962", *Space Res.* *V*, 423, 1965.